

INVERSE HEAT CONDUCTION-MICROSTRUCTURE

PROBLEM

AN ONLINE INPUT ESTIMATION ALGORITHM FOR A COUPLED INVERSE
HEAT CONDUCTION-MICROSTRUCTURE PROBLEM

BY

SALAM K ALI, B.SC., M.SC.

A Thesis

Submitted to the school of Graduate Studies

In Partial Fulfillment of the Requirements

For the Degree

Doctor of Philosophy

McMaster University

© Copyright by Salam K Ali, September 2009

DOCTOR OF PHILOSOPHY (2009)

McMaster University

(Mechanical Engineering)

Hamilton, Ontario

TITLE: An Online Input Estimation Algorithm for a Coupled Inverse Heat Conduction-
Microstructure Problem

AUTHOR: Salam K Ali, M.Sc. (Saddam University)

SUPERVISORS: Associate Professor Mohamed S. Hamed and
Professor Marilyn F. Lightstone

NUMBER OF PAGES: xvii, 181

ABSTRACT

This study focuses on developing a new online recursive numerical algorithm for a coupled nonlinear inverse heat conduction-microstructure problem. This algorithm is essential in identifying, designing and controlling many industrial applications such as the quenching process for heat treating of materials, chemical vapor deposition and industrial baking. In order to develop the above algorithm, a systematic four stage research plan has been conducted.

The first and second stages were devoted to thoroughly reviewing the existing inverse heat conduction techniques. Unlike most inverse heat conduction solution methods that are batch form techniques, the online input estimation algorithm can be used for controlling the process in real time. Therefore, in the first stage, the effect of different parameters of the online input estimation algorithm on the estimate bias has been investigated. These parameters are the stabilizing parameter, the measurement errors standard deviation, the temporal step size, the spatial step size, the location of the thermocouple as well as the initial assumption of the state error covariance and error covariance of the input estimate. Furthermore, three different discretization schemes; namely: explicit, implicit and Crank-Nicholson have been employed in the input estimation algorithm to evaluate their effect on the algorithm performance.

The effect of changing the stabilizing parameter has been investigated using three different forms of boundary conditions covering most practical boundary heat flux conditions. These cases are: square, triangular and mixed function heat fluxes. The most important finding of this investigation is that a robust range of the stabilizing parameter

has been found which achieves the desired trade-off between the filter tracking ability and its sensitivity to measurement errors. For the three considered cases, it has been found that there is a common optimal value of the stabilizing parameter at which the estimate bias is minimal. This finding is important for practical applications since this parameter is usually unknown. Therefore, this study provides a needed guidance for assuming this parameter.

In stage three of this study, a new, more efficient direct numerical algorithm has been developed to predict the thermal and microstructure fields during quenching of steel rods. The present algorithm solves the full nonlinear heat conduction equation using a central finite-difference scheme coupled with a fourth-order Runge-Kutta nonlinear solver. Numerical results obtained using the present algorithm have been validated using experimental data and numerical results available in the literature. In addition to its accurate predictions, the present algorithm does not require iterations; hence, it is computationally more efficient than previous numerical algorithms.

The work performed in stage four of this research focused on developing and applying an inverse algorithm to estimate the surface temperatures and surface heat flux of a steel cylinder during the quenching process. The conventional online input estimation algorithm has been modified and used for the first time to handle this coupled nonlinear problem. The nonlinearity of the problem has been treated explicitly which resulted in a non-iterative algorithm suitable for real-time control of the quenching process. The obtained results have been validated using experimental data and numerical results obtained by solving the direct problem using the direct solver developed in stage

three of this work. These results showed that the algorithm is efficiently reconstructing the shape of the convective surface heat flux.

ACKNOWLEDGEMENTS

I wish to express my deepest appreciation to my supervisors Dr. Mohamed S. Hamed and Dr. Marilyn F. Lightstone for their invaluable guidance, endless support, valuable advice and encouragement throughout the period of this research.

I would like to thank my supervisory committee and comprehensive examination members, Dr. Stephen Tullis, Dr. Bartosz Protas, Dr. Sumanth Shankar, and Prof. John Luxat for their direction and advice in different stages of this work. Many thanks are also to the whole staff of the Mechanical Engineering Department for their help and cooperation.

I would like to thank my colleagues of the Thermal Processing Laboratory (TPL) and the Computational Fluid Dynamic (CFD) laboratory at McMaster University: Cathy, Deep, Charles, Morteza, Hassan Morsy, Ramin, Fusheng, Allaa Khafagy, Ahmed Omer, Mohamed Dhafar, Abbas, Di, George. We shared many stressful and joyful moments. Fortunately, only the pleasant moments are remembered.

Without the duaa, continuous support, encouragement and inspiration of my mother, this endeavor would not have been possible. The support of my sister and brothers has always been a strong factor in motivating me throughout my long education journey.

Lastly, I owe my heartfelt gratitude to my wife Hiba, my daughter Noor, and my son Muhammad for their love, patience, support, and encouragement. Without you, my dream would not have come true.

DEDICATION

To

The Memory of My Father

My Dear Mother

My Beloved Family

Hiba, Noor, and Muhammad

My Sister and Brothers

TABLE OF CONTENTS

ABSTRACT.....	iii
ACKNOWLEDGEMENTS.....	vi
TABLE OF CONTENTS.....	viii
LIST OF FIGURES.....	xii
CHAPTER ONE: INTRODUCTION	1
1.1 Introduction.....	2
1.2 Inverse Heat Conduction Problem Formulation.....	5
1.3 Literature Review.....	8
1.3.1 Direct Inverse Methods.....	8
1.3.2 Optimization Based Methods.....	11
1.3.3 Observer Based Methods.....	13
1.4 Kalman Filter.....	16
1.5 Research Objectives.....	21
1.6 Thesis outline.....	28
1.7 References.....	30
CHAPTER TWO: STRUCTURE OF THE ONLINE INPUT ESTIMATION ALGORITHM.....	39
2.1 Introduction.....	40

2.2 Derivation of Kalman filter equations	41
2.3 Derivation of the real time recursive least squares estimator	49
2.4 References.....	50

CHAPTER THREE: NUMERICAL STUDY OF THE MODELING ERROR IN THE ONLINE INPUT ESTIMATION ALGORITHM USED FOR INVERSE HEAT CONDUCTION PROBLEMS (IHCPS).....54

Abstract.....	56
3.1 Introduction.....	57
3.2 Problem Description	59
3.3 Online Input Estimation Algorithm	63
3.4 Simulation Cases.....	66
3.5 Problem Observability	67
3.6 Results and Discussion	68
3.7 Conclusions.....	75
3.8 Acknowledgements.....	75
3.9 References.....	76
3.10 Supplementary Material.....	76

CHAPTER FOUR: AN EFFICIENT NUMERICAL ALGORITHM FOR THE PREDICTION OF THERMAL AND MICROSTRUCTURE FIELDS DURING QUENCHING OF STEEL RODS.....80

Abstract.....	82
Keywords.....	82
Nomenclature.....	82
4.1 Introduction.....	84
4.2 Computational Model.....	88
4.2.1 The Thermal Field Model.....	90
4.2.2 The Phase Transformation Model.....	95
4.3 Structure of the Numerical Algorithm.....	98
4.4 Case Study of Infinite 1080 Carbon Steel Rod.....	102
4.5 Results and Discussion.....	105
4.6 Summary and Conclusions.....	113
4.7 Acknowledgments.....	114
4.8 References.....	114
4.9 Supplementary Material.....	116
CHAPTER FIVE: A MODIFIED ONLINE INPUT ESTIMATION ALGORITHM FOR INVERSE MODELING OF STEEL QUENCHING.....	119
Abstract.....	121
Nomenclature.....	121
5.1 Introduction.....	125

5.2 Problem Formulation	125
5.2.1 Thermal Field Model	130
5.2.1.1 Online input estimation algorithm for Steel Quenching Process.....	139
5.2.2 Microstructure Model	146
5.3 Computational Procedure.....	150
5.4 Case Study	154
5.5 Results and Discussion	156
5.6 Conclusion	167
5.7 Acknowledgments.....	167
5.8 References.....	168
CHAPTER SIX: RESEARCH CONTRIBUTIONS AND RECOMMENDATIONS FOR FUTURE WORK.....	174
6.1 Research Contributions.....	175
6.2 Recommendations for Future Work.....	180

LIST OF FIGURES

Figure 1.1 Schematic of the inverse heat conduction problem (IHCP). 6

Figure 2.1 schematic diagram of the prediction-correction nature of the Kalman filter...42

Figure 3.1 One-dimensional linear inverse heat conduction problem. 60

Figure 3.2 The effect of the stabilizing parameter Q on the estimate bias (time step $\Delta t=0.005$ and $R=1E-6$). 69

Figure 3.3 The effect of the stabilizing parameter Q on the estimate bias for the robust range. 69

Figure 3.4 The effect of the stabilizing parameter (Q) within the robust range on the square wave estimated heat flux ($\Delta t=0.005$ and $R=1E-6$). 70

Figure 3.5 The effect of the stabilizing parameter (Q) within the robust range on the triangular wave estimated heat flux ($\Delta t=0.005$ and $R=1E-6$). 71

Figure 3.6 The effect of the stabilizing parameter (Q) within the robust range on the mixed wave estimated heat flux ($\Delta t=0.005$ and $R=1E-6$). 71

Figure 3.7 A comparison between the exact heat flux and the estimated one with the optimal value of Q ($\Delta t=0.005$ and $R=1E-6$). 72

Figure 3.8 The effect of the temporal and the special discretizations on the estimate bias ($Q=0.01$ and $\Delta t=0.005$) for the square wave heat flux. 73

Figure 3.9 The effect of the thermocouple location and the measurement error standard deviation (σ) on the estimate bias ($Q=0.01$ and $\Delta t=0.005$) for the square wave heat flux 74

Figure 4.1 One-dimensional quenching problem.....	89
Figure 4.2 The computational domain and the uniformly spaced nodal points.....	91
Figure 4.3 Schematic representation of the scheil’s additivity principle and the calculation of the temperature dependant parameters $A(T)$ and $B(T)$ from TTT diagram.	96
Figure 4.4 Simplified flow chart of the computational procedure of the present algorithm.	100
Figure 4.5 TTT diagram for Plain Carbon 1080 Steel [13].	102
Figure 4.6 Dimensions of the case study part.	103
Figure 4.7 The variation of heat transfer coefficient with temperature used in the case study.	103
Figure 4.8 Thermophysical properties of plain carbon 1080 steel [13].....	104
Figure 4.9 A comparison between the transient temperatures of different numerical algorithms and the experimental data reported in [12].	105
Figure 4.10 A comparison between the temperature profile at the rod center predicted by the present algorithm and the experimental data reported in [12].	106
Figure 4.11 A comparison between the microstructure distributions predicted by the previous algorithms [11, 13 and 15] and the present algorithm.	107
Figure 4.12 The volume fraction of pearlite at three different locations inside the rod as a function of time.....	108
Figure 4.13 Variation of the volume fraction of Austenite, Pearlite and martensite at $r=12.03$ mm with time	109

Figure 4.14 A comparison between the microstructure distributions of different numerical algorithms presenting the effect of heat generation.	110
Figure 4.15 A comparison between the temperature profile at the rod center predicted by the present algorithm and those predicted by Woodard while neglecting the effect of heat generation.....	111
Figure 4.16 The effect of the nonlinear term on the thermal field of the quenched steel rod.	112
Figure 4.17 A comparison between the temperature profiles predicted by different numerical algorithms with experimental data when the nonlinear term is neglected.....	113
Figure 4.18 A comparison between the temperature profiles predicted by the numerical algorithm with the experimental data of Fernandes et al. [8].	117
Figure 4.19 A comparison between the pearlite volume fraction predicted by the numerical algorithm with the experimental data of Fernandes et al. [8].	118
Figure 5.1 One-dimensional quenching problem.....	131
Figure 5.2 The computational domain and the uniformly spaced nodal points.....	134
Figure 5.3 Schematic representation of the Scheil's additivity principle and the calculation of the of the Temperature dependant parameters $A_T(T)$ and $B_T(T)$ from TTT diagram.	147
Figure 5.4 Simplified flow chart of the computational procedure of the present inverse algorithm.step from the microstructure calculations, and then used in the heat equation to calculate the thermal field of the next time step.	151
Figure 5.5 TTT diagram for Plain Carbon 1080 Steel.	153

Figure 5.6 The variation of thermophysical properties with temperature used in the case study.....	155
Figure 5.7 A comparison between the exact and the estimated convective heat transfer coefficient of steel quenching process.	157
Figure 5.8 A comparison between (a) the temperature profile predicted by the present algorithm and the experimental data reported in [33], and (b) the transient temperatures of the Kalman filter, different direct numerical algorithms and the experimental data reported in [33]......	158
Figure 5.9 A comparison between (a) the pearlite volume fraction (b) the martensite volume fraction and (c) the retained austenite volume fraction predicted by the previous direct solution algorithms [32,34,35,36] and the present inverse algorithm.....	160
Figure 5.10 A comparison between the inverse solver pearlite volume fraction and that of the direct solver with time for two locations.....	161
Figure 5.11 A comparison between the inverse solver volume fraction of different phases and these of the direct solver.....	162
Figure 5.12 A comparison between the inverse solver pearlite volume fraction and that of the direct solver with time for four locations.....	163
Figure 5.13 Schematic representation of the cooling curves for four locations inside the quenched cylinder on the TTT diagram.....	164
Figure 5.14 Variation of the Estimate Bias with (a) the spatial step size, (b) the time step size, and (c) the measurement error standard deviation.....	166

PREFACE

This PhD thesis is structured in a sandwich thesis style based on the following published and submitted articles:

1. Ali, S. K., Hamed, M. S., and Lightstone, M. F., A Modified Online Input Estimation Algorithm for Inverse Modeling of Steel Quenching, accepted for publication in the Journal of Numerical Heat Transfer/ B, 2009.
2. Ali, S. K., Hamed, M. S., and Lightstone, M. F., Inverse Estimation of Heat Transfer Coefficients in Heat Treating Process, presented in the Inverse Problem Symposium, Michigan State University, May 31 to June 2, 2009.
3. Ali, S. K., Hamed, M. S., and Lightstone, M. F., An Efficient Numerical Algorithm for the Prediction of Thermal and Microstructure Fields during Quenching of Steel Rods, Journal of ASTM International, Vol. 5, No. 10, 2008.
4. Ali, S. K., Hamed, M. S., and Lightstone, M. F., Numerical study of the modeling error in the online input estimation algorithm used for inverse heat conduction problems (IHCPs), Journal of Physics: Conf. Ser. 135 012004, 2008.
5. Ali, S. K., Lightstone, M. F., and Hamed M. S., Parametric Study of Input estimation Algorithm Used for Inverse Heat Conduction Problems, 15th Annual Conference of the CFD Society of Canada, Ontario, Canada, May 27-31, 2007.

INTRODUCTION

CHAPTER 1

1.1 Introduction

The Inverse Heat Conduction Problem (IHCP) involves the estimation of a boundary heat flux, heat source history, or convective heat transfer coefficient by using interior transient temperature measurements in a solid object. The theory and application of inverse heat conduction problems have been significantly developed over the past few decades. IHCP has important applications in various branches of science and engineering. For example, aerodynamic heating of space vehicles occurs during re-entry in the atmosphere and information on the surface temperature of the thermal shield is required. This information cannot be directly obtained with temperature sensors placed directly on the surface due to environmental obstacles. Therefore, temperature sensors are embedded inside the body. The surface temperatures are estimated by using inverse analysis. Inverse analysis can also be used to estimate the thermophysical properties of the shield during operation at high temperatures [1]. Another important application where inverse heat conduction analysis can play an important role is in the nuclear industry [2]. IHCP can be used to estimate the critical heat flux of the fuel sheath as well as the prediction of the inner wall temperature of nuclear reactors. Other examples of IHCP are the determination of quenching heat transfer coefficients under very rapid transient conditions [3], the prediction of temperature or heat flux at the workpiece interface of machine cutting [4], manufacturing process control and the cooling control of electronic components [5].

Calculation of the temperature distribution within a solid body using thermal conditions at the boundary is a direct problem. In contrast, the estimation of heat flux at the boundary using temperature measurements taken within the body is an inverse

problem. In the cause and effect context, the direct problem is the determination of the effects or consequences from known causes while the inverse problem is the estimation of the causes of the desired or observed effects. In many situations, the direct measurement of the cause is not practical and one is forced to estimate the cause from the observation of the effect.

Inverse heat conduction problems are mathematically ill-posed problems because they do not have solutions that are continuously dependent on the input data. This is in contrast to direct problems, which are well-posed. Hadamard [6] in 1923 introduced the concept of well-posed problems. The idea of Hadamard is that a mathematical problem is well-posed if its solution exists and is stable and unique. In other words, the solution should continuously depend on the input data and any small perturbation in the input data should only cause a small change in the solution. In contrast, in an ill-posed problem a small disturbance in the input could lead to a large error in the solution.

The physical reason for the ill-posedness of the inverse heat estimation problem is that variations in the surface conditions of a solid body are lagged and damped toward the interior because of the diffusive nature of the heat conduction. As a consequence, large variations in the thermal conditions at the boundary have to be estimated from small changes in the measurements. Furthermore, error and noise in the measurements can mistakenly lead to large fluctuations in the estimated boundary thermal conditions. As such, special techniques are required to obtain stable solutions for ill-posed problems.

Numerous methods have been developed to solve inverse heat conduction problems [7]. The exact matching method is one of the earliest reported methods.

Shumakov in 1957 and Stolz in 1960 developed two models to analytically solve the problem of transient heat conduction by using the exact matching technique [8,9]. In the Stolz's model, the boundary heat flux is estimated sequentially using one temperature sensor as well as one time step. The results of this method are very sensitive to measurement error especially when the time step is small due to the lag and damping effect resulted from the diffusive nature of the heat conduction process. This flaw makes this method not practically feasible. The sequential function specification method of Beck [10] overcame the limitations of Stolz's method by using future information available in a number of future temperature measurements to minimize the prediction error in the least squares procedure.

Tikhonov [11] introduced a regularization technique to solve IHCPs by modifying the objective function in the least squares procedure. In this method, the objective function includes two terms; the first term is representing the prediction error while the second term includes a regularization parameter used to overcome the ill-posedness and controls the unphysical fluctuation in the estimates and hence enhancing the stability of the solution. The thermal boundary conditions are determined by solving IHCP as a whole time domain solution in which all of the heat flux components are simultaneously estimated for all times. The space marching algorithm is another solution method by which the spatial domain is divided into a direct region for which all boundary conditions are known, and an inverse region for which the boundary conditions are only partially known. Starting from the easily obtained solution in the direct region, it estimates the thermal field in the inverse region by using the finite differencing technique [12].

Most of the above methods are batch form algorithms and they require a complete data set before the computation begins. However, in many situations, it is necessary to carry out the estimation in real time. Some examples are: the vulcanization of complex rubber moldings, real time monitoring of nuclear reactor [13] and the baking of ceramic wafers for annealing, oxidation and chemical vapor deposition [14]. In these cases, the heat flux imposed on the boundary determines the temperature distribution in the system therefore; accurate determination of the heat flux is a crucial step in the operation of the process. This boundary heat flux may need to be adjusted and updated frequently during the process, so a real time sequential algorithm has to be adapted where initial a priori estimation is continually updated based on current experimental measurements. A detailed literature review about the inverse heat conduction solution techniques will be given in section 1.3 of this chapter.

1.2 Inverse Heat Conduction Problem Formulation

Let Ω represents a bounded domain in R^{Ω} , that is occupied by a material having the following thermophysical properties: ρ is the density, C_p is the heat capacity, and κ is the thermal conductivity. Assume that the domain has the four boundaries Ω_N , Ω_E , Ω_S and Ω_W , where the boundaries Ω_E , Ω_S and Ω_W have known thermal boundary conditions while the boundary condition of Ω_N is an unknown heat flux, as shown in Figure 1.1.

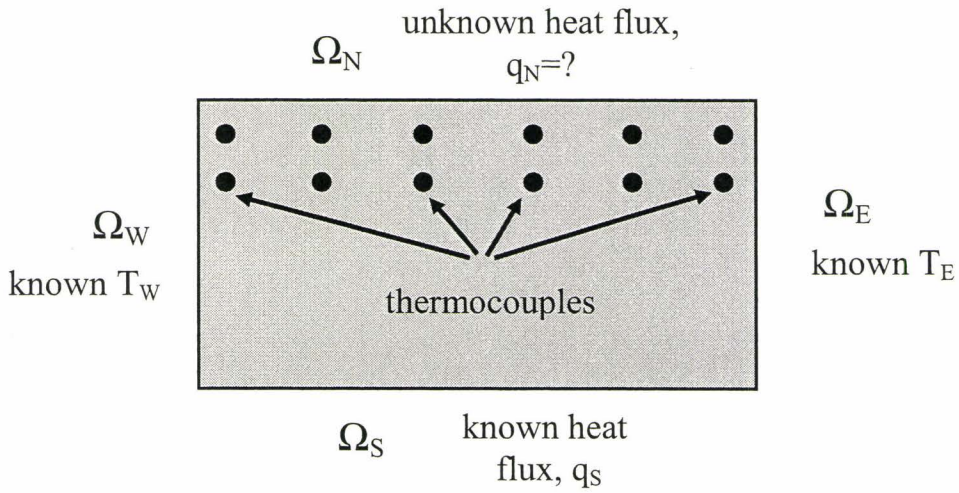


Figure 1.1 Schematic of the inverse heat conduction problem (IHCP).

Some temperature measurements are known at M points within the domain. The objective of the inverse heat conduction analysis is to estimate the unknown boundary condition, q_N . The governing equation of the heat transfer process in this domain is the transient heat conduction equation given by:

$$\rho C_p \frac{\partial T}{\partial t} = \nabla \cdot (\kappa \nabla T), \quad \text{in } \Omega, \quad \text{for } t > 0 \quad (1.1)$$

$$T(x, t) = T_E, \quad \text{on } \Omega_E, \quad \text{for } t > 0 \quad (1.2)$$

$$T(x, t) = T_W, \quad \text{on } \Omega_W, \quad \text{for } t > 0 \quad (1.3)$$

$$\kappa \frac{\partial T(x, t)}{\partial n} = q_S, \quad \text{on } \Omega_S, \quad \text{for } t > 0 \quad (1.4)$$

$$\kappa \frac{\partial T(x, t)}{\partial n} = q_N \text{ (unknown), on } \Omega_N, \text{ for } t > 0 \quad (1.5)$$

$$T(x, 0) = T_o(x), \text{ in } \Omega, \text{ for } t > 0 \quad (1.6)$$

$$Y(x_i, t_j) = T(x_i, t_j), \text{ in } \Omega, \text{ for } i = 1, 2, 3, \dots, M \text{ and } j = 1, 2, 3, \dots, N_t \quad (1.7)$$

where N_t is the number of time steps.

Generally, inverse problems are solved by minimizing an objective function with some regularization techniques used in the estimation procedure, as will be clarified in the literature review, next section. With some statistical assumptions, the objective function, S , that provides minimum variance estimates is the ordinary least squares norm [1], defined as the sum of squared residuals as

$$\begin{aligned} S(q_N) &= \{Y(x_i, t_j) - \hat{T}(x_i, t_j)\}^T \{Y(x_i, t_j) - \hat{T}(x_i, t_j)\} \\ &= \sum_{\substack{i=1 \\ j=1 \\ i=M \\ j=N_t}} \{Y(x_i, t_j) - \hat{T}(x_i, t_j)\}^2 \end{aligned} \quad (1.8)$$

where Y and \hat{T} are the vectors containing the measured and estimated temperatures respectively, and the superscript T indicates the transpose of the vector. The estimated temperatures are obtained from the solution of the direct problem with estimates for the unknown heat flux at the surface.

1.3 Literature Review

As previously stated, the inverse heat conduction problems are ill-posed problems where their solutions are unstable and sometimes not unique. Therefore, in order to solve IHCPs, some sorts of regularization are required. The regularization, in this context, is a mathematical treatment by which an ill-posed problem is converted into a well-posed problem where its solution is unique and very close to the solution of the original ill-posed problem. This solution is stable and more robust since a small change in the input data due to measurements errors does not cause a large variation in the solution [7].

Based on the method of regularizing the inverse heat conduction problem, solution methods can be classified into three main categories [15]. The first category is based on the direct inverse methods; the second is based on the dynamic observers while the third is based on the optimization solution methods. The solution of the direct inverse methods is based on formulating a linear relationship between heat flux and temperatures. The dynamic observer based methods apply the optimal control theory to the inverse heat conduction problem. The prominent characteristic of this category is that these methods allow for online estimation. The inverse heat conduction problems are transformed into optimization problems in the third category.

1.3.1 Direct Inverse Methods

The standard compact form of the linear IHCP can be represented by the following matrix form equation; $T=X q$, where X is the sensitivity coefficient matrix, which describes the relationship between the response of the estimated temperature, T , and any

change in the boundary heat flux, q . The direct inverse operation cannot be directly applied to the above equation to estimate q since the sensitivity matrix, X , is singular [15]. Many regularization techniques have been developed and used to overcome the ill-posedness of these methods. The most widely used in the literature are the Tikhonov regularization and the future times.

Tikhonov [16] developed a whole time domain regularization method based on the modified objective function and sensitivity matrix relationship of the direct heat conduction equation. Tikhonov's idea is to add a term to the objective function that reduces or eliminates undesirable oscillations in the estimation results. He introduced three types of regularization, namely, zeroth-order, first-order and second-order regularization. For example, the modified objective function of Tikhonov whole domain zeroth-order regularization is:

$$S(q) = \sum_{i=1}^I (Y_i - T_i)^2 + \alpha \sum_{i=1}^I q_i^2 \quad (1.9)$$

Where q_i is the unknown boundary heat flux that needs to be estimated by the inverse analysis at time t_i , Y is the temperature measurement, T is the estimated temperature, α is the regularization parameter, and I is the number of time steps. The second term in equation (1.9) is the whole domain zeroth-order regularization term. A proper value of the regularization parameter, α , should be carefully selected to improve the stability of the solution. Tikhonov recommended that α be selected in such a way that the minimum value of the objective function and the sum of squares of the measurement errors are

equal [16]. More details about a proper choice of Tikhonov regularization parameter can be found in [1,2,7,15,16].

Beck [2] used future time steps to regularize the IHCP and estimate boundary heat fluxes in many applications [7]. The information of future temperatures is used in a smoother algorithm to enhance the stability of the solution by reducing the sensitivity to the measurement errors. If the number of future measurements is r , the modified objective function of this method is;

$$S(q_M) = \sum_{i=1}^r (Y_{M+i-1} - T_{M+i-1})^2 \quad (1.10)$$

If the value of r is set to unity, the method is simplified into Stolz method of exact matching [9]. Beck's method is known as the sequential function specification method. It is so called because its solution depends on the shape of the initial assumption of the function being estimated. Constant and linear heat flux functional forms [2] have been used. Although the solution at each time step uses a number of future temperature measurements, only one component of the boundary heat flux is estimated corresponding to the current time step. This feature makes it possible to use a very small time step. However, using a number of future time steps limits this method to batch form estimation. This method can be used for both linear and nonlinear IHCPs.

The ill-posedness of the above sensitivity matrix of the IHCP has been dealt with by applying the singular value decomposition method [17,18]. In this method the sensitivity matrix is decomposed into three matrices as follows.

$$X = U\Sigma V^T \quad (1.11)$$

Where $U \in R^{n \times n}$ and $V \in R^{n \times n}$ are orthogonal matrices and $\Sigma \in R^{n \times n}$ is a diagonal matrix with nonnegative diagonal elements such that $\Sigma_1 \geq \Sigma_2 \geq \Sigma_3 \geq \dots \geq \Sigma_{\min(n,n)} \geq 0$. The smallest positive singular values of matrix Σ make the minimum norm solution of the inverse heat conduction problems very sensitive to measurement errors. Therefore, these smallest singular values of matrix X should be truncated and removed in order to enhance the solution stability. The truncation index can be selected by applying the discrepancy principle [18].

Low-pass filters have also been employed to solve inverse heat conduction problems. Blum and Marquardt [19] solved the IHCPs by mapping it into the z domain. While Luttich et al. [20] used s -domain transform to solve IHCPs. The low-pass filter techniques and the singular value decomposition are similar in handling the ill-posedness of IHCP in the sense that both methods filter out the high frequency signals.

1. 3.2 Optimization Based Methods

In this category of IHCP solution techniques, optimization is also employed to solve IHCP, among which the steepest descent method [16], the Conjugate Gradient Method (CGM) [1, 15], the Newton-Raphson and the quasi Newton methods have been explored.

The objective function usually used in this category is the ordinary least squares norm. It is given by the following form for multiple sensors (N):

$$S(q_M) = \sum_{m=1}^N \int_{t=0}^{t_f} \{Y_m(t) - T(x_{meas}, t)\}^2 dt \quad (1.12)$$

where Y_m is the measurement, T is the predicted measurement and t_f is the duration of the experiment. The above objective function is minimized under a constraint specified by the direct problem that is part of the solution procedure.

Steepest descent method is the most basic gradient method. The idea of this method is to move downwards on the objective function along the direction of the highest variation (gradient), in order to locate its minimum value. The use of the gradient direction in this method is not very efficient since the steepest descent method starts with large variations in the objective function, but as the minimum value is almost reached, the convergence rate becomes very slow.

The conjugate gradient method improves the convergence rate of the steepest descent method by choosing directions of descent using linear combination of the gradient direction with directions of descent of previous iterations [1, 15, 21-25]. Both the steepest descent and the conjugate gradient methods use the same procedure for the evaluation of the search step size. Due to its excellent search algorithm, CGM has been extensively used for solving IHCPs. The conjugate gradient method with adjoint problem has been used for parameter and function estimation problems [26-32]. If a priori information is available about the unknown variable, the problem can be solved as a parameter estimation problem. On the other hand, if there is no a priori information of the unknown variable then the problem is solved as a function estimation problem.

Employing the CGM to solve IHCPs requires solving the following subproblems: the direct problem, the inverse problem, the sensitivity problem, the adjoint problem, the gradient equation, the iterative procedure and the stopping criterion. The solution is usually obtained through an optimal searching. While the steepest descent and conjugate gradient methods use gradients of the objective function in their iterative procedures, the Newton-Raphson method also uses information of the second derivative, Hessian matrix, of the objective function in order to minimize the objective function and to achieve a faster convergence rate with more computational cost due to the complexity of the computation. In quasi Newton methods, the Hessian matrix appearing in the Newton-Raphson method is approximated in such a way that it does not involve the second derivatives. The approximation of the Hessian matrix is based on the first derivatives. As a result, the quasi Newton method has a slower convergence rate than the Newton-Raphson method; however, it is computationally faster [33]. Calculating the gradient is more computationally expensive than calculating the function value, and calculating the Hessian matrix is more computationally expensive than calculating the gradient. However, the optimization technique that does not involve the Hessian matrix usually requires many more iterations, and is often faster.

1.3.3 Observer Based Methods

Many types of observer structures have been used in solving IHCP including Beck's sequential observer [3,34], state and disturbance [35], and Kalman filter observer [36]. An important characteristic in this category is that it allows for online estimation. This

kind of estimation is also called digital filter estimation algorithm [3]. The concept of an observer based method can be clarified as follows [35]:

Consider a discrete-time system where the state of the system (T_k) is governed by the following process equation:

$$T_{k+1} = AT_k + Bq_k \quad (1.13)$$

where T_{k+1} is an estimate of the real state of the system based on the information from the previous state T_k . A is the state transition matrix from time k to $k+1$, B is the input matrix and q_k is a known input vector.

The measurement equation is:

$$z_k = HT_k \quad (1.14)$$

An observer, is a dynamical system that provides an estimate of the state of the system, \hat{T}_{k+1} , based on the input, q_k , and the output measurements z_k . This can be achieved by copying the dynamics of the system and incorporating a feedback from the difference between the system output and the output generated using the estimates of the state. That is:

$$\hat{T}_{k+1} = A\hat{T}_k + Bq_k + K_f(z_k - \hat{z}_k) \quad (1.15)$$

The term $K_f(z_k - z_k)$ in equation (1.15) is a feedback that indicates the error of the estimate. Therefore, the gain coefficient K_f must be selected in such a way that the above equation is stable and the estimation errors tend to zero.

With Beck's sequential observer it is first necessary to determine filter coefficients K_f which requires using one of the inverse solution techniques such as sequential and whole domain procedures. After determining the filter coefficients, the filter algorithm can be used efficiently for online analysis.

The state and disturbance observer has been used for the first time to solve IHCPs by Marquardt and Auracher in 1990 [35]. The most important strengths of this approach are the insensitivity to measurement noise and the ease of implementation. The shortcomings of this method are the unavoidable phase lag and its deficiency in reproducing abruptly changing in the unknown boundary heat flux.

The Kalman filter design technique [36] is used to obtain a Kalman type observer [37]. The unknown parameters are combined with the original state vector as new variables to form a new set of state equations. The Kalman filter technique is then used to solve this new set of equations and predict the state parameters.

There are various thermal problems that have been solved by applying an adaptive filter solution methods such as the Kalman filter. The solution of these problems is based on the optimal control theory. The main task in the simulation of a thermal system is the determination of its state vector and some unknown parameters from incomplete information. Temperature is the state vector in a thermal system and boundary conditions, thermal properties and shape of boundaries are examples of the state parameter that can

be identified by simulation of a thermal system. The following section provides an overview of using Kalman filter as an estimator in parameter estimation algorithms of heat transfer problems.

1.4 Kalman Filter

Kalman filter is a statistical estimator that belongs to a class of algorithms known as Bayesian filtering algorithms. It solves inverse problems using statistical inversion theory and assuming that the state vector, initial estimate and its error covariance are Gaussian random variables. In the statistical inversion theory, the ill-posed inverse problem is converted into a well-posed problem by recasting the problem in a larger space of probability distribution employing Bayesian inference [38-42]. The solution of the converted problem is not a single estimate, however, it is a probability distribution known as a posterior distribution from which a single estimate can be obtained by employing some stochastic probabilistic estimators such as the Kalman filter.

The deterministic techniques of solving IHCPs, such as those mentioned in the preceding sections, assume that the mathematical models (governing equations) are perfectly representing the physical phenomena. Furthermore, the measurement errors are characterized in terms of their norms in these techniques. These norms are usually assumed as real numbers. There are also some uncontrolled input disturbances to the system that are not considered in the IHCPs deterministic methods. However, in the numerical solutions, the mathematical models must be discretized, which introduces a new source of error. Also, in practice, the norm of the measurements error is usually a

random variable with a specified mean. Therefore, the deterministic solutions of IHCPs that give single estimates of the unknown variables do not rigorously consider the stochastic nature of the model and measurement uncertainties. Hence, they are not as reliable as the probabilistic methods in solving ill-posed inverse problems. The probabilistic approaches provide a complete characterization of both the model noise as well as the measurements noise. Furthermore, the probabilistic methods are able to better quantify the uncertainties of the estimates by computing their statistical moments.

Kalman filter was derived by Kalman [36] in 1960 as an optimal linear estimator. It recursively estimates the state of a linear dynamic system as a conditional mean using some measurements. These measurements are linearly related to the state of the system and are corrupted by uncorrelated Gaussian white noise of zero mean. Kalman filter optimality is based on the fact that the mean squared error of the estimates is minimized.

This filter has been used in numerous applications [43-48]. It was first applied for parameter estimation of an inverse heat conduction problem by Scarpa and Milano [49] in 1991. The thermal diffusivity as well as the error resulting from the uncertainty in the thermocouple locations were identified by introducing some noise in the transient temperature measurements. The state vector was augmented with the estimated parameters to form a new set of state equations. The Kalman filter technique was used to solve this new set of equations and to predict the state parameters. This parameter estimation approach is called a joint estimation. It is worth mentioning that there was a previous attempt to use Kalman filter for a parameter estimation problem by Simbrirskii in 1976 [50]. Simbrirskii estimated temperature dependent thermal conductivity without

considering the uncertainty in the sensors locations. In contrast to the joint estimation, the dual estimation represents a decoupled type of approach where two separate estimators are used to estimate the state vector and the unknown parameters. For example the online input dual estimation approach developed by Tuan et al. [51].

Tuan et al. [51] proposed a recursive online estimation method to solve two-dimensional linear inverse heat conduction problems. They combine the Kalman filter technique and the Recursive Least Squares Estimator (RLSE) [52]. In this method, the Kalman filter generates the residual innovation sequence, followed by the use of a real time recursive least squares method to predict the value of the parameters employing the generated innovation sequence. They used the algorithm to estimate two separate unknown heat fluxes on two different boundaries in real time. The algorithm is simple in concept and computationally efficient.

If the system model or measurement model is nonlinear, the standard Kalman filter cannot be directly applied. However, it can be extended to handle nonlinear systems. There are two main approaches by which the standard Kalman filter can be extended for nonlinear problems. The first approach is called the perturbation Kalman Filter (PKF) in which the state space model is linearized around a nominal trajectory by using Taylor series expansion [43]. The second approach is called the Extended Kalman Filter (EKF) in which the state space model is linearized around the most recent time estimates [53]. PKF is faster since the real time implementation parameters such as the state transition matrices and the filter gains are not functions of the estimates and do not

need to be updated at each iteration. However, it is less robust against nonlinear approximation errors than the EKF.

The review paper of Sorenson [54] demonstrated the developments in the method of least-squares estimation from its first derivation by Gauss to the new form of Kalman. Sorenson noticed that Kalman filter with its easy implementation on a digital computer can be regarded as an efficient computational solution of the least squares method. In addition, Sorenson noted that Kalman filter can be applied with significant success to nonlinear systems.

Jang et al. [55] applied two different approaches for online estimation of nonlinear chemical process problems. The first approach was based on the extended Kalman filter while the second approach applied nonlinear optimization methods to minimize the error in the estimate. The results of this study showed that the extended Kalman filter is sensitive to several factors such as the initial guess of the state variables, the statistics of the input and measurements noise, and the degree of nonlinearity of the system.

Scarpa and Milano [56] used a Kalman smoothing technique to estimate time dependent surface heat flux at one boundary of a one-dimensional system using measurements of temperature profile at an interior location within a solid slab. They used future temperature measurements to smooth the estimation. Therefore, their algorithm is only applicable for offline estimations.

Employing different discretization techniques, the online input estimation algorithm of Tuan et al. [51], has been subsequently applied for solving different

problems including estimating the contact conductance during metal casting, interface conductance between periodically contacting surfaces, and solidification [57-62].

Ji and Jang experimentally evaluated the application of Kalman filter for inverse heat conduction problems [63]. The heat flux was augmented in the temperature state vector and both are estimated simultaneously. The results of this investigation showed a good agreement with the experimental results.

Cartesegna et al. [64] applied an inverse technique to estimate the thermophysical and mass transfer properties of a porous insulating material under transient thermal conditions. The Kalman filter was used as a parameter estimator in this study. Results showed that Kalman filter could be an interesting approach for estimating the global transport performance of porous materials in the presence of moisture.

Daoas and Radhouani [65] applied an extended version of the Kalman filter to estimate time-dependent surface heat flux in a one-dimensional nonlinear IHCP using experimental temperature measurements. They used the extended Kalman filter with a number of future measurements as a smoothing technique. The proposed method is an offline technique for the estimation of surface temperatures and surface heat flux. Their results showed that this algorithm is capable of handling the time lag and measurement errors if the number of future temperature measurements is carefully chosen.

Wang et al. [66] developed an online adaptive-weighting input estimation algorithm to solve nonlinear heat conduction problems. The nonlinearity resulted from the thermophysical properties being temperature dependent. This algorithm incorporates an extended Kalman filter with the real time recursive least squares estimator to estimate

a time varying unknown heat source in a one-dimensional transient problem. This study showed that the extended Kalman filter can be efficiently used for handling nonlinear inverse heat conduction problems. This algorithm has been modified later by Chen and Cheng to handle a highly nonlinear thermal system [67].

Milano et al. [68] surveyed ten years worth of research in implementing inverse algorithms to estimate thermophysical properties from dynamic experiments. Those algorithms were based on the parameter estimation theory by using Kalman filtering technique. They concluded from this review that the use of statistical algorithms like Kalman filter in the parameter estimation can be considered as the most reliable and comprehensive approach.

1.5 Research Objectives

Based on the presented literature review of the general methods used to solve inverse heat conduction problems, it is clear that the first and second groups of methods are batch form algorithms which cannot be used for online estimations. Moreover, the whole time domain Tikhonov regularization method has one clear disadvantage that is if the inverse solution is carried out over a long period of time, the matrix dimension and the computational cost will be increased accordingly. The disadvantage of the conjugate gradient method is that it is incapable of uniform convergence of the approximation because gradients approach zero value during the final time step.

In industrial applications, some parameters or boundary heat flux must be determined and adjusted online rather than in batch form. Thus batch form algorithms

cannot be used for those applications. In contrast, the discrete Kalman filter algorithm can be readily implemented for online real time analysis. Furthermore, the discrete Kalman filter approach is much more computationally efficient than other methods [3]. This online algorithm does not require accumulating the measurements after they are processed. Therefore, the required capacity of the computational equipment is significantly reduced using the recursive estimation method since every new output of Kalman filter only requires the previous output and the current observed data. In addition, Kalman filter outperforms the other methods particularly in treating noisy measurements since it belongs to stochastic type estimators as previously mentioned.

It can be easily concluded from the Kalman filter literature review that the research in the field of parameter and input estimation using Kalman filter has been geared toward signal processing rather than thermal engineering. However, previous work has been done by different researchers using Kalman filter as an estimator to solve IHCPs [45-53]. The first time the Kalman filter was applied to solve IHCPs was in 1991 [45]. Since then this technique has been used mostly for solving the thermal field of linear inverse heat conduction problems [49-51,56-63,65-67]. However, there are many industrial processes such as thermal processing of metals where the thermal field is coupled with the microstructure field. The main objective of this work is to develop a new real-time recursive algorithm that is capable of handling coupled thermal-microstructure fields to estimate the transient thermal boundary conditions of nonlinear inverse heat conduction problems using the observer based theory of Kalman filter. The algorithm should be able to handle measurement errors efficiently and tracking the time

varying surface heat flux and surface temperature robustly and adaptively. In order to achieve this task, a systematic four stage research plan was devised. The details of the four stages are as follows:

Stage 1: The online dual input estimation algorithm has been derived and developed by Tuan et al. [51]. As indicated in the literature review, it is very efficient online technique to solve IHCP. However, some important issues require further investigation as discussed below. In this stage, an online input estimation algorithm using Kalman filter and real time recursive least square method has been coded to solve a one-dimensional linear inverse heat conduction problem. The main objectives of this stage of the research work were:

1. Develop a full understanding of the performance of the dual online input estimation algorithm developed by Tuan et al. [51]. This would primarily include understanding the effect of the tuning parameters of the algorithm, namely, the stabilizing parameter of the Kalman filter Q and the forgetting factor of the least squares algorithm γ on the accuracy of the estimates. A thorough understanding of these issues would help in developing this algorithm for more complicated and coupled applications such as steel quenching.
2. Examine the influence of spatial and temporal discretizations of the heat conduction equation, the location of the temperature sensor, and the measurement noise level and its covariant matrix R on the quality of the estimate.
3. Another issue that needed to be addressed in this work is the effect of the initial value of the state estimate covariance errors matrix P in the Kalman filter algorithm and the

value of the input (heat flux) estimate error covariance matrix P_b in the recursive least squares algorithm. In all his work, Tuan et al. [51,57-62,66,67] has assigned very large values for these two matrices. He assigned 10^{10} for P and 10^8 for P_b which causes the estimator to ignore the few initial estimates [51].

Stage 2: Kalman filter has been extensively investigated since its derivation by Kalman in 1960 [36] and a number of alternative Kalman filtering algorithms have been proposed which are theoretically equivalent or close to the original formulation [59]. However, all previous investigations using the online input estimation techniques for heat transfer applications have been based on employing only the continuous time conventional Kalman filter [51,57-62,66,67]. The implicit Kalman filter is an alternative filter which could be used to incorporate various desirable features including enhancing numerical stability and computational accuracy or reducing computational requirements.

Depending on the discretization scheme used for the heat conduction problem, different types of Kalman filter can be obtained. Using an explicit scheme leads to an explicit Kalman filter. With an explicit scheme a smaller time step is often needed to improve the accuracy of the algorithm or to provide good stability, very small time steps, however, are not always recommended in inverse heat conduction problems due to its diffusive nature [3]. This issue associated with the use of explicit Kalman filter for solving inverse heat conduction problems has been addressed in the second stage of this study.

In this stage of the research work, the implicit, explicit, and Crank-Nicholson Kalman filters have been applied to the problem of inverse heat conduction to investigate their ability in improving the estimate of the boundary heat flux.

The implicit Kalman filter takes the following form:

The process equation:

$$A_1(k)T(k+1) = A_2(k)T(k) + D[q(k) + w(k)] \quad (1.16)$$

where T is the state vector of dimensional n , $q(k)$ is the input vector, $w(k)$ is the process stochastic disturbance, $A_1(k)$ and $A_2(k)$ are known matrices from which the state transition matrix can be estimated, $D(k)$ is the input transition matrix, and $k=1, 2, \dots$ is the discrete time index.

The measurement equation:

$$z(k+1) = H(k+1)T(k+1) + v(k+1) \quad (1.17)$$

where $z(k+1)$ is the measurements vector, $H(k+1)$ is the measurement matrix and $v(k+1)$ is the measurement noise vector.

If matrix A_1 has rank less than n then the above system is often called descriptor or singular system. The traditional discrete dynamic system is a special case of Equation (1.16) when $A_1=I$. If A_1 is non singular for all k , then the implicit system can be formulated as an explicit form and the traditional Kalman filter can be applied to obtain the minimum variance state estimate of Equation (1.16). The main objectives of this stage of the research work were:

1. Investigate the numerical stability of the online input estimation algorithm using different discretization schemes including implicit, explicit and Crank-Nicholson schemes.
2. Study the effect of using implicit, Crank-Nicholson, and explicit Kalman filter on the performance of the online input estimation algorithm.

Stage 3: The last two stages of this study were devoted to investigate the feasibility of modifying the online input estimation algorithm to handle coupled inverse heat conduction-microstructure problems, namely, steel quenching processes.

Quenching is an important process in industrial heat treatment operations in which the temperature of the part is reduced to a desired value using a liquid jet, gas jet, or immersion in a liquid bath. Quenching in steel is even more important due to phase transformations that take place. During a phase transformation, heat is generated which influences the thermal field of the steel. The phase transformation in steel is dependent on the thermal field developed during quenching. Therefore different types of steel microstructures can be obtained depending on the cooling rate.

Deformation, thermal and residual stresses, and surface hardness of steel are strongly related to the microstructure and the phases presented inside the material. Thus, the phase transformation in steel during quenching should be efficiently controlled in order to produce steel with a certain set of mechanical properties. This can be achieved effectively by controlling the quenching process. Traditionally quenching conditions are determined by experimental work which does not provide information about the microstructure during the process and only gives the final microstructure. This way of

obtaining quenching conditions can lead to non-optimal material properties and some associated financial consequences to the industry [69].

There are two main scenarios in numerical modeling of heat treatment of steel by quenching. The first scenario is related to the situation where quenching conditions are known and the goal is to compute the produced microstructure, surface hardness, residual stresses and distortions. The second scenario considers the situation where the quenching conditions need to be estimated to produce a desired microstructure in order to achieve a certain set of mechanical properties.

The former case is addressed by solving a direct heat transfer problem using the given boundary conditions to calculate the thermal field and the corresponding microstructure, surface hardness, and distribution of residual stresses inside the steel. The latter case is addressed by using transient temperatures (cooling rate) corresponding to the required microstructure as input to an inverse heat conduction algorithm in order to estimate the required convective heat transfer coefficient that provides the required cooling rate. In both types of problems: direct and inverse, the phase transformation model must be coupled with the thermal field model to simultaneously evaluate the thermal field as well as the microstructure field inside the part.

The same microstructure model that is used for direct problems will be used for inverse problems. Therefore, the direct problem with the microstructure model is solved first in stage three of the present work to check the validity and reliability of the used microstructure model. In addition, solving a direct problem of steel quenching would provide a thorough understanding and validation of the phase transformation model.

Moreover, results of the direct problem will be used as input to the inverse solver, which was carried out in stage four of this study.

Stage 4: The final goal of this work was to develop a new inverse algorithm to simulate the heat treatment process of steel quenching. This algorithm was based on combining the online input estimation methodology with steel microstructure models. Achieving this task would provide a tool for online controlling the process of steel quenching which, in turn, would lead to large savings in both efforts and cost of achieving optimal material properties.

1.6 Thesis outline

This thesis consists of six chapters. Chapter 1 introduces the concept of inverse heat conduction problems with its general formulation. It also provides detailed literature review of different solution techniques that have been used for solving inverse heat conduction problems. This review includes the application of Kalman filter for thermal systems. This chapter is concluded with research objectives and thesis outline.

Chapter 2 presents the historical development of the online input estimation algorithm and its application in tracking and navigation applications and its modification by Tuan et al. [51] for inverse heat conduction problems. This chapter includes the mathematical derivation of Kalman filter and its modification as part of the online input estimation algorithm.

Chapter 3 consists of two publications. The first publication is a paper published in the Journal of Physics: Conference Series in 2008. The paper reports a parametric study of

the effect of some important parameters that affect the performance of the online input estimation algorithm in its application for inverse heat conduction problems. Special attention has been given to the modeling error used as the stabilizing parameter in the algorithm. The second part of this chapter is a conference publication devoted to investigating the effect of using different types of Kalman filter, resulted from employing different discretization techniques, on the performance of the online input estimation algorithm. This publication was presented in the 15th Annual Conference of the CFD Society of Canada, Toronto, Ontario, May 27-31, 2007.

Chapter 4 is a journal paper published in the *Journal of ASTM International*, Vol. 5, Issue 10, 2008. This paper reports a new algorithm for the prediction of the thermal and microstructure fields of a steel rod during quenching. The full nonlinear heat conduction equation in the cylindrical coordinates was used in this investigation. The nonlinearity of the problem was handled by employing implicit linearization which led to a very efficient and accurate algorithm. No iterations were needed and hence, the computational time was reduced significantly.

Chapter 5 is a journal paper that has been accepted for publication in the *Journal of Numerical Heat Transfer/B*. The paper introduces a modified version of the online input estimation algorithm for a coupled problem of steel quenching. Since its derivation by Tuan et al. in 1996 [51], the online input estimation algorithm has been only used for solving the thermal field of many inverse heat conduction problems. In this work, the feasibility of applying this algorithm for a coupled heat conduction/microstructure

problem has been investigated and validated. The outcome of this work showed the reliability of this algorithm in handling such problems.

The sixth chapter of this thesis summarizes the significant research contributions as well as some recommendations for future research work.

1.7 References

1. Ozisik, M. N., and Orlande, H. R. B., “Inverse Heat Transfer, Fundamentals and Applications”, Taylor & Francis, New York, 2000.
2. Beck, J. V., Blackwell, B., and St. Clair, C. R., Jr, ” Inverse heat conduction-III Posed Problems”, John Wiley, New York. 1985.
3. Heming, C, Xieqing, H., and Jiabin, X., Comparison of Surface Heat-Transfer Coefficients Between Various Diameter Cylinders During Rapid Cooling, *Journal of Materials Processing and Technology*, vol. 138, pp. 399-402, 2003.
4. Wang, C. C., and Chen, C. K., Three-Dimensional Inverse Heat Transfer Analysis During the Grinding Process, *Journal of Mechanical Engineering Science*, Vol. 216, Part C, pp. 199-212, 2002.
5. Janicki, M., Zubert, M., and Napieralski, Application of Inverse Problem Algorithms for Integrated circuit temperature estimation, *Microelectronics Journal*, Vol. 30, No. 11, pp. 1099–1107, 1999.
6. Hadamard, J., *Lectures on Cauchy’s Problem in Linear Differential Equations*, Yale University Press, New Haven, CT, 1923.
7. Woodbury, K. A., *Inverse Engineering Handbook*, CRC Press, New York, 2002.

8. Shumakov, N. V., A Method for the Experimental Study of the Process of heating a solid body, Soviet Physics - Technical Physics, Translated by American Institute of Physics, Vol. 2, pp. 771-781, 1957.
9. Stolz, G. Jr., Numerical Solution to an Inverse Problem of Heat Conduction for Simple Shapes, Journal of Heat Transfer, Vol. 82, pp. 20-26, 1960.
10. Beck, J. V., Calculation of Surface Heat Flux from an Internal Temperature History, ASME Paper, 62-HT-46, 1962.
11. Tikhonov, A. N., Solution of Incorrectly Formulated Problems and the Regularization Methods, Soviet mathematics - Doklady, Vol. 4, No. 4, pp. 1035-1038, 1963.
12. Raynaud, M., and Bransier, J., A New Finite-Difference Method for Nonlinear Inverse Heat Conduction Problem, Numerical Heat Transfer, Vol. 9, pp. 27-42, 1986.
13. Ji, C. C., Tuan, P. C., and Jang, H. Y., A Recursive Least-Squares Algorithm for On-Line 1-D Inverse Heat Conduction Estimation, International Journal of Heat and Mass Transfer, vol. 40, no. 9, pp. 2081-2096, 1997.
14. Nulman, J., and Krusius, J.P., and Gat, A., Rapid Thermal Processing of Thin Gate Dielectrics-Oxidation of Silicon, IEEE Electron device Lett., EDL-6, pp. 205, 1985.
15. Xue, X., Luck, R., and Berry, J. T., Comparisons and Improvements Concerning the Accuracy and Robustness of Inverse Heat Conduction Algorithms, Inverse Problems in Science and Engineering, Vol.13, No.2, pp. 177-199, 2005.
16. Tikhonov, A. N., and Arsenin, V. Y., Solution of ILL-Posed problems, Washington, DC, 1977.

17. Shenefelt, J., Luck, R., Taylor, R. P., and Berry, J.T., “Model Reduction Solution for Inverse Heat Conduction Problems Employing Matrix Transfer”, *International Journal of Heat and Mass Transfer*, Vol. 45, pp. 67-74, 2002.
18. Hansen, P. C., *Rank-deficient and Discrete Ill-posed Problems: Numerical Aspects of Linear Inversion*, SIAM, 1998.
19. Blum, J. C., and Marquardt, W., An Optimal Solution to Inverse Heat Conduction Problems Based on Frequency-Domain interpretation and observers, *Numerical Heat Transfer, Part B*, Vol. 32, pp.453-478, 1997.
20. Luttich, T., Mhamdi, A., and Marquardt, W., Design, Formulation and Solution of Multi-dimensional Inverse Heat Conduction Problems, *Numerical Heat Transfer, Part B*, Vol. 47, No. 2, pp. 111-133, 2005.
21. Alifanov, O. M., Artyukhin, E. and Romyantsev, A., *Extreme Methods for Solving Ill-Posed Problems with Applications to Inverse heat Transfer Problems*, Begell House, New York, 1995.
22. Daniel, J. W., *The Approximate Minimization of Functionals*, Prentice Hall, Englewood Cliffs, 1971.
23. Jaluria, Y., *Design and Optimization of Thermal Systems*, McGraw Hill, 1998.
24. Fletcher, R. and Reeves, C. M., Function Minimization by Conjugate Gradient, *Compt. Journal*, Vol. 7, pp.149-154, 1964.
25. Fletche, R., *Practical Methods of Optimization*, John Wiley & Sons, 2000.
26. Fletche, R., and Reeves, C. M., Function Minimization by Conjugate Gradients, *Computer Journal*, Vol. 7, pp. 149-154, 1964.

27. Kammerer, W. I., and Nashed, M. Z., On the Convergence of the Conjugate Gradient Method for Singular Linear Operator Equations, *Journal of Numerical Analysis*, Vol. 9, pp. 165-181, 1972.
28. Alifanov, O. M., and Artyukhin, E. A., Regularized Numerical Solutions of Nonlinear Inverse Heat Conduction Problem, *Journal of engineering Physics*, Vol. 29, pp. 934-938, 1975.
29. Alifanov, O. M., Determination of Heat Loads from a Solution of Nonlinear Inverse problem, *High Temperatures*, Vol. 15, pp. 498-504, 1977.
30. Jarny, Y., Ozisik, M. N., and Bardou, J. P., A General Optimization Method Using Adjoint Equation for Solving Multidimensional Inverse Heat Conduction, *International Journal of Heat and Mass Transfer*, Vol. 34, pp. 2911-2919, 1991.
31. Huang, C. H., and Ozisik, M. N., Inverse Problem of Determining the Unknown Strength of an Internal Plane Heat Source, *Journal of Franklin Institute*, pp. 751-764, 1992.
32. Carvalho, R. N., Orlande, H. R., and Ozisik, M. N., Estimation of the Boundary Heat Flux in Grinding Via the Conjugate Gradient Method, *Heat Transfer Engineering*, Vol. 21, pp. 71-82, 2000.
33. Marcelo, J. C., and Orlande, H. R., and George, S. D., Inverse and Optimization Problems in Heat Transfer, *Proceedings of the 10th Brazilian Congress of Thermal Science and Engineering*, Nov. 29-Dec. 03, 2004.
34. Beck, J. V., Filter solutions for the nonlinear inverse heat conduction problem, *Inverse Problems in Science and Engineering*, Vol. 16, No. 1, pp. 3-20, 2008.

35. Marquardt, W., and, Auracher, H., An Observer-Based Solution of Inverse Heat Conduction Problems, *International Journal of Heat and Mass Transfer*, Vol. 33, No. 7, pp. 1545-1562, 1990,
36. Kalman, R.E., A New Approach to Linear Filtering and Prediction Problem, *ASME J. Basic Eng.*, Series 82d, pp. 35-45, 1960.
37. Ji, C. C., and Jang, H. Y., Experimental Investigation in Inverse Heat Conduction Problem, *Numerical Heat Transfer, Part A*, Vol. 34, pp. 75-91, 1998.
38. Kaipio, J., and Somersalo, E., *Statistical and Computational Inverse Problems*, Springer Science & Business Media, New York, 2005.
39. Wang, J., and Zabararas, N., A Bayesian Inference Approach to Inverse Heat Conduction Problem, *International Journal of Heat and Mass Transfer*, Vol. 47, pp. 3927-3941, 2004.
40. Narayanan V. A., and Zabararas, N., Stochastic Inverse Heat Conduction Using a Spectral Approach, *International Journal for Numerical Methods in Engineering*, Vol. 60, pp. 1569-1593, 2004.
41. Emery, A. F., Estimating Parameters and Refining Thermal Models by Using the Extended Kalman Filter Approach, *Journal of Heat Transfer*, Vol. 126, pp. 809-817, 2004.
42. Vogel, C. R., *Computational Methods for Inverse Problems*, SIAM, 2002.
43. Grewal, M. S., Application of Kalman filtering to the calibration and Alignment of Inertial Navigation systems, *Proc. PLANS, 86-Position Location and navigation Symposium*, Las Vegas, NV, 1986.

44. Grewal, M. S., and Miyasako, R. S., Gyro Compliance Estimation in the Calibration and Alignment of Inertial Measurements Units, Proc. Eighteen Joint Service Conf. on data Exchange for Inertial Systems, San Diego, CA, 1986.
45. Chui, C. K., and Chen, G., Kalman Filtering with Real Time Applications, Springer-Verlag, New York, 1987.
46. Sorenson, H. W., Kalman Filtering: Theory and application, IEEE Press, Piscataway, NJ, 1985.
47. Maybeck, P. S., Stochastic Models, Estimation, and Control, Vol. 1, Academic Press, San Diego, CA, 1979.
48. Grewal, M. S., and Andrews, A. P., Kalman Filtering: Theory and Practice Using Matlab, Second Edition, John Wiley & Sons, Inc., 2001.
49. Scarpa, F., Bartolini, R., and Milano, Guido, State Space (Kalman) Estimator in the Reconstruction of Thermal Diffusivity from Noisy Temperature Measurements, High Temperatures-High Pressure, Vol. 23, pp. 633-642, 1991.
50. Simbirskii, D. F., Solution of an Inverse Problem of Heat Conduction, Using Optimal Filtering, Journal of Engineering Physics, Vol. 14, pp. 925-931, 1976.
51. Tuan, P. C., Ji, C. C., Fong, L. W., Huang, W. T. , An Input Estimation Approach to Online Two-Dimensional Inverse Heat Conduction Problem, Numerical Heat Transfer, Part B, Vol. 29, pp. 345-363, 1996.
52. Shalom, Y. B., Li, X. R., and Kirubarajan, T., Estimation with Applications to Tracking and Navigation, John Wiley, New York, 2001.

53. Jawinski, A. H., Stochastic Processing and Filtering Theory, New York, NY: Academic Press, 1970.
54. Sorenson, H. W., Least-Squares Estimation: from Gauss to Kalman, IEEE Spectrum, pp. 63-68, July 1970.
55. Jang, S. S., Joseph, B., and Mukal, H., Comparison of Two Approaches to Online Parameter and State Estimate of Nonlinear Systems, Ind. Eng. Chem. Process Des. Dev., Vol. 25, pp. 809-814, 1986.
56. Scarpa, F., and Milano, G., Kalman Smoothing Technique Applied to the Inverse Heat conduction Problem, Numerical Heat Transfer, Part B, Vol. 28, PP. 79-96, 1995.
57. Tuan, P. C., Lee, S. H., and Hou, W. T., An Efficient On-line Thermal Input Estimation Method Using Kalman Filter and recursive Least Square Algorithm, Inverse Problems in Eng., Vol. 5, PP. 309-333. 1997.
58. Tuan, P. C., and Ju, M. C., The Validation of the Robust Input Estimation Approach to Two-Dimensional Inverse Heat Conduction Problems, Numerical Heat Transfer, Part B, Vol. 37, pp. 247-265, 2000.
59. Tuan, P. C., and Ju, M. C., Adaptive Weighting Input Estimation Algorithm for One Dimensional Cylindrical Inverse Heat Conduction Problems, Proc. Natl. Sci. Council. ROC (A), Vol. 25, No. 3, PP. 163-171, 2001.
60. Chen, T. C., Adaptive Weighting Input Estimation Method to Contact Conductance During Metal Casting Problem, Numerical Heat Transfer, Part B, Vol. 39, pp. 405-419, 2001.

61. Chen, T. C., and Tuan, P. C., Inverse Problem of Estimating Interface Conductance Between Periodically Contacting Surfaces using the Weighting Input Estimation Method, *Numerical Heat Transfer, Part B*, Vol. 41, pp. 477-492, 2002.
62. Chen, T. C., and Tuan, P. C., Input Estimation Method Including Finite-Element Scheme for Solving Inverse Heat Conduction Problems, *Numerical Heat Transfer, Part B*, Vol. 47, pp. 277-290, 2005.
63. Ji, C. C., and Jang, H. Y., Experimental Investigation in Inverse Heat Conduction Problem, *Numerical Heat transfer, Part A*, Vol. 34, pp. 75-91, 1998.
64. Cartesegna, M., Scarpa, F., and Milano, G., Simultaneous Identification of Thermophysical and Moisture Transport Properties in Porous Insulating Materials, *High Temperature- High Pressure*, vol. 32, No. 1, pp.53-60, 2000.
65. Daouas, N., and Radhouani, M. S., A New Approach of The Kalman Filter Using Future Temperature Measurements for Nonlinear Inverse Heat Conduction Problems, *Numerical Heat Transfer, Part B*, Vol. 45, No. 6, pp. 565-585, 2004.
66. Wang, H. M., Chen, T. C., Tuan, P. C., and Den, S.G., Adaptive-Weighting Input-Estimation Approach to Nonlinear Inverse Heat-Conduction Problems, *Journal of Thermophysics and Heat Transfer*, Vol. 19, No. 2, 209-216, 2005.
67. Chen, T. C. , Cheng, C. H., Jang, H. Y., and Tuan, P. C., Using Input Estimation to Estimate Heat Source in Nonlinear Heat Conduction Problem, *Journal of Thermophysics and Heat Transfer*, Vol. 21, No. 1, 166-172, 2007.

68. Milano, G., Scarpa, F., Righini, F., and Bussolino, G. C., Ten Years of Parameter estimation Applied to Dynamic Thermophysical Property Measurements, *International Journal of Thermophysics*, Vol. 22, No. 4, pp. 1227-1240, 2001.
69. Shuhui, M., Aparna, S. V., Makiko, T., and Darrell, K. R., Quenching-Understanding, Controlling and Optimizing the Process, *Proceeding of the Fourth International Conference on Quenching and Control of Distortion*, 20-23 may, Beijing, 2003.

***STRUCTURE OF THE ONLINE INPUT ESTIMATION
ALGORITHM***

CHAPTER 2

2.1 Introduction

The input estimation methodology was first derived by Chan et al. in 1978 to estimate acceleration input vector of maneuvering targets such as aircrafts [1]. It consists of a conventional Kalman filter, a statistical detector and an acceleration input least squares estimator. The scheme at each time step uses a sliding window that contains a number of measurements to estimate the target acceleration where its norm is then compared against a specific threshold in a statistical detection process. If the norm is more than the threshold, the estimated acceleration is used to correct the Kalman filter state and covariance estimates. This batch form algorithm was modified later by Bolger in 1987 by formulating it in a recursive form [2]. The recursive formulation of Bolger had been revised by Hou and Shaanxi in 1989 by using the correct form of Kalman filter equations [3]. The results of the above investigations showed that this algorithm can be effectively tracking maneuvering targets.

The online form of input estimation algorithm has been derived for inverse heat conduction applications by Tuan et al. in 1996 [4]. The new algorithm was used to solve a two-dimensional linear inverse heat conduction problem. This method, input estimation, is based on using the conventional Kalman filtering approach combined with the real time recursive least squares algorithm (RLSE) to estimate the two input unknown heat fluxes on two different boundaries.

Tuan et al. modified the batch form input estimation algorithm of Chan et al. [1] to an online recursive form for real time estimating of a time varying unknown input by using a fading memory scalar known as the forgetting factor, γ . This parameter can also

be used to control the input gain of recursive least squares estimation in order to give the acceptable trade-off between the filter tracking ability, filter response, and its sensitivity to measurement errors, filtering capability. Tuan et al. firstly used this factor as a constant tunable parameter varying between 0 and 1 [4]. This approach was modified later by Tuan et al. [5]. In the new approach the constant forgetting factor is replaced by an adaptive weighting forgetting factor $\gamma(k)$ by taking it as a function of residual innovation, the difference between the actual and predicted measurements, at each time step. The results showed that this approach is reliable in tracking unknown boundary heat flux and efficiently handled the noisy measurements.

The online input estimation algorithm has been applied to different applications including estimating contact conductance during metal casting, estimating interface conductance between periodically contacting surfaces, and solidification employing different discretization techniques [4-19]. This approach involves the application of residual innovation sequence produced by the Kalman filter, and followed by the use of real time least squares method to predict the value of the parameters (unknown boundary heat fluxes). The next section provides an overview of the derivation of the Kalman filter equations as well as the real time recursive least squares estimator.

2.2 Derivation of Kalman filter equations

Kalman filter is a set of mathematical equations that recursively compute the state, $T(k + 1)$, of a linear dynamical system at time $k + 1$ from the previous state estimate, $T(k)$, at time k and the new measurement, $z(k + 1)$. It first predicts a state of a system

using the previous estimate and the process dynamic of the system. Then it corrects (update) this prediction after receiving a feedback from the system in the form of noisy measurements. The prediction-correction process of Kalman filter can be represented by the schematic diagram shown in Figure 2.1. Since it is recursive, Kalman filter needs only the previous estimate and current measurement in order to estimate the new state of the system. This is a very important feature of Kalman filter which makes it very attractive for online implementation. Thus, the most important feature is that the unknown is of a real time estimate followed by a measurement that is taken at the current time.

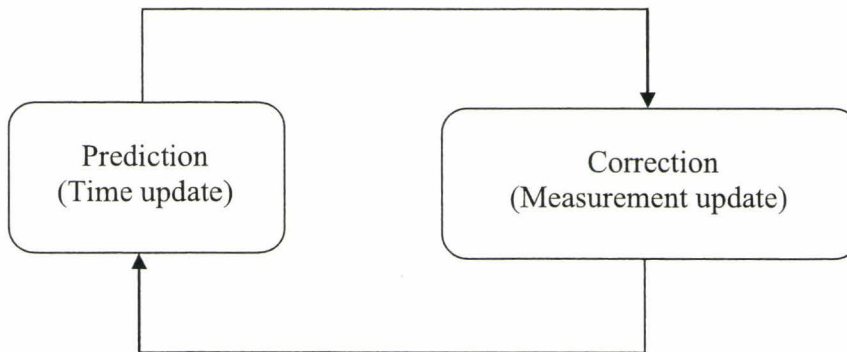


Figure 2.1 Schematic diagram of the prediction-correction nature of the Kalman filter.

Consider a discrete time state space representation of a linear form of heat conduction process described by the following two equations:

Process Equation:

$$T(k + 1) = A(k)T(k) + D(k)[q(k) + w(k)] \quad (2.1)$$

Measurement Equation:

$$z(k + 1) = H(k + 1)T(k + 1) + v(k + 1) \quad (2.2)$$

where $T(k)$ and $T(k + 1)$ are respectively the temperature state vectors of the system at time k and $k + 1$, $A(k)$ is the state transition matrix, $D(k)$ is the input matrix, $q(k)$ is the input represented by the boundary heat flux, $z(k + 1)$ is the measurement vector at time $k + 1$, $H(k + 1)$ is the measurement matrix, $w(k)$ is the process noise and $v(k)$ is the measurement noise. Both the process noise and the measurement noise are assumed to be zero mean uncorrelated Gaussian and white noise sequences with covariance $Q(k)$ and $R(k)$ respectively given by:

$$E[w(k)w^T(n)] = \begin{cases} Q(k) & \text{if } n = k \\ 0 & \text{if } n \neq k \end{cases} \quad (2.3)$$

$$E[v(k)v^T(n)] = \begin{cases} R(k) & \text{if } n = k \\ 0 & \text{if } n \neq k \end{cases} \quad (2.4)$$

Moreover, the process noise $w(k)$ is uncorrelated with the measurement noise $v(k)$, that is,

$$E[w(k)v^T(n)] = 0 \quad \text{for all } k \text{ and } n \quad (2.5)$$

Assuming that there is an initial estimate of the process $T(k)$ at time k . This estimate is based on all the previous information about the process before time k . Also, assuming that the error associated with this estimate is given by:

$$e(k) = T(k) - \hat{T}(k) \quad (2.6)$$

where $T(k)$ is the true state of the system and $\hat{T}(k)$ is the predicted state. Therefore, the state prediction covariance, also known as error covariance matrix, is defined by:

$$P(k) = E[e(k)e^T(k)] = \left\{ [T(k) - \hat{T}(k)][T(k) - \hat{T}(k)]^T \right\} \quad (2.7)$$

The state prediction is obtained by applying the operator of expectation conditioned on the sequence of measurements available at time k , defined by the vector Z^k . This estimation is called the conditional mean given by:

$$E[T(k+1/k)|Z^k] = E\left\{ [A(k)T(k) + D(k)[q(k) + w(k)]] | Z^k \right\} \quad (2.8)$$

Since the process noise $w(k)$ is Gaussian white noise of zero mean, the above equation becomes:

$$\hat{T}(k+1/k) = A(k)T(k/k) + D(k)q(k) \quad (2.9)$$

The prediction error is obtained from subtracting Equation 2.9 from Equation (2.1) as follows:

$$e(k+1/k) = T(k+1) - \hat{T}(k+1/k) \quad (2.10)$$

Substituting Equations 2.1 and 2.9 in Equation 2.10, yields

$$e(k + 1/k) = A(k)[T(k) - \hat{T}(k + 1/k) + D(k)w(k)] \quad (2.11)$$

The state prediction error covariance is found by applying the operator of expectation conditioned on Z^k on the above equation

$$P(k + 1/k) = E[e(k + 1/k)e^T(k + 1/k)|Z^k] \quad (2.12)$$

$$P(k + 1/k) = A(k)E[e(k + 1/k)e^T(k + 1/k)|Z^k]A^T(k) + D(k)E[w(k)w^T(k)]D^T(k)$$

$$P(k + 1/k) = A(k)P(k/k)A^T(k) + D(k)Q(k)D^T(k) \quad (2.13)$$

Similarly, the predicted measurement is obtained by finding the expected value of the measurement equation, Equation 2.2, conditioned on Z^k

$$\hat{z}(k + 1/k) = E[z(k + 1)|Z^k] \quad (2.14)$$

$$\hat{z}(k + 1/k) = E[H(k + 1)T(k + 1) + v(k + 1)|Z^k]$$

$$\hat{z}(k + 1/k) = H(k + 1)\hat{T}(k + 1/k) \quad (2.15)$$

Subtracting Equation 2.15 from Equation 2.2 yields the measurement prediction error:

$$\bar{z}(k + 1/k) = z(k + 1) - \hat{z}(k + 1/k)$$

$$\bar{z}(k + 1/k) = H(k + 1)e(k + 1/k) + v(k + 1) \quad (2.16)$$

Note that \bar{z} is also known as the innovation residual.

Thus, the measurement prediction covariance is given by:

$$S(k+1) = E[\bar{z}(k+1/k)\bar{z}^T(k+1/k)|Z^k]$$

$$S(k+1) = H(k+1)P(k+1/k)H^T(k+1) + R(k+1) \quad (2.17)$$

Kalman's idea is that the new information in the measurement can be used to improve the prior estimation. He updated the prior estimation to obtain the posterior estimation by using a linear relationship between the predicted estimate and the new measurement as follows,

$$\hat{T}(k+1/k+1) = \hat{T}(k+1/k) + K(k+1)[z(k+1) - \hat{z}(k+1/k)] \quad (2.18)$$

where $K(k+1)$ is Kalman gain works as a weighting matrix between the predicted state and the measurement. It is worth mentioning that $\hat{T}(k+1/k)$ and $\hat{T}(k+1/k+1)$ are respectively the predicted and corrected estimates for the same time step $(k+1)$ [20].

Using Equations 2.15 and 2.16, the above equation can be written as:

$$\hat{T}(k+1/k+1) = \hat{T}(k+1/k) + K(k+1)\bar{z}(k+1) \quad (2.19)$$

The updated error covariance matrix of the updated state at time $k+1$ can be obtained by

$$\begin{aligned}
& P(k + 1/k + 1) \\
&= E \left[\{T(k + 1) - \hat{T}(k + 1/k + 1)\} \{T(k + 1) - \hat{T}(k + 1/k + 1)\}^T \middle| Z^k \right] \quad (2.20)
\end{aligned}$$

Substituting Equations 2.2, 2.15, and 2.19 in Equation 2.20, yield:

$$\begin{aligned}
P(k + 1/k + 1) &= E[\{e(k + 1/k) - K(k + 1)[H(k + 1)T(k + 1) + v(k + 1) - \\
&\quad H(k + 1)\hat{T}(k + 1/k)]\} \{e(k + 1/k) - K(k + 1)[H(k + 1)T(k + 1) + \\
&\quad v(k + 1) - H(k + 1)\hat{T}(k + 1/k)]\}^T | Z^k] \quad (2.21)
\end{aligned}$$

Note that the prediction error, $e(k + 1/k)$, is uncorrelated to the measurement noise, $v(k + 1)$.

By performing the above expectation in Equation 2.21, the following general expression for the updated error covariance (posterior covariance) can be obtained:

$$\begin{aligned}
P(k + 1/k + 1) &= [I - K(k + 1)H(k + 1)]P(k + 1/k)[I - K(k + 1)H(k + 1)]^T + \\
&\quad K(k + 1)R(k + 1)K^T(k + 1) \quad (2.22)
\end{aligned}$$

$$\begin{aligned}
P(k + 1/k + 1) &= \\
&P(k + 1/k) - K(k + 1)H(k + 1)P(k + 1/k) - P(k + 1/k)H^T(k + 1)K^T(k + 1) + \\
&K(k + 1)[H(k + 1)P(k + 1/k)H^T(k + 1) + R(k + 1)]K^T(k + 1) \quad (2.23)
\end{aligned}$$

This expression for the updated error covariance is a function of any gain $K(k + 1)$, and the goal now is to find the optimal Kalman gain that minimizes the updated

covariance matrix. The optimal Kalman filter can be obtained by applying the minimum mean square error criterion. This can be done by differentiating Equation 2.23 with respect to $K(k + 1)$ and equating it to zero and finding the optimal Kalman filter gain. The resulting optimal Kalman filter is given by:

$$K(k + 1) = P(k + 1/k)H^T(k + 1)S^{-1}(k + 1) \quad (2.24)$$

Substituting Equation 2.24 in Equation 2.23 yields the following expressions for the updated error covariance matrix:

$$P(k + 1/k + 1) = P(k + 1/k)H^T(k + 1)S^{-1}(k + 1)H(k + 1)P(k + 1/k)$$

$$P(k + 1/k + 1) = P(k + 1/k) - K(k + 1)S(k + 1)K^T(k + 1)$$

$$P(k + 1/k + 1) = [I - K(k + 1)H(k + 1)]P(k + 1/k) \quad (2.25)$$

The above Kalman filter equations are classified into two main groups [21]. The first group is called the time update equations by which the state of the system and the error covariance matrix are predicted for the next time step. The second group is called the measurement update equations by which the predicted estimates of the first group are corrected by using the new information contained in the new measurement. The previous two groups along with the Kalman gain can be summarized below:

Time update equations

A priori state prediction

$$\hat{T}(k + 1/k) = A(k)T(k/k) + D(k)q(k) \quad (2.26)$$

A priori state-error covariance matrix

$$P(k + 1/k) = A(k)P(k/k)A^T(k) + D(k)Q(k)D^T(k) \quad (2.27)$$

Kalman gain

$$K(k + 1) = P(k + 1/k)H^T(k + 1)S^{-1}(k + 1) \quad (2.28)$$

Measurements update equations

State prediction update

$$\hat{T}(k + 1/k + 1) = \hat{T}(k + 1/k) + K(k + 1)\bar{z}(k + 1) \quad (2.29)$$

A posteriori (update) state-error covariance matrix

$$P(k + 1/k + 1) = [I - K(k + 1)H(k + 1)]P(k + 1/k) \quad (2.30)$$

2.3 Derivation of the real time recursive least squares estimator

The recursive least square estimator is developed based on using two Kalman filters in the Kalman filter estimator. These two Kalman filters generate two different innovation residuals. The first innovation residual is the observed innovation sequence that is produced by the mismatched Kalman filter assuming no boundary heat flux [3]. The second innovation residual, known as a hypothetical innovation sequence, is produced by the hypothetical Kalman filter assuming known boundary heat flux.

The idea behind employing two Kalman filters is to formulate a linear regression relationship between the observed innovation residual of the mismatched Kalman filter and the hypothetical innovation residual of the hypothetical Kalman filter as a function of the unknown boundary heat flux. This relationship can be considered as a measurement equation for the unknown boundary heat flux, the input, where the recursive least squares estimation technique can be used to estimate the unknown input. The derivation of this measurement equation is given in chapter five for the steel quenching process and for the sake of brevity will not be repeated here.

Having given the mathematical derivation of the Kalman filter and the real time recursive least squares estimator that constitute the online input estimation algorithm. The next chapter will present parametric study for the applicability of the online input estimation algorithm for the one dimensional inverse heat conduction problem considering different functions of boundary heat flux.

2.4 References

1. Chan, Y. T., Hu, A. G., and Plant, J. B., A Kalman Filter Based Tracking Scheme with Input Estimation, IEEE Transactions on Aerospace and Electronic Systems, Vol. AES-15, No. 2, pp. 237-244, 1979.
2. Bogler, P. L., Tracking a Maneuvering Target Using Input Estimation, IEEE Transactions on Aerospace and Electronic Systems, Vol. AES-23, No. 3, pp. 298-310, 1987.

3. Hou, M., and Shaanxi, X., Comment on Tracking a Maneuvering Target Using Input Estimation, IEEE Transactions on Aerospace and Electronic Systems, Vol. AES-25, No. 2, pp. 280-280, 1989.
4. Tuan, P. C., Ji, C. C., Fong, L. W., Huang, W. T. , An Input Estimation Approach to On-line Two-Dimensional Inverse Heat Conduction Problem, Numerical Heat Transfer, Part B, Vol. 29, pp. 345-363, 1996.
5. Tuan, P. C., and Ju, M. C., The Validation of the Robust Input Estimation Approach to Two-Dimensional Inverse Heat Conduction Problems, Numerical Heat Transfer, Part B, Vol. 37, pp. 247-265, 2000.
6. Tuan, P. C., Lee, S. H., and Hou, W. T., An Efficient On-line Thermal Input Estimation Method Using Kalman Filter and recursive Least Square Algorithm, Inverse Problems in Eng., Vol. 5, PP. 309-333. 1997.
7. Ji, C. C., Tuan, P. C., and Jang, H. Y., A Recursive Least-Squares Algorithm for On-Line 1-D Inverse Heat Conduction Estimation, International Journal of Heat and Mass Transfer, vol. 40, no. 9, pp. 2081-2096, 1997.
8. Tuan, P. C., and Hou, W. T., Adaptive Robust Weighting Input Estimation Method For the 1-D Inverse Heat Conduction Problem, Numerical heat Transfer B, vol. 34, pp. 439-456, 1998.
9. Ji, C. C., and Jang, H. Y., Experimental Investigation in Inverse Heat Conduction Problem, Numerical Heat transfer, Part A, Vol. 34, pp. 75-91, 1998.
10. W. S. Lee, Y. H. Ko, and C. C. Ji, A Study of an Inverse Method for the Estimation of Impulseive Heat Flux, Journal of the Franklin Institute, vol 337, 661-671, 2000.

11. Chen, T. C., Adaptive Weighting Input Estimation Method to Contact Conductance During Metal Casting Problem, Numerical Heat Transfer, Part B, Vol. 39, pp. 405-419, 2001.
12. Tuan, P. C., and Ju, M. C., Adaptive Weighting Input Estimation Algorithm for One Dimensional Cylindrical Inverse Heat Conduction Problems, Proc. Natl. Sci. Council. ROC (A), Vol. 25, No. 3, PP. 163-171, 2001.
13. Chen, T. C., and Tuan, P. C., Inverse Problem of Estimating Interface Conductance Between Periodically Contacting Surfaces using the Weighting Input Estimation Method, Numerical Heat Transfer, Part B, Vol. 41, pp. 477-492, 2002.
14. Chen, T. C., and Tuan, P. C., Input Estimation Method Including Finite-Element Scheme for Solving Inverse Heat Conduction Problems, Numerical Heat Transfer, Part B, Vol. 47, pp. 277-290, 2005.
15. Wang, H. M., Chen, T. C., Tuan, P. C., and Den, S.G., Adaptive-Weighting Input-Estimation Approach to Nonlinear Inverse Heat-Conduction Problems, Journal of Thermophysics and Heat Transfer, Vol. 19, No. 2, 209-216, 2005.
16. Jang, H. Y., Tuan, P. C., Chen, T. C., and Chen, T. S., Input estimation Method Combined With the Finite-Element Scheme to Solve IHCP Hollow-Cylinder Inverse Heat Conduction Problem, Numerical Heat Transfer A, vol. 50, 263-280, 2006.
17. Chen, T. C. , Cheng, C. H., Jang, H. Y., and Tuan, P. C., Using Input Estimation to Estimate Heat Source in Nonlinear Heat Conduction Problem, Journal of Thermophysics and Heat Transfer, Vol. 21, No. 1, 166-172, 2007.

18. Cheng, T. C., and Liu, C. C., Jang, H. Y., and Tuan, P. C., Inverse Estimation of Heat Flux and Temperature in multi-layer gun Barrel, *International Journal of Heat and Mass transfer*, Vol. 50, pp. 2060-2068, 2007.
19. Cheng, T. C., and Liu, C. C., Inverse Estimation of Time-varied Heat Flux and Temperature on 2-D Gun Barrel using Input Estimation Method with Finite-element Scheme, *Defence Science Journal*, vol. 58, pp. 57-76, January 2008.
20. Shalom, Y. B., Li, X. R., and Kirubarajan, T., *Estimation with Applications to Tracking and Navigation*, John Wiley, New York, 2001.
21. Haykin, S., *Kalman Filtering and Neural Networks*, New York, John Wiley and Sons Inc., 2001.

***NUMERICAL STUDY OF THE MODELING ERROR IN THE
ONLINE INPUT ESTIMATION ALGORITHM USED FOR
INVERSE HEAT CONDUCTION PROBLEMS (IHCPS)***

CHAPTER 3

Chapter Three Preface

This work has been previously published in:

- Ali, S. K., Hamed, M. S. and Lightstone, M.F., Numerical study of the modeling error in the online input estimation algorithm used for inverse heat conduction problems (IHCPs), Journal of Physics: Conf. Ser. 135 012004, 2008.

The whole article is the first part of this chapter.

- Ali, S. K., Lightstone, M. F. and Hamed, M. S., Parametric Study of Input estimation Algorithm Used for Inverse Heat Conduction Problems, presented in the 15th Annual Conference of the CFD Society of Canada, Ontario, Canada, May 27-31, 2007.

Part of this article is the supplementary material for this chapter.

Numerical study of the modeling error in the online input estimation algorithm used for inverse heat conduction problems (IHCPs)

Abstract

A numerical investigation has been conducted to study the effect of modeling error in the state equation on the performance of the online input estimation algorithm in its application to the inverse heat conduction problems. This modeling error is used as a tuning parameter known as the stabilizing parameter in the online input estimation algorithm of the inverse heat conduction problems. Three different cases which cover most forms of the boundary heat flux functions have been considered. These cases are: square wave, triangular wave and mixed wave heat fluxes. The investigation has been carried for a one dimensional inverse heat conduction problem. Temperature measurements required for the inverse algorithm were generated by using a numerical solution of the direct heat conduction problem employing the three boundary heat flux functions. The most important finding of this investigation is that a robust range of the stabilizing parameter has been found which achieves the desired trade-off between the filter tracking ability and its sensitivity to measurement errors. For all three considered cases, it has been found that there is a common optimal value of the stabilizing parameter at which the estimate bias is minimal. This finding is very important for practical applications since this parameter is unknown practically and this study provides a needed guidance for assuming this parameter. The effect of changing other important parameters

in the online input estimation algorithm on its performance has also been studied in this investigation.

3.1 Introduction

Online input estimation algorithm of the inverse heat conduction problems was derived and developed by Tuan et al. [1]. This algorithm has been used for solving many problems of one and two dimensional linear inverse heat conduction problems [1-3]. It employs two estimators. The first estimator is the Kalman filter by which the temperature state vector is estimated and used to generate the residual innovations. The residual innovations are the difference between the measured temperatures and the estimated temperatures. The second estimator is the real time recursive least squares by which the boundary heat flux is estimated using a linear regression relationship between the residual innovations and the unknown boundary heat flux. The most important feature of this algorithm is the real time estimation since it can be applied to the control of industrial processes.

There are two tuning parameters in this algorithm. The first one is the modeling error, known as the stabilizing parameter, Q , in the Kalman filter estimator, while the second one is the “forgetting factor”, γ , in the real time least squares estimator. Values of Q and γ affect the performance of the input estimation algorithm because they influence the trade-off between the filter tracking ability and its sensitivity to measurement errors. Tuan et al. [2] provided an efficient relationship for the calculation of the forgetting

factor as a ratio of the standard deviation of measurement errors and the residual innovation at each time step.

Therefore, the stabilizing parameter, Q , becomes the only tuning parameter that can be used to provide the desired trade-off. A large value of Q results in a fast response filter at the cost of large sensitivity to measurement error which leads to undesired fluctuations in the heat flux estimates. While a small value might lead to a very slow response filter.

The main objective of this study is to investigate the effect of changing the stabilizing parameter Q on the performance of the online input estimation algorithm. This stabilizing parameter is representing all sources of errors in the model, including: the error due to the dynamical representation of temperature; the error due to the parameters representation and the error due to the discretization of the heat equation. However, these errors are not practically known and therefore a quantifying study of this parameter is essential for designing Kalman filter as part of an online input estimation algorithm.

The optimality of Kalman filter requires that the system should be completely observable. Therefore, the observability of the considered problem has been investigated as well. This is important for the present analysis because the study was intended to investigate the effect of changing only the stabilizing parameter Q on the performance of the algorithm. The performance of the algorithm is measured by the estimate bias of the input (heat flux) given by [4]:

$$B = \left[\frac{1}{n} \sum_{k=1}^n (q_k - \hat{q}_k)^2 \right]^{1/2} \quad (3.1)$$

where q_k and \hat{q}_k are the dimensionless exact and estimated heat flux respectively, and n is the total number of time steps.

To the authors' knowledge, there has been no study in the literature investigating the effect of the stabilizing parameter on the performance of the online input estimation algorithm. Other important parameters requiring systematic assessment of their effect include: the standard deviation of measurement error, time step size, spatial step size, location of the thermocouples, initial assumption of the state estimate error covariance matrix in the Kalman filter estimator, P , as well as the input (heat flux) estimate error covariance matrix in the recursive least squares estimator, Pb . Thus, the present study includes investigating the effects of the above parameters on the estimate bias of the online input estimation algorithm.

3.2 Problem Description

The considered problem is one dimensional geometry shown in Figure 3.1. It is initially at a uniform temperature and then subjected to a transient heat flux on one side while insulated on the other side where the thermocouple is placed.

The governing equation of this problem is the one-dimensional, linear, heat conduction equation:

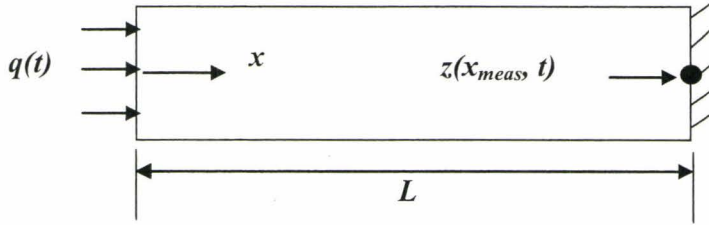


Figure 3.1 One-dimensional linear inverse heat conduction problem.

$$\rho c \frac{\partial T}{\partial t} = k \frac{\partial^2 T}{\partial x^2} \quad 0 \leq x \leq L, \quad t > 0 \quad (3.2)$$

The boundary conditions are given by Equations 3.3 and 3.4

$$q(0, t) = -k \frac{\partial T}{\partial x} \quad t > 0 \quad (3.3)$$

$$\frac{\partial T}{\partial x} = 0 \quad x = L, \quad t > 0 \quad (3.4)$$

The initial condition is

$$T(x, 0) = T_0 \quad 0 \leq x \leq L \quad (3.5)$$

Temperature measurements at $x=L$, are given by:

$$z(L, t) = T(L, t) + v(t) \quad t > 0 \quad (3.6)$$

where $v(t)$ is the measurement errors assumed to be a zero mean Gaussian white noise.

The following parameters have been used to make the above equations in dimensionless form:

$$T^*(x^*, t^*) = \frac{T - T_0}{q_0 L / k}, \quad x^* = \frac{x}{L}, \quad t^* = \frac{\alpha t}{L^2}, \quad \alpha = \frac{k}{\rho c}, \quad q^* = \frac{q}{q_0} \quad (3.7)$$

where q_0 is a nominal value of the surface heat flux, ρ is the density, c is the specific heat, k is the thermal conductivity, α is the thermal diffusivity and t^* is the dimensionless time. After omitting the asterisk (*) for notational convenience, the above equations become:

$$\frac{\partial T}{\partial t} = \frac{\partial^2 T}{\partial x^2} \quad 0 \leq x \leq 1, \quad t > 0 \quad (3.8)$$

$$q(0, t) = -\frac{\partial T}{\partial x} \quad t > 0 \quad (3.9)$$

$$\frac{\partial T}{\partial x} = 0 \quad x = 1, \quad t > 0 \quad (3.10)$$

$$z(1, t) = T(1, t) + v(t) \quad t > 0 \quad (3.11)$$

The spatial derivative of the above heat conduction Equation 3.8 has been discretized by using an explicit central finite difference scheme with a spatial step size Δx to obtain the continuous time state space model [1]:

$$\frac{dT}{dt} = a_1 T(t) + b_1 [q(t) + w(t)] \quad (3.12)$$

where T is $(N \times 1)$ temperature state vector, $w(t)$ is the process noise assumed to be Gaussian white noise of zero mean and independent of the measurement noise $v(t)$, a_1 is $(N \times N)$ coefficient matrix and b_1 is an $(N \times 1)$ input coefficient matrix. For the present problem a_1 and b_1 are given by the following equations:

$$a_1 = \frac{1}{\Delta x^2} \begin{bmatrix} -2 & 2 & 0 & 0 & 0 & \dots & 0 \\ 1 & -2 & 1 & 0 & 0 & \dots & 0 \\ 0 & 1 & -2 & 1 & 0 & \dots & 0 \\ \vdots & & & \ddots & & & \vdots \\ \vdots & & & & \ddots & & \vdots \\ 0 & \dots & & 1 & -2 & 1 & 0 \\ 0 & \dots & & 0 & 1 & -2 & 1 \\ 0 & \dots & & 0 & 0 & 2 & -2 \end{bmatrix} \tag{3.13}$$

$$b_1 = \frac{2}{\Delta x} [1 \ 0 \ 0 \ 0 \ \dots \dots \dots \ 0]^T \tag{3.14}$$

Equation 3.12 is then discretized over time with a time step Δt to get the discrete time state space model that is needed for implementing the Kalman filter. The resulted discrete time state space model is:

$$T(k + 1) = A T(k) + D [q(k) + w(k)] \tag{3.15}$$

and the measurement equation becomes:

$$z(1, k) = T(1, k) + v(k) \tag{3.16}$$

The operators A and D are the state transition matrix and the input matrix, respectively.

These two operators are given by [3]:

$$A = \exp(a_1 \Delta t) \quad (3.17)$$

$$D = \int_{k \Delta t}^{(k+1) \Delta t} \exp[a_1(k+1)\Delta t - \tau] b_1 d\tau \quad (3.18)$$

The variance of the process noise input vector, $w(k)$, and the measurement noise vector, $v(t)$, are given by $E\{w(k)w^T(j)\} = Q\delta_{kj}$ and $E\{v(t)v^T(j)\} = R\delta_{kj} = \sigma^2\delta_{kj}$, respectively. The superscript T refers to the matrix transpose, δ is the Kronecker delta function. The parameter Q is the model error covariance matrix which attempts to compensate any mismatches in the model. It is assumed to be diagonal, and in the present problem is (1x1) matrix used as a stabilizing parameter. The operator R is the measurement noise covariance matrix and σ is the standard deviation of the measurement error. Note that the values of R depend on the accuracy of the measurement sensor.

3.3 Online Input Estimation Algorithm

The online input estimation algorithm consists of two estimators. The Kalman filter estimator and the real time recursive least squares estimator. The Kalman filter estimator employs two Kalman filters. The first one called the hypothetical filter assuming a known boundary heat flux (the input vector) while the second filter is called the mismatch filter

assuming zero boundary heat flux. A relationship between the actual innovation residual of the first filter (the hypothetical Kalman filter) and the theoretical innovation residual of the second filter (the mismatch Kalman filter) is formulated as a function of the boundary heat flux. Then the real time recursive least squares estimator estimates the boundary heat flux that best fits that relationship applying the concept of Minimum Mean Squared Error Estimate (MMSE). The detailed derivation of this algorithm has been presented in sections 2.2 and 2.3. The following is a summary of the equations of each estimator:

Kalman filter equations

State prediction

$$T(k/k-1) = AT(k-1/k-1) \quad (3.19)$$

State covariance prediction

$$P(k/k-1) = AP(k-1/k-1)A^T + DQD^T \quad (3.20)$$

Innovation covariance

$$s(k) = HP(k/k-1)H^T + R \quad (3.21)$$

Filter gain

$$K(k) = P(k/k-1)H^T s^{-1}(k) \quad (3.22)$$

Update state covariance

$$P(k/k) = [I - K(k)H] P(k/k-1) \quad (3.23)$$

Innovation

$$\bar{z}(k) = z(x_{meas}, k) - H T(k/k - 1) \quad (3.24)$$

Update state estimate

$$T(k/k) = T(k/k - 1) + K(k) \bar{z}(k) \quad (3.25)$$

Recursive least squares equations

First sensitivity matrix

$$C(k) = H [A M(k - 1) + I] D \quad (3.26)$$

Second sensitivity matrix

$$M(k) = [I - K(k)H][A M(k - 1) + I] \quad (3.27)$$

Gain

$$Kb(k) = \gamma^{-1} P b(k - 1) C^T(k) * [C(k) \gamma^{-1} P b(k - 1) C^T(k) + s(k)]^{-1} \quad (3.28)$$

Error covariance of the input estimate

$$P b(k) = [I - Kb(k)C(k)] \gamma^{-1} P b(k) \quad (3.29)$$

Input estimation

$$\hat{q}(k) = \hat{q}(k - 1) + Kb(k) * [\bar{z}(k) - C(k)\hat{q}(k - 1)] \quad (3.30)$$

where T is the temperature state vector, A is the state transition matrix given by Equation 3.17, D is the input matrix given by Equation 3.18, H is the measurement matrix given by

[0 0 0 1] for the considered problem where only one thermocouple is used at the insulated boundary, γ is a scalar called the “forgetting factor” which works as a weighting factor in the recursive least square estimator. In the present study, γ , is given by [2]:

$$\gamma(k) = \begin{cases} 1 & |\bar{z}(k)| \leq \sigma \\ \frac{\sigma}{|\bar{z}(k)|} & |\bar{z}(k)| > \sigma \end{cases} \quad (3.31)$$

where σ is the standard deviation of the measurement error (the square root of R), $\bar{z}(k)$ is the innovation (residual) obtained from Kalman filter by Equation 3.24.

3.4 Simulation Cases

An example similar to that presented by Tuan et al. [3] has been used in the present study. The problem uses a linear one dimensional geometry and the sensor is located at the insulated boundary, figure 1. The domain is initially at a uniform temperature and a transient heat flux is applied at $x=0$. Transient temperature “measurements” are taken at $x=L$ by solving the direct heat conduction problem. Then these temperatures are corrupted by Gaussian white noise to simulate the actual temperature measurements. These transient temperature measurements are then used as an input to the inverse problem.

Three different cases have been used to investigate the effects of changing the modeling error, Q , on the estimate bias, B , of the online input estimation algorithm. The first case is a square wave boundary heat flux given by:

$$q(0, t) = \begin{cases} 0 & 0 \leq t \leq 1.05 \\ 1 & 1.05 \leq t \leq 2.1 \\ 0 & 2.1 \leq t \leq 3.2 \end{cases} \quad (3.32)$$

The second case is a triangular wave heat flux given by:

$$q(0, t) = \begin{cases} 0 & 0 \leq t \leq 1 \\ 2 * (t - 1) & 1 \leq t \leq 1.5 \\ -2 * (t - 2) & 1.5 \leq t \leq 2 \\ 0 & 2 \leq t \leq 3.2 \end{cases} \quad (3.33)$$

The third case is a mixed wave heat flux consists of sinusoidal, square, and triangular waves given by:

$$q(0, t) = \begin{cases} 0.5 * (1 + \sin t) & 0 \leq t \leq 3.2 \\ 0 & 3.2 \leq t \leq 4.2 \\ 1 & 4.2 \leq t \leq 5.2 \\ 0 & 5.2 \leq t \leq 6 \\ 0.5 * (t - 6) & 6 \leq t \leq 8 \\ -0.5 * (t - 10) & 8 \leq t \leq 10 \\ 0 & 10 \leq t \leq 10.5 \\ 1 & 10.5 \leq t \leq 11.5 \\ 0 & 11.5 \leq t \leq 12.8 \\ 0.5 * (1 + \sin t) & 12.8 \leq t \leq 15.6 \\ 0 & 15.6 \leq t \leq 16.5 \end{cases} \quad (3.34)$$

3.5 Problem Observability

The observability is a tool that can be used to investigate the internal state of a system by employing any information about the system input and output. The system is assumed to be completely observable if the rank of the observable matrix is equal to the rank of the state vector of the system. That is:

$$\text{Rank}[H^T, (H A)^T, (H A^2)^T, \dots \dots \dots, (H A^{N-1})^T] = N \quad (3.35)$$

In order to check the observability of the considered problem, the spatial domain of the considered problem has been discretized into 11 nodes so that the state vector of the problem is (11x1) and the state transition matrix A is (11x11). A single thermocouple was used, so the measurement matrix H is (1x11). After evaluating the state transition matrix A , using Equation 2.17, and the measurement matrix H , the observability matrix was determined and its rank was calculated and was equal to the dimension of the state vector N . Therefore, the considered problem was found completely observable. It is worth noting that the observability of the problem can be also checked by spectral decomposition of the observability matrix.

3.6 Results and Discussion

For the three cases, the square wave, the triangular wave and the mixed wave heat fluxes, the effect of changing the stabilizing parameter for the range of (0.0001 to 100) has been investigated. The results are shown in Figure 3.2. This figure indicates that there is a common robust range of the stabilizing parameter that gives a good estimate of the time varying boundary heat flux.

For the three cases the same value of the stabilizing parameter ($Q=0.01$) gives a minimum value of the estimate bias as shown in Figure 3.3. In practice the value of the stabilizing parameter is usually unknown. Therefore the above value of stabilizing

parameter could be used for most functions of one dimensional boundary heat flux that need to be estimated by online inverse input estimation methodology.

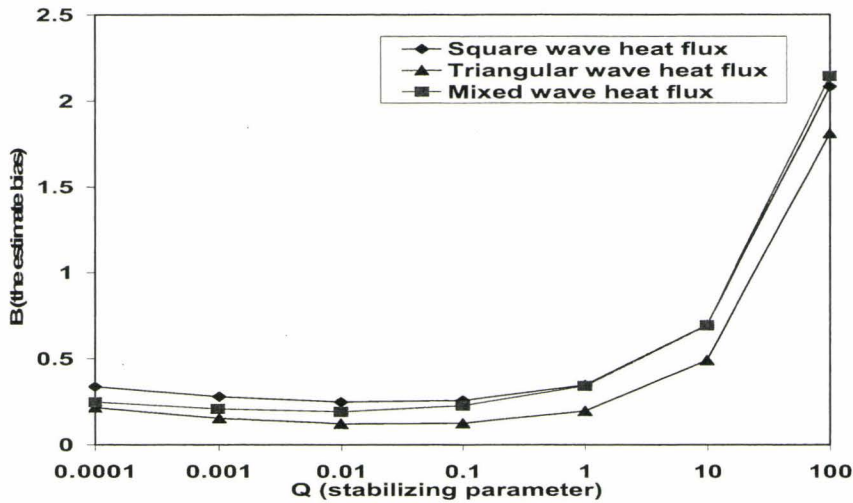


Figure 3.2 The effect of the stabilizing parameter Q on the estimate bias (time step $\Delta t=0.005$ and $R=1E-6$).

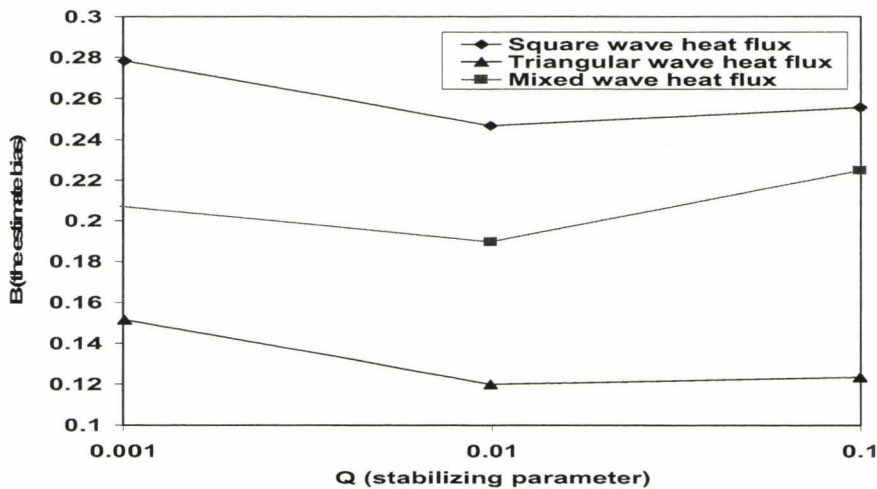


Figure 3.3 The effect of the stabilizing parameter Q on the estimate bias for the robust range.

Figures 3.4, 3.5 and 3.6 show the estimated heat flux for the full simulation time for the robust range of the stabilizing parameter for the three considered cases. It can be seen from line 4 that with a stabilizing parameter ($Q=0.1$) larger than its optimal value, the algorithm responds faster to the time varying heat flux but with a large sensitivity to the measurement error as indicated by the oscillations in the estimates. In contrast, with a smaller value of Q (0.001), the oscillations in the estimates are suppressed but the algorithm responds slower and the tracking time lag is large, line 2. Figure 3.7 and line 3 in Figures 3.4 and 3.5 represent the estimated heat flux corresponding to the optimal value of the stabilizing parameter ($Q = 0.01$) that gives a minimum estimate bias. It is clear that the estimated heat flux has been improved with this value of Q where the oscillations and the tracking time lag are both decreased.

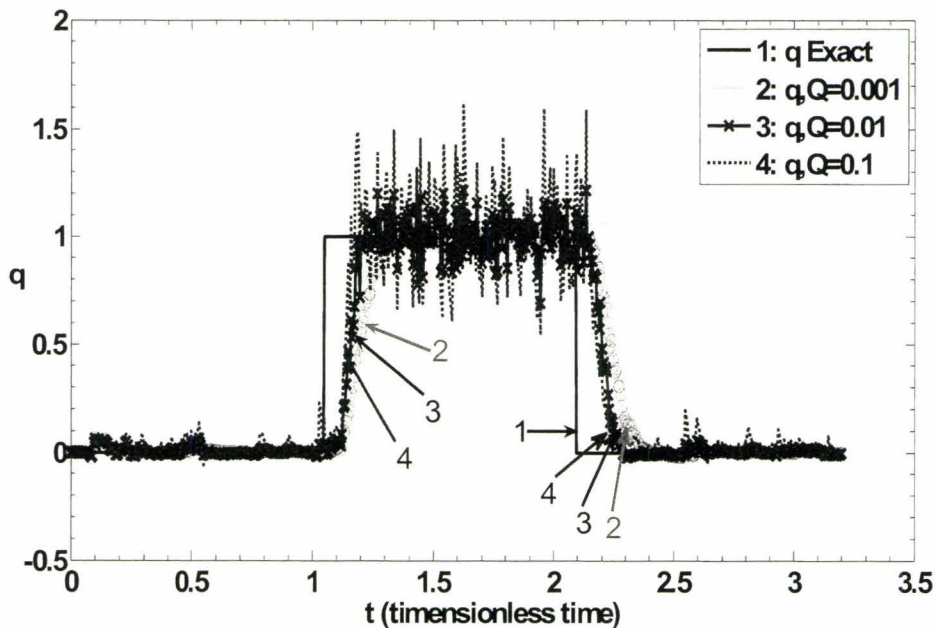


Figure 3.4 The effect of the stabilizing parameter (Q) within the robust range on the square wave estimated heat flux ($\Delta t=0.005$ and $R=1E-6$).

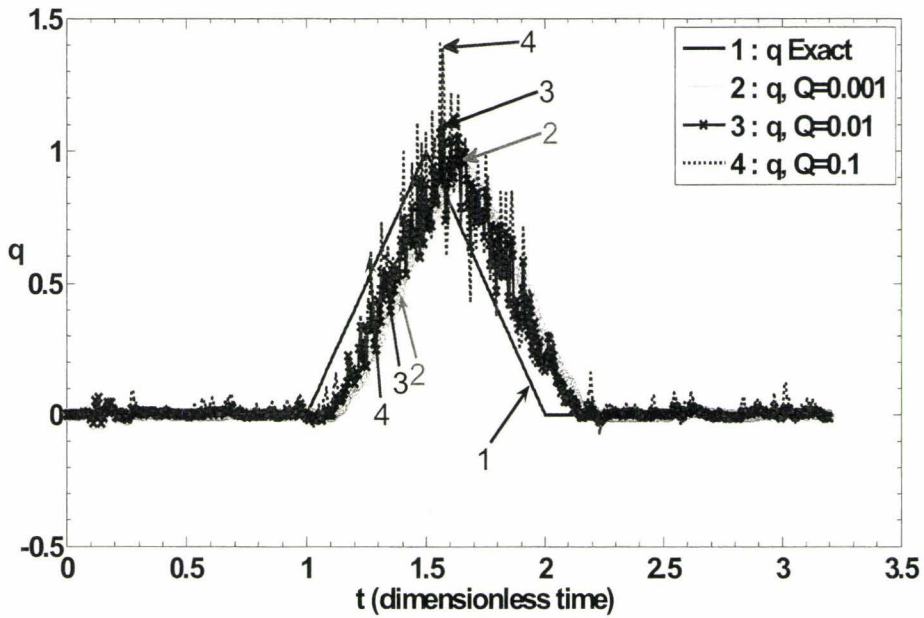


Figure 3.5 The effect of the stabilizing parameter (Q) within the robust range on the triangular wave estimated heat flux ($\Delta t=0.005$ and $R=1E-6$).

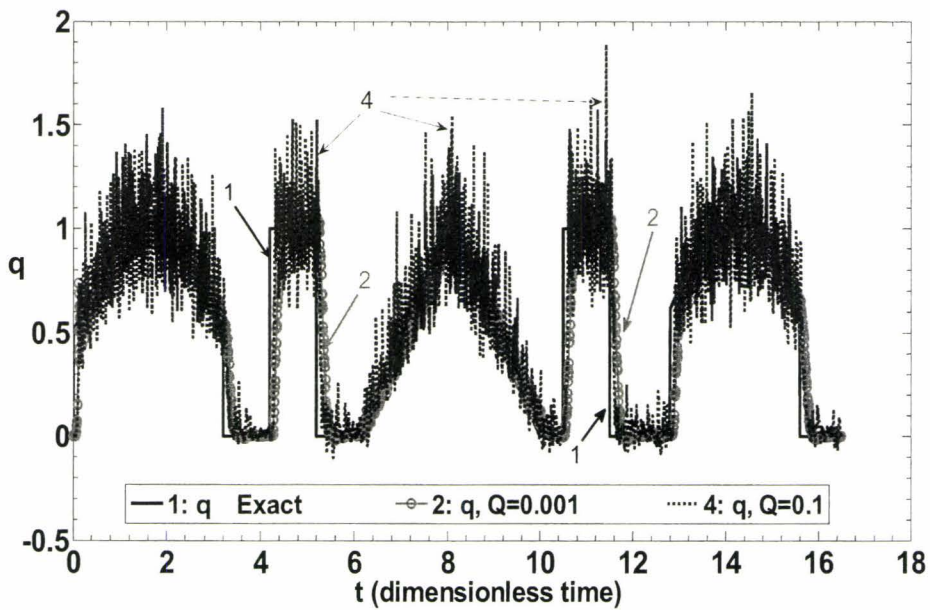


Figure 3.6 The effect of the stabilizing parameter (Q) within the robust range on the mixed wave estimated heat flux ($\Delta t=0.005$ and $R=1E-6$).

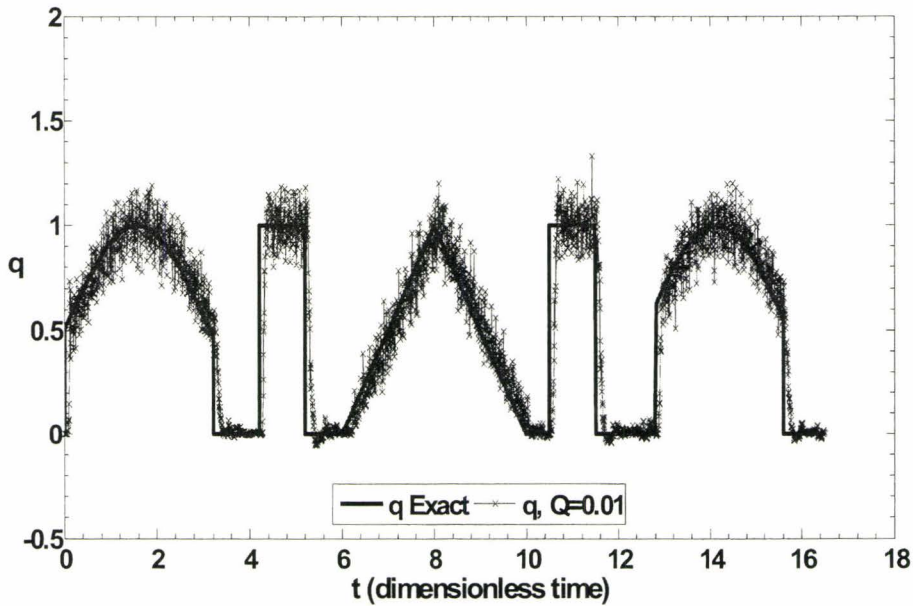


Figure 3.7 A comparison between the exact heat flux and the estimated one with the optimal value of Q ($\Delta t=0.005$ and $R=1E-6$).

The effect of the spatial step size, Δx , and the time step size, Δt , on the estimate bias, B , for the case of square wave heat flux is shown in Figure 3.8. As seen from this figure, the estimate bias of the input estimation algorithm is not affected by the spatial step size. The effect of time step size on the estimate bias has been investigated for the same stabilizing parameter ($Q=0.01$). The result showed that there is a specific time step that gives a minimum estimate bias. However, the same stabilizing parameter satisfies a minimum estimate bias for different time steps. Note that the dimensionless time used in the present study is also known as a dimensionless Fourier number, Equation 3.7.

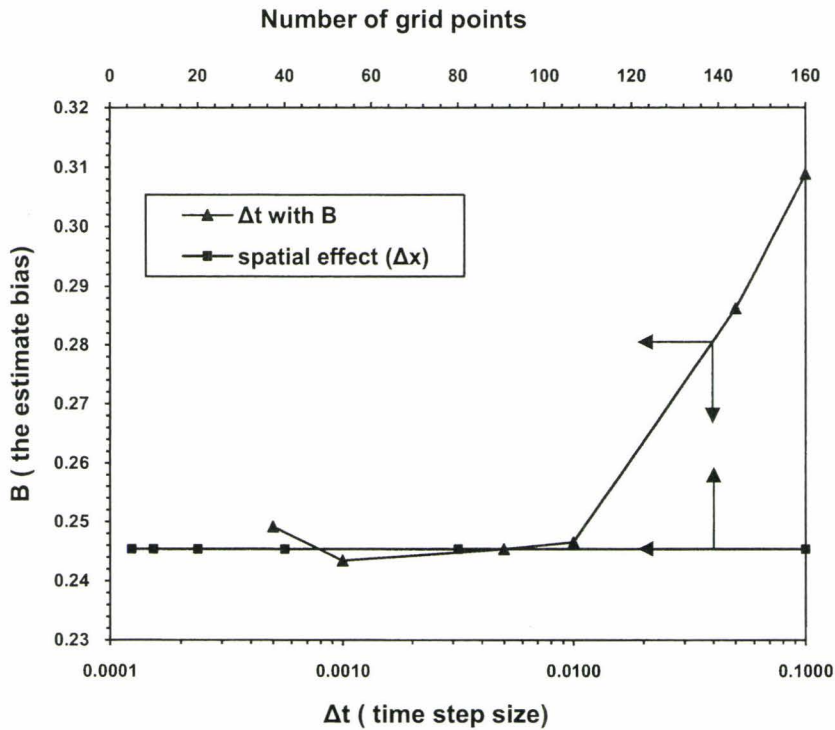


Figure 3.8 The effect of the temporal and the special discretizations on the estimate bias ($Q=0.01$ and $\Delta t=0.005$) for the square wave heat flux.

The curve represents the relationship between the standard deviation of the measurement error, σ , and the estimate bias, B , shown in Figure 3.9 indicates that the estimate bias increases as the standard deviation of the measurement errors increased. The effect of the thermocouple location on the estimate bias is also shown in Figure 3.9. As expected, better estimates are obtained as the thermocouple moves closer to the active boundary.

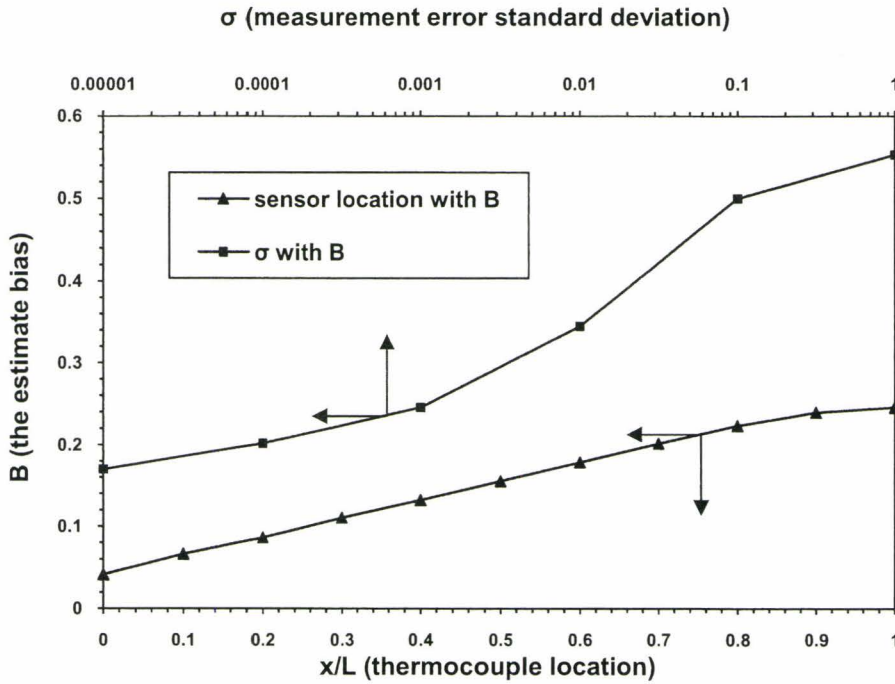


Figure 3.9 The effect of the thermocouple location and the measurement error standard deviation (σ) on the estimate bias ($Q=0.01$ and $\Delta t=0.005$) for the square wave heat flux

Finally, the initial values that are assumed for both the state estimate error covariance matrix in the Kalman filter estimator, P , and the heat flux estimate error covariance matrix in the recursive least squares estimator, Pb , have been investigated. In all his work, Tuan et al. [1-3] assigned very large values for them: 10^{10} for P and 10^8 for Pb and he recommends that the filter will ignore the first few estimates. In this work it is found that there is no effect of these assumptions on the estimator performance at later times. However, large values increase the convergence time to the steady state condition when the state covariance matrix coincides with its prediction leading to an optimal value for the filter gain, $K(k)$, Equation 3.22. Moreover, large values cause the algorithm

estimates to violate the physical law of energy conservation. Therefore, these values can be reasonably assumed based on the prior information of the initial conditions of the given problem.

3.7 Conclusions

In this study, three different simulation examples have been used to study the effect of changing the modeling error in the state equation on the estimate bias of the online input estimation algorithm in its application to the one dimensional inverse heat conduction problems. The results showed that there is a common robust range for stabilizing parameter (modeling error) that can be used to estimate efficiently various cases of the unknown input boundary heat flux in one-dimensional IHCPs.

The results of the square wave example showed that there is an optimal time step that gives a minimum estimate bias. Also, the algorithm performance is not very sensitive to the spatial step size used in discretizing the heat conduction equation. The thermocouple should be located very close to the unknown heat flux to enhance the estimate. Finally reasonable values for both P and Pb are recommended. These values can be assumed based on the prior information of the initial conditions of the given problem.

3.8 Acknowledgements

This work is supported and funded by the Sciences and Engineering Research Council of Canada (NSERC), the Centre for Materials and Manufacturing/Ontario Centres of Excellence (OCE-CMM), and the OCE-McMaster thermal processing Consortium.

3.9 References

1. Tuan, P. C., Ji, C. C., Fong, L. W., Huang, W. T. , An Input Estimation Approach to On-line Two-Dimensional Inverse Heat Conduction Problem, Numerical Heat Transfer, Part B, Vol. 29, pp. 345-363, 1996.
2. Tuan, P.C., and Ju, M.C., The Validation of the Robust Input Estimation Approach to Two-Dimensional Inverse Heat Conduction Problems, Numerical Heat Transfer, Part B, Vol. 37, pp. 247-265, 2000.
3. Tuan, P.C., Lee, S.H., and Hou, W.T., An Efficient On-line Thermal Input Estimation Method Using Kalman Filter and recursive Least Square Algorithm, Inverse Problems in Eng., 5, PP. 309-333. 1997.
4. Beck, J. V., Blackwell, B., and St. Clair, C. R., Jr, Inverse heat conduction-III Posed Problems, John Wiley, New York. 1985.

3.10 Supplementary Material

In order to apply a Kalman filter to the inverse heat conduction problems, the heat conduction equation should be converted into the state space representation. Two main approaches can be used.

In the first approach, the only spatial derivative of the heat conduction equation is discretized using a central finite difference scheme to get the Continuous Time State Space Model (CTSSM), Equation 3.12. Then, the continuous time state space heat equation is integrated with respect to time to obtain the discrete time state space model,

Equation 3.15, which is required for applying the Kalman filter. This approach has been used in the previous article of this chapter.

In the second approach the discrete time state space model of the heat equation is obtained directly by discretizing both time and spatial derivatives. Three different discretizing schemes have been used to see their effect on the performance of the input estimation algorithm. These schemes are explicit, implicit and Crank-Nicholson.

The resulted discrete time state space model of the heat equation using the explicit scheme, where the spatial derivative is discretized at n time level, is:

$$T(k + 1) = a_2 T(k) + b_2 [q(k) + w(k)] \quad (3.36)$$

Here the state transition matrix $A = a_2$ and the input matrix $D = b_2$ and the time step Δt is embedded in both a_2 and b_2 .

The discrete time state space model of the heat equation using the implicit scheme, where the spatial derivative is discretized at $n+1$ time level, is:

$$a_3 T(k + 1) = T(k) + b_3 [q(k) + w(k)] \quad (3.37)$$

Then

$$T(k + 1) = a_3^{-1} T(k) + a_3^{-1} b_3 [q(k) + w(k)] \quad (3.38)$$

So, here the state transition matrix $A = a_3^{-1}$ and the input matrix $D = a_3^{-1} b_3$.

Finally, the Crank-Nicholson finite difference discretization scheme has been used to obtain the discrete time state space model of the heat equation and the resulted equation is:

$$a_4 T(k+1) = a_5 T(k) + b_4 [q(k) + w(k)] \quad (3.39)$$

$$a_4 T(k+1) = a_4^{-1} a_5 T(k) + a_4^{-1} b_4 [q(k) + w(k)] \quad (3.40)$$

where the state transition matrix $A = a_4^{-1} a_5$ and the input matrix $D = a_4^{-1} b_4$.

The above four cases that include, the continuous time state space model (CTSSM), explicit, implicit and Crank-Nicholson schemes have been applied to the problem of one dimensional inverse heat conduction problem described in the first part of this chapter employing the square wave boundary heat flux introduced previously. Table 3.1 shows the results of this investigation. For the first approach (CTSSM), the explicit and the Crank-Nicholson schemes the estimate bias is 0.2442 while it is 0.2347 for the implicit scheme. Since the estimate bias is almost same for the above approaches thus there is a very slight effect for the use of these different approaches on the estimate bias of the input estimation algorithm of the linear inverse heat conduction problems. However, the first approach (CTSSM), implicit and Crank-Nicholson are preferable than the explicit scheme because they are unconditionally stable. Furthermore, the CTSSM is almost 38% faster than the other methods where their executing times are almost the same.

Approach	Estimate Bias	Stability	Executing time
CTSSM	0.2442	Unconditionally stable	Faster (38% less)
Explicit scheme	0.2442	Conditionally stable	Almost Same executing time
Implicit scheme	0.2432	Unconditionally stable	
Crank-Nicholson	0.2442	Unconditionally stable	

Table 3.1 The results of using different discretization schemes.

***AN EFFICIENT NUMERICAL ALGORITHM FOR THE
PREDICTION OF THERMAL AND MICROSTRUCTURE
FIELDS DURING QUENCHING OF STEEL RODS***

CHAPTER 4

Chapter Four Preface

This work has been previously published in:

- Ali, S. K., Hamed, M. S. and Lightstone, M.F., An Efficient Numerical Algorithm for the Prediction of Thermal and Microstructure Fields during Quenching of Steel Rods, Journal of ASTM International, Vol. 5, Issue 10, 2008.

Permission has been granted by the publisher to include this material in this thesis.

An Efficient Numerical Algorithm for the Prediction of Thermal and Microstructure Fields during Quenching of Steel Rods

Abstract

This paper presents a new, more efficient numerical algorithm that has been developed to predict thermal and microstructure fields during quenching of steel rods. The present algorithm solves the full nonlinear heat conduction equation using a central finite-difference scheme coupled with a fourth-order Runge-Kutta nonlinear solver. Numerical results, obtained using the present algorithm, have been validated using experimental data and numerical results available in the literature. In addition to its accurate predictions, the present algorithm does not require iteration; hence, it is computationally more efficient than previous numerical algorithms.

Keywords

Steels quenching, phase transformation, heat treatment, numerical algorithm

Nomenclature

A = Temperature dependent coefficient, Equation 4.18

B = Temperature dependent coefficient, Equation 4.18

C_p = Specific heat

F = Volume fraction

H = Enthalpy

h = Heat transfer coefficient

k = Thermal conductivity

Nr = total number of spatial nodal points

\dot{Q} = Latent heat of the phase transformation

q_{out} = Heat flux at the rod's surface

R = Outer radius of the rod

r = Radius of the rod

T = Temperature

t = Time

Greek Symbols

α_M = Koistinen and Marburger coefficient, Equation 4.24

ρ = Density

τ_f = Phase transformation starting time

τ_s = Phase transformation ending time

Subscripts

a = Austenite

M = Martensite

m = Any phase

p = Pearlite

4.1 Introduction

Quenching is an essential heat treating process for achieving high levels of hardness and toughness in metal components. Quenching is also a sensitive process that sometimes results in significant distortion and cracking problems. Our ability to predict and, hopefully, to limit unwanted levels of distortion, cracking, and residual stresses depends, to a large extent, on accurate predictions of thermal and microstructure fields during quenching.

Quenching of steel is even more complex due to phase transformation that occurs during the quenching process. During the phase transformation process, latent heat is released which alters the thermal field of the steel. The phase transformation in steel depends on the thermal field developed during quenching. Therefore, different types of steel microstructures can be obtained by using different quenching cooling rates.

Modeling of the thermal field and the accompanying phase transformation and mechanical properties has attracted a lot of attention of many researchers [1-9]. Two types of modeling have been used. In the first type, the evolution of the microstructure is uncoupled from the thermal field. The disadvantage of this model is that it provides little information about the actual microstructure [1,2]. In the second type of modeling, the microstructure evolution is coupled with the thermal field [5-9]. This modeling technique is preferred by many researchers since it provides detailed information about phase transformation and its evolution with respect to the developed thermal field.

Inoue and Tanaka [5] used the finite element method to simulate the temperature history, the microstructure, and the residual stresses of a 0.43 % carbon steel circular

cylinder quenched by water. The thermal expansion coefficient was used to model the microstructure transformation during quenching. Therefore, the microstructure phase transformation was uncoupled from the temperature and stress fields calculations in this model. The drawback of this model is that many simplifications were assumed to determine the microstructure of the quenched part. These simplifications reduce the information that can be obtained from this model about the microstructure. In addition to that, the heat generation due to phase transformation was neglected in this investigation.

Subsequently, the above model has been modified and improved over 20 years by Inoue et al. [6,7]. They proposed and implemented the metallo-thermomechanical theory to develop a finite element code known as HEARTS. In this code the phase transformation calculations were coupled to the thermal and stress fields calculations. This code was used to simulate the quenching process of two- and three- dimensional engineering problems.

Fernandes et al. [8] developed a mathematical model coupling the evolution of phase transformation with the temperature field during quenching of a 1080 carbon steel cylinder. The diffusional transformation has been divided into incubation and growth periods which were treated separately. The incubation period was treated by using the Scheil's additivity principle [3], while the growth period was modeled by applying the Johnson-Mehl-Avrami formula [1,2]. The diffusionless transformation was modeled by using the Koistinen and Marburger law [4]. The temperature field was calculated by solving the heat conduction equation using an implicit finite-difference algorithm. The

heat generated due to phase transformation appears in the heat equation as a heat source term. Numerical results of this study were in good agreement with the experimental data.

Denis et al. [10] presented a mathematical model for predicting the phase transformations of a 1042 carbon steel cylinder during rapid heating and cooling. The model was used to describe the kinetics of austenization during heating, the austenite carbon content and grain size at the end of heating, and the kinetics of the transformations during cooling. The rule of additivity along with Johnson-Mehl-Avrami model was used for the microstructure transformation calculations. This model has been applied to a cylindrical specimen that was subjected to high thermal gradients. The comparison with the experimental data showed that this model was good in describing the heating process. However, there was deviation between the numerical results and the experimental data during the cooling process.

Wang et al. [11] used a two-dimensional finite element algorithm to simulate quenching of 1080 carbon steel cylinders undergoing nonisothermal transformations and exposed to a temperature dependent convective heat transfer coefficient at the boundary. Temperature dependent thermophysical properties were used. The model was also applied to simulate quenching of a 2024 aluminum component. This algorithm has been validated later against the experimental data published by the same authors [12]. The transient temperatures predicted by the numerical simulation were in good agreement with the corresponding measurements.

Woodard et al. [13] used a finite element algorithm to analyze the temperature and the microstructure of 1080 carbon steel cylinders during quenching. The finite

element procedure was very similar to that used by Wang et al. [11]. However, this investigation was focused on investigating the effect of including heat generation due to phase transformation on the thermal field and on the microstructure of the quenched parts. The model was applied to predict the temperature and microstructure distributions as well as the hardness of 1080 steel cylinders quenched using three different quenchants, water and two synthetic polymers. The results indicated the importance of including the effect of heat generation on the predicted microstructures.

Homberg [14] developed a mathematical model to simulate the Jominy end-quench test used in constructing continuous cooling curves. This model uses Scheil's additivity rule with the Johnson-Mehl-Avrami equation for modeling the diffusional transformation while it replaces the Koistinen-Marburger formula with a rate law procedure. This martensitic rate law takes into account the irreversibility of the diffusionless process. However, the martensitic rate law was computationally expensive. The model was applied for plain carbon steel C1080 and C100. The numerical results showed that the Johnson-Mehl-Avrami equation describes well the austenite to pearlite transformation after the incubation period.

Recently Kang and Im [15] developed a three-dimensional finite element algorithm to predict the volume fraction of multi phases generated during quenching of a 1080 carbon steel cylinder. This algorithm was also used to simulate quenching of low carbon steel mechanical parts such as differential bevel gear and cam lobe. In this model, the generation of latent heat due to phase transformation has been considered. The additivity rule and the Johnson-Mehl-Avrami equation have been applied for the

diffusional transformation while Koistinen and Marburger's equation has been used for the martensitic diffusionless transformation. The validity and reliability of the numerical results of the thermal and phase transformation fields were compared with the experimental data of Wang et al. [12].

To the best of the authors' knowledge, all previous work in the literature treated the nonlinearity of the problem by using explicit linearization where a linear form of the heat equation is used. The dependency of the thermophysical properties on the temperature were handled by explicit linearization with an iterative solution procedure. In contrast, the present methodology has adapted a new nonlinear solution technique by using a complete nonlinear form of the heat conduction equation. The complete equation is solved using a fourth-order Runge-Kutta nonlinear solution technique coupled with a central finite difference scheme. The thermophysical properties are taken as a function of the current temperature that is being solved. This approach removes the need for iterations; hence, it is more efficient computationally. The present algorithm has been applied and tested to simulate the quenching problem of an infinite 1080 carbon steel rod.

4.2 Computational Model

In order to numerically calculate the deformation, residual stresses, and surface hardness during quenching of a heat treated part, the thermal field and the microstructure of all present phases must be determined first.

The algorithm of simulating a quenching process consists of the following three major elements: first, calculation of the thermal field given the convective heat transfer

coefficient, second, calculation of the microstructure distribution by using data from the Time-Temperature-Transformation (TTT) diagram of the material and, finally, calculation of the mechanical properties of the processed part including: deformation, residual stresses, and surface hardness. It is worth noting here that the first two steps are coupled through heat generation arising from the microstructure chemistry (latent heat of formation).

In the present study only the first two steps are considered. The thermal field is obtained by solving the nonlinear heat conduction equation using a fourth-order Runge-Kutta method. The Johnson-Mehl-Avrami equation has been used to model the diffusional transformation [1], while the diffusionless transformation has been modeled by employing the Koistinen and Marburger's equation [4]. The details of the computational procedure will be given in the next section.

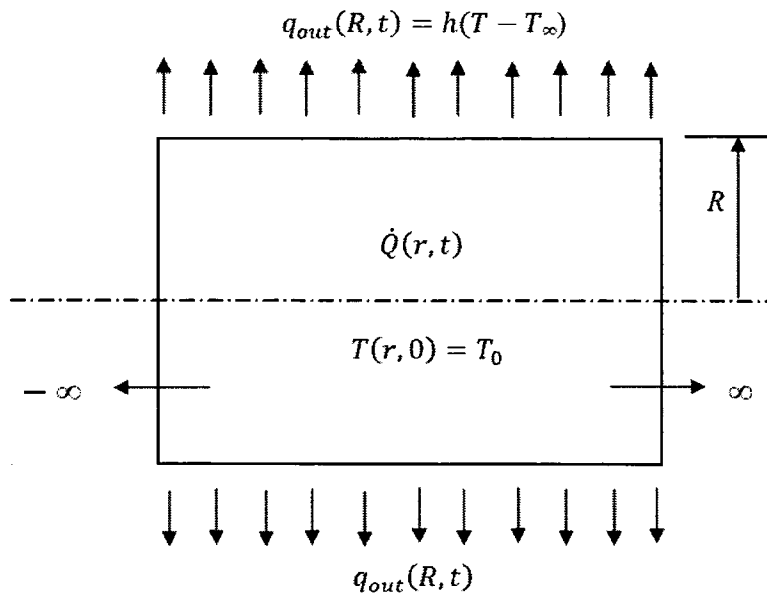


Figure 4.1 One-dimensional quenching problem.

4.2.1 The Thermal Field Model

Consider an infinite rod initially at a uniform temperature T_0 as shown in Figure 4.1. This rod is quenched by exposing it to a coolant at a temperature T_∞ .

The mathematical model governing the thermal field inside the infinite rod is the following one-dimensional nonlinear heat conduction equation:

$$\rho(T)C_p(T)\frac{\partial T}{\partial t} = \frac{1}{r}\frac{\partial}{\partial r}\left(k(T)r\frac{\partial T}{\partial r}\right) + \dot{Q}(r, t) \quad (4.1)$$

where $\rho(T)$ is the density, $C_p(T)$ is the specific heat, $k(T)$ is the thermal conductivity and $\dot{Q}(r, t)$ is the latent heat generated due to the phase transformation.

The infinite rod is subjected to the following set of boundary and initial conditions:

At $r=0$

$$\frac{\partial T(0, t)}{\partial r} = 0 \quad (4.2)$$

At $r=R$

$$q_{out}(R, t) = -k(T)\frac{\partial T}{\partial r} = h(T(R, t) - T_\infty) \quad (4.3)$$

$$T(r, 0) = T_0 \quad (4.4)$$

$$\dot{Q}(r, 0) = 0 \quad (4.5)$$

where R is the outer radius of the rod, h is a known heat transfer coefficient, and $T(R,t)$ is the temperature at the rod surface.

After spatial differentiation, the temperature time derivative in Equation 4.1 can be written as follows:

$$\frac{\partial T}{\partial t} = \frac{k(T)}{\rho(T)C_p(T)} \frac{\partial^2 T}{\partial r^2} + \frac{1}{\rho(T)C_p(T)} \frac{k(T)}{r} \frac{\partial T}{\partial r} + \frac{\partial k(T)}{\partial T} \frac{1}{\rho(T)C_p(T)} \left\{ \frac{\partial T}{\partial r} \right\}^2 + \frac{\dot{Q}(r,t)}{\rho(T)C_p(T)} \quad (4.6)$$

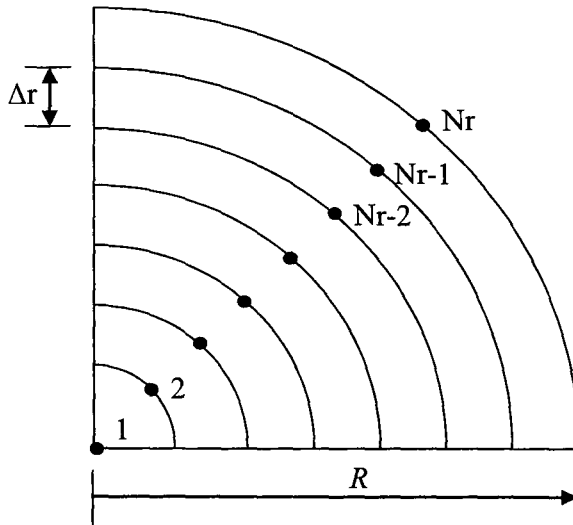


Figure 4.2 The computational domain and the uniformly spaced nodal points.

Using central finite difference approximations to discretize the spatial derivatives, Equation 4.6 can be written as follows:

$$\begin{aligned}
\frac{\partial T(i, t)}{\partial t} &= \frac{k(T)}{\rho(T)C_p(T)} \left\{ \frac{T_{i+1} - 2T_i + T_{i-1}}{\Delta r^2} \right\} + \frac{k(T)}{\rho(T)C_p(T)} \frac{1}{r_i} \left\{ \frac{T_{i+1} - T_{i-1}}{2\Delta r} \right\} \\
&+ \frac{1}{\rho(T)C_p(T)} \frac{\partial k(T)}{\partial T} \left\{ \frac{T_{i+1} - T_{i-1}}{2\Delta r} \right\}^2 + \frac{\dot{Q}(i, t)}{\rho(T)C_p(T)} \quad \text{for } i \\
&= 1, 2, \dots, Nr
\end{aligned} \tag{4.7}$$

where Nr is the total number of spatial nodal points shown in Figure 4.2, and Δr is radial step size.

Applying the boundary condition, Equation 4.2, at the center of the rod ($i=1$) in Equation 4.7 yields:

$$\frac{\partial T(1, t)}{\partial t} = \frac{2k(T)}{\rho(T)C_p(T)} \left\{ \frac{T_2 - T_1}{\Delta r^2} \right\} + \frac{\dot{Q}(1, t)}{\rho(T)C_p(T)} \tag{4.8}$$

Equation 4.7 at the last node (the node at the surface $i=Nr$) becomes:

$$\begin{aligned}
\frac{\partial T(Nr, t)}{\partial t} &= \frac{k(T)}{\rho(T)C_p(T)} \left\{ \frac{T_{Nr+1} - 2T_{Nr} + T_{Nr-1}}{\Delta r^2} \right\} + \frac{k(T)}{\rho(T)C_p(T)} \frac{1}{r_{Nr}} \left\{ \frac{T_{Nr+1} - T_{Nr-1}}{2\Delta r} \right\} \\
&+ \frac{1}{\rho(T)C_p(T)} \frac{\partial k(T)}{\partial T} \left\{ \frac{T_{Nr+1} - T_{Nr-1}}{2\Delta r} \right\}^2 + \frac{\dot{Q}(Nr, t)}{\rho(T)C_p(T)}
\end{aligned} \tag{4.9}$$

Discretizing the boundary condition at the surface of the rod ($i=Nr$) using a central finite expression yields:

$$T_{Nr+1} = T_{Nr-1} - \frac{2\Delta r}{k(T)} q_{out} \quad (4.10)$$

Substituting Equation 4.10 in Equation 4.9 yields:

$$\begin{aligned} \frac{\partial T(Nr, t)}{\partial t} = & \frac{2k(T)}{\rho(T)C_p(T)} \left\{ \frac{T_{Nr-1} - T_{Nr}}{\Delta r^2} \right\} + \frac{2q_{out}}{\rho(T)C_p(T)} \frac{1}{\Delta r} - \frac{1}{r_{Nr}} \frac{q_{out}}{\rho(T)C_p(T)} \\ & + \frac{1}{\rho(T)C_p(T)} \frac{\partial k(T)}{\partial T} \left\{ \frac{q_{out}}{k(T)} \right\}^2 + \frac{\dot{Q}(Nr, t)}{\rho(T)C_p(T)} \end{aligned} \quad (4.11)$$

The system of equations, Equations 4.7, 4.8 and 4.11 is solved using the fourth-order Runge-Kutta nonlinear solver method [16].

The thermophysical properties in the above equations were treated as a function of both the temperature and the volume fraction of the present phases because the microstructure of the quenched steel is composed of various phases depending on the thermal field. Therefore, the mixture rule was adapted to calculate the thermophysical properties of the material, where any property (P) at any point inside the solid is assumed to be a linear combination of the corresponding property of each phase multiplied by the volume fraction of that phase, as given by the following equation:

$$P(F_m, T) = \sum_m^n P_m(T) F_m \quad (4.12)$$

where P could be any property such as the density, the specific heat, or the thermal conductivity, n is the number of the present phases, and F_m is the volume fraction of the m th phase.

The heat generation during phase transformation is calculated by the following equation:

$$\dot{Q}(i, t) = \sum_m \Delta H_m(T) \frac{\Delta F_m}{\Delta t} \quad (4.13)$$

where $\Delta H_m(T)$ is the temperature dependent enthalpy change due to the phase transformation. Depending on the type of phase transformation, this enthalpy change can be calculated for 1080 carbon steel from the following equations:

1. For austenite to pearlite transformation [13, 15]:

$$\Delta H_{a-p} (J/m^3) = 1.56 \times 10^9 - 1.5 \times 10^6 T \quad (4.14)$$

or

$$\Delta H_{a-p} (J/m^3) = (953 + 0.409T - 0.0012T^2) \times 10^6 \quad (4.15)$$

2. For austenite to martensite transformation [13]:

$$\Delta H_{a-M} (J/m^3) = 640 \times 10^6 \quad (4.16)$$

4.2.2 The Phase Transformation Model

There are two main types of transformation that could occur during steel quenching. The first one is a diffusional transformation while the second one is a diffusionless transformation. The transformation from austenite to pearlite is an example of the first type. This transformation takes place in two stages: the first stage is the nucleation process, also known as the incubation period, while the second stage is the growth process. The nucleation stage is modeled using the Scheil's additivity rule where the cooling rate is divided into isothermal intervals corresponding to the number of time steps on the Time-Temperature-Transformation (TTT) diagram shown in Figure 4.3. For each time step j , $(\Delta t_j / \tau_{sj})$ is calculated and summed:

$$\sum_j (\Delta t_j / \tau_{sj}) \quad (4.17)$$

When this summation equals one, the incubation period is considered complete [15]. The quantity τ_{sj} is the transformation starting time taken from the TTT diagram which depends on the temperature.

The growth stage of the diffusional transformation is modeled by using the following Johnson-Mehl-Avrami equation [15]:

$$F_m(t) = 1 - \exp[-A(T) \times t_j^{B(T)}] \quad (4.18)$$

where $F_m(t)$ is the volume fraction of phase m , $A(T)$ and $B(T)$ are temperature dependent parameters which can be calculated from the isothermal TTT diagram, t_j is the

transformation time representing the time elapsed from the beginning of the diffusional transformation.

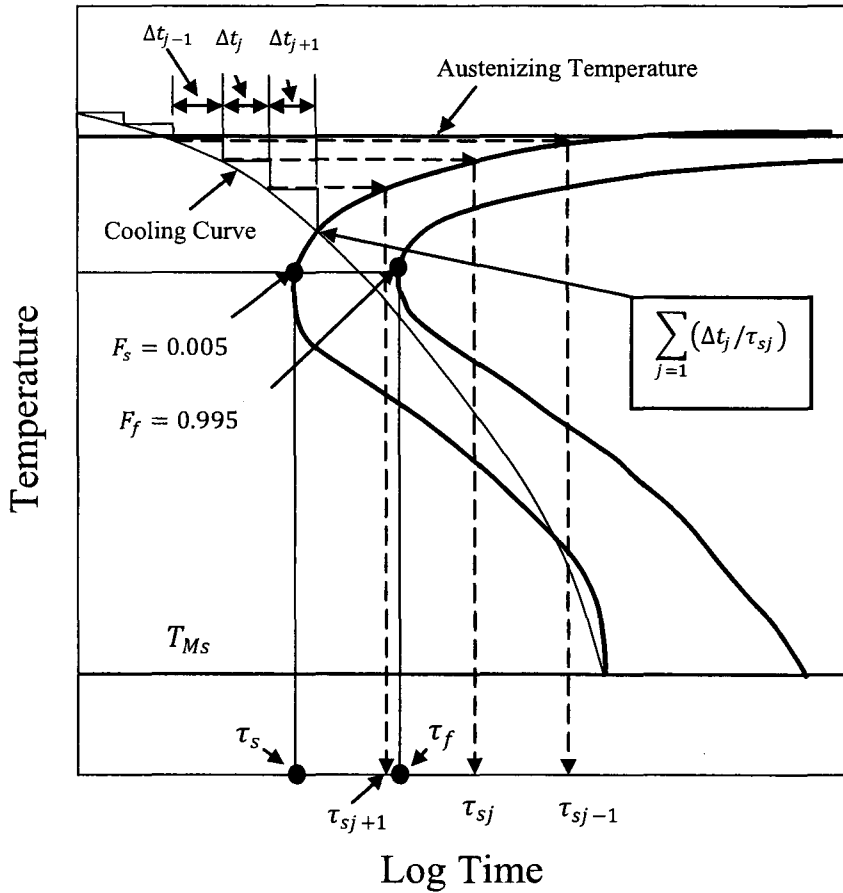


Figure 4.3 Schematic representation of the Scheil's additivity principle and the calculation of the temperature dependent parameters $A(T)$ and $B(T)$ from TTT diagram.

The above equation is developed primarily for isothermal transformation. However, it is proven that it can be used efficiently for nonisothermal transformations if

the two parameters $A(T)$ and $B(T)$ are updated at each time step [8-15]. These parameters can be updated for the austenite to pearlite transformation using the TTT diagram.

The two C-curves on the TTT diagram, Figure 4.3, represent the start and the end of the diffusional transformation (austenite to pearlite). The first curve on the right is assumed to be at pearlite volume fraction equals to 0.005, F_s , while the second curve corresponds to pearlite volume fraction, F_f , equals to 0.995. At each time step, the starting time of diffusional transformation, $\tau_s(T)$, and the ending time $\tau_f(T)$ are taken from the TTT diagram.

Using the above values of F_s and F_f , Equation 4.18 becomes:

$$F_s = 0.005 = 1 - \exp(-A(T) * \tau_s^{B(T)}) \quad (4.19)$$

$$F_f = 0.995 = 1 - \exp(-A(T) * \tau_f^{B(T)}) \quad (4.20)$$

The above two equations are solved at each time step for the two parameters $A(T)$ and $B(T)$ and the solution is given by the following two equations:

$$B(T) = \frac{\ln\{\ln(0.995)\} - \ln\{\ln(0.005)\}}{\ln\{\tau_s(T)\} - \ln\{\tau_f(T)\}} \quad (4.21)$$

$$A(T) = -\ln(0.995) \tau_s^{-B(T)} \quad (4.22)$$

The transformation time t_j in Equation 4.18 is calculated from the following equation:

$$t_j = \Delta t_j + \left[\frac{\ln \left\{ \frac{1}{1 - F_m^{(j-1)}} \right\}}{A(T)} \right]^{1/B(T)} \quad (4.23)$$

where $F_m^{(j-1)}$ is the volume fraction of the m th phase present at the previous time step, $j-1$, and Δt_j is the current time step.

The diffusionless transformation of austenite to martensite is only function of temperature. This transformation is calculated using the following Koistinen-Marburger formula [15]:

$$F_M(T) = [1 - \exp\{-\alpha_M(T_{MS} - T)\}] \left(1 - \sum_m F_m \right) \quad (4.24)$$

where $F_M(T)$ is the volume fraction of the martensite, F_m is the volume fraction of the other phases, α_M is the Koistinen and Marburger coefficient and it is equal to $1.1 \times 10^{-2} K^{-1}$ for 1080 carbon steel, T_{MS} is the martensitic transformation start temperature. Since pearlite, ferrite, and bainite cannot be transferred to martensite, the equation is therefore multiplied by $(1 - \sum_m F_m)$.

4.3 Structure of the Numerical Algorithm

The structure of the present numerical algorithm is shown in Fig. 4.4. The algorithm is initialized by entering the following input data: the initial conditions, the physical

geometry, and data taken from the isothermal Time-Temperature-Transformation (TTT) diagram of the material. The thermal field is then calculated using a fourth order Runge-Kutta nonlinear solver. For each time step, the temperature time derivative (slopes) is calculated at four locations in time [16]. Then the temperature is calculated as a weighted average of the temperatures estimated based on the calculated slopes of the previous step.

After calculating the thermal field, calculation of the microstructure transformations starts by applying the additivity rule, Equation 4.17, incorporating the data from the TTT diagram to calculate the nucleation period. Once the nucleation period is completed, the growth transformation is calculated by using the Johnson-Mehl-Avrami equation, Equation 4.18. In this study only the austenite to pearlite transformation is considered and is assumed to only take place above the nose of the TTT diagram [11].

The temperature of each node is compared with the martensitic transformation starting temperature (T_{MS}), Figure 4.3, and if it is smaller, the martensite volume fraction is calculated using the Koistinen-Marburger formula, Equation 4.24.

In the previous works [8-15], at each time step the thermal field calculations are carried out assuming no heat generation due to the phase transformation primarily. At the same time step, upon completing the microstructure calculation and if there is heat generation due to the phase transformation, this heat generation is added to the heat equation and the calculation of the thermal field is repeated along with the microstructure calculation. This iterative solution procedure continues until a specific convergence criterion is satisfied. Furthermore, the nonlinearity due to the thermophysical properties being temperature dependant is handled by explicit linearization. These thermophysical

properties are calculated based on the temperatures of the previous time step and then updated at each iteration level until convergence is achieved.

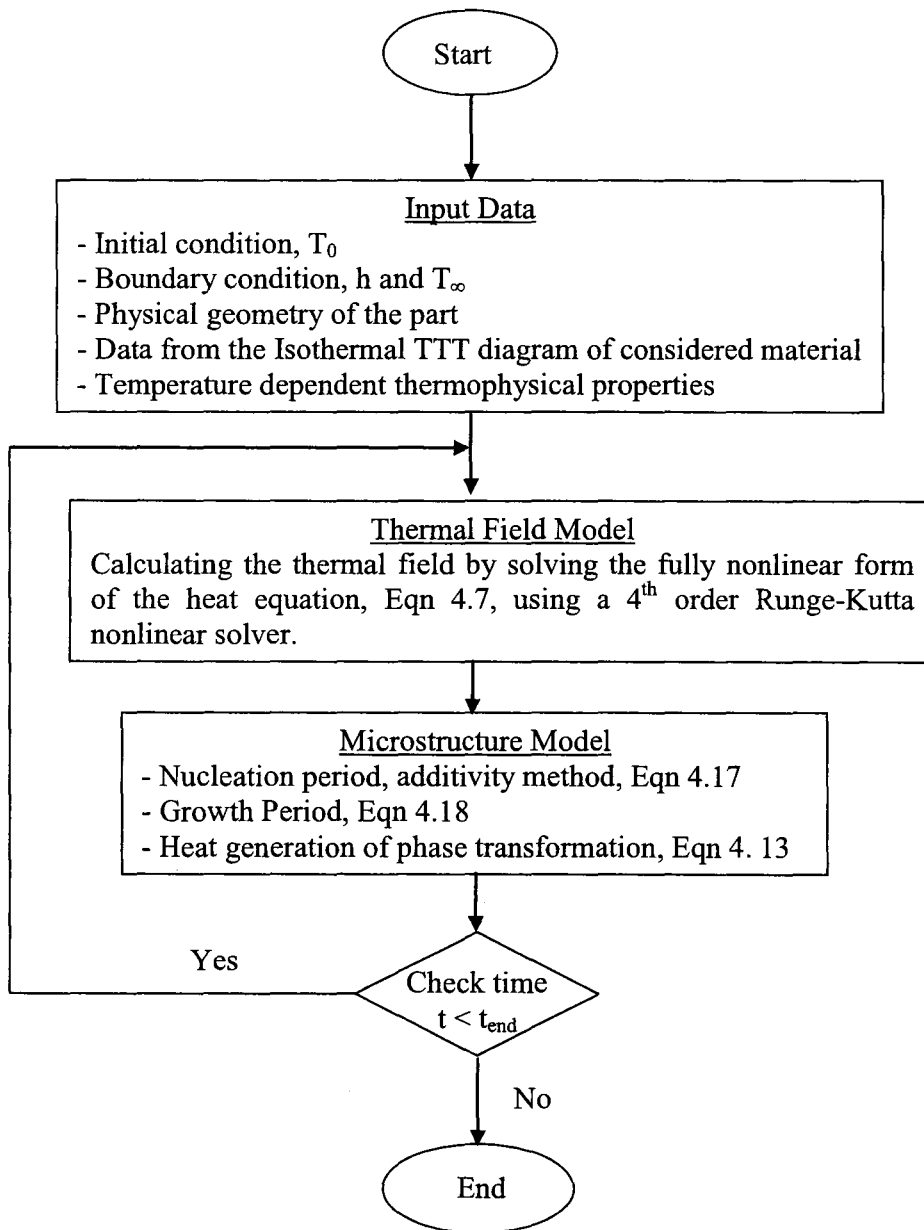


Figure 4.4 Simplified flow chart of the computational procedure of the present algorithm.

The computational procedure of the previous models is very time consuming, for example, the model developed by Kang and Im [15] was applied to simulate the same problem considered in this study. In his study, Kang modeled only 1/12 of the physical geometry of the problem in order to reduce the computational time. This may indicate that the analysis time was an issue in his model. In contrast, the present model handles the nonlinearity of the thermophysical properties by considering them as functions of the temperature being solved as well as using a fourth-order Runge-Kutta nonlinear solver. In addition to that, the heat generation of the phase transformation is handled in the present model explicitly, where it is calculated at the end of each time step from the microstructure calculations, and then used in the heat equation to calculate the thermal field of the next time step. This procedure eliminates the need for the iterative procedure adapted by the previous models, and hence the computational time of the present model is reduced significantly. For example, the solution of the entire physical geometry of the case study was obtained by using a personal computer with a Pentium 4 processor and 2 GB RAM. The computational time on this computer was only 30 seconds. Note that attention has been given to ensure that the current results are both time step size and spatial step size independent.

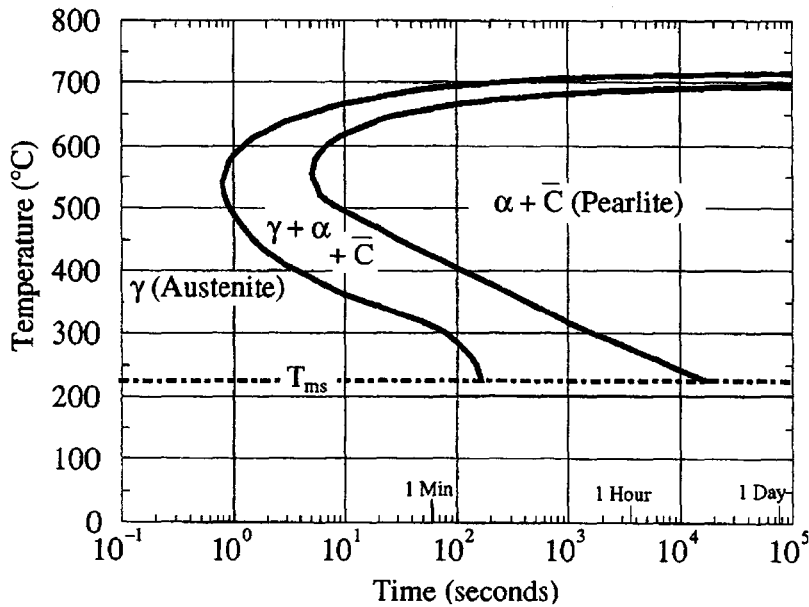


Figure 4.5 TTT diagram for Plain Carbon 1080 Steel [13].

4.4 Case Study of Infinite 1080 Carbon Steel Rod

The present model has been validated by simulating a quenching problem of an infinitely long 1080 plain carbon steel rod. The TTT diagram of this material is shown in Figure 4.5. This problem had been experimentally and numerically investigated by many researchers [11-13,15]. The rod is initially kept at the austenizing temperature of 850 °C and then quenched in 22.5 °C water. Three thermocouples were imbedded in the rod at three different locations. The first thermocouple is at the surface (point A in Figure 4.6); second thermocouple is at point B at a distance of 1.27 mm from the surface and the third thermocouple is at the centre of the rod (point O). The rod's dimensions are shown in Figure 4.6. The variation of the heat transfer coefficient with the quenched rod surface temperature used in the present study taken from Ref [13] is shown in Figure 4.7. The

dependency of the thermophysical properties on the temperature of the 1080 carbon steel is shown in Figure 4.8 [13].

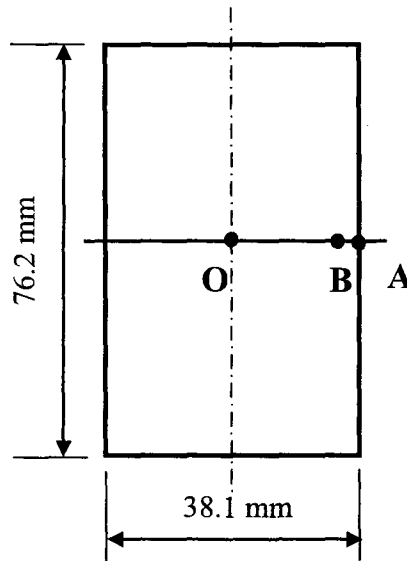


Figure 4.6 Dimensions of the case study part.

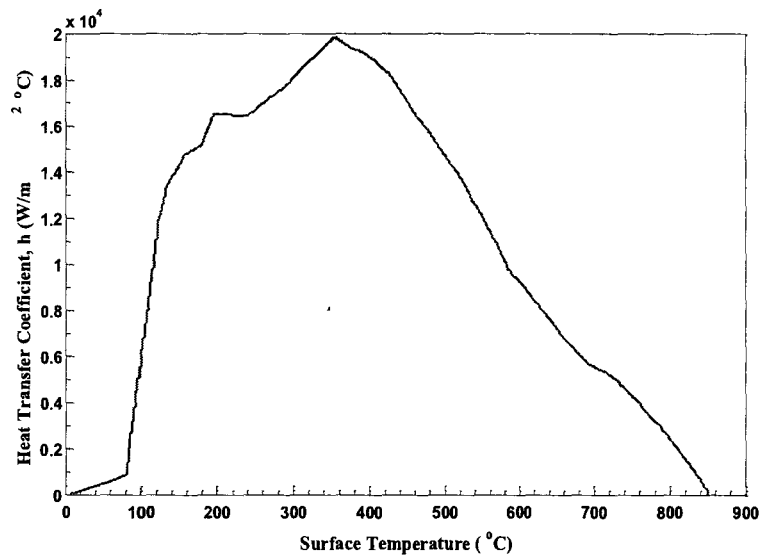


Figure 4.7 The variation of heat transfer coefficient with temperature used in the case study.

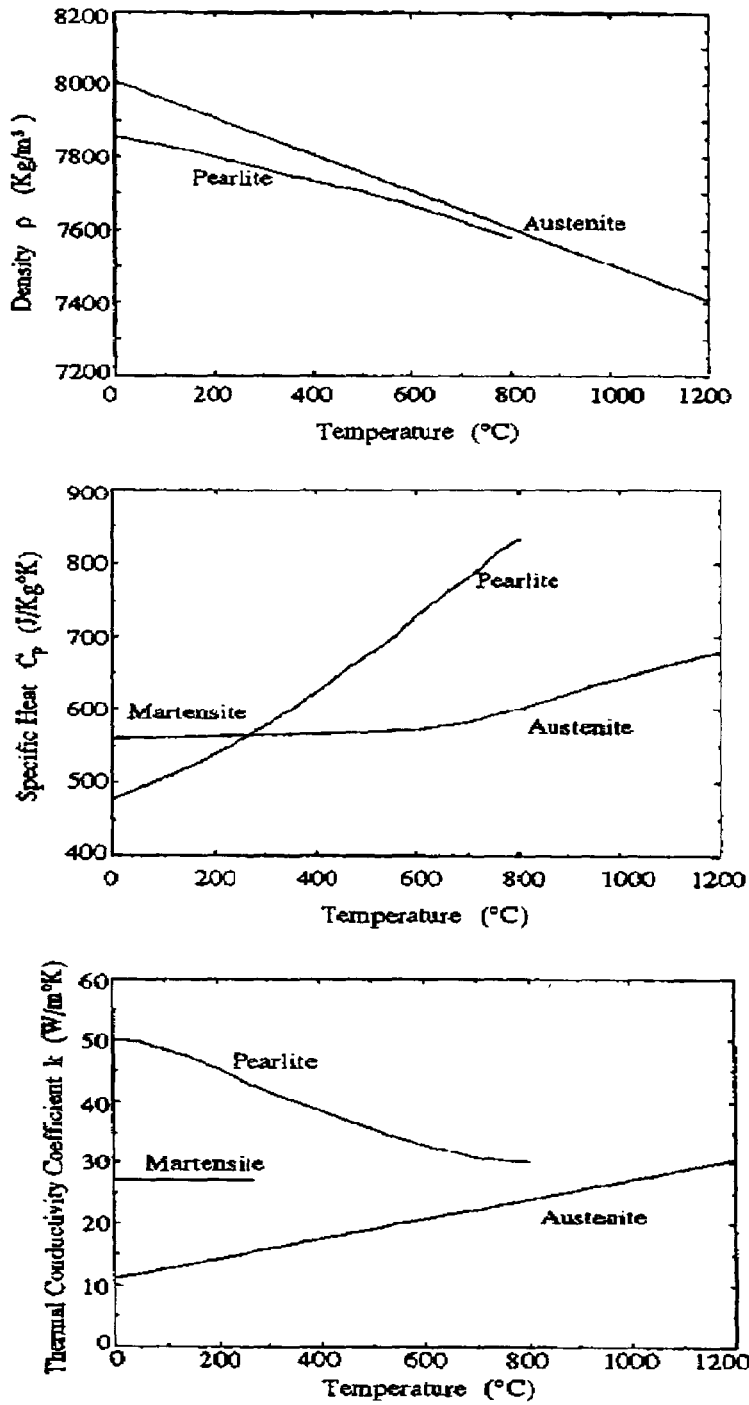


Figure 4.8 Thermophysical properties of plain carbon 1080 steel [13].

4.5 Results and Discussion

The present algorithm has been used to solve the case study problem described in the previous section. The numerical results have been compared with the experimental data in Ref [12] as well as the available numerical results reported in Refs [11,13,15].

Figure 4.9 shows a comparison between the predicted and experimental temperature transient for two different locations in the quenched steel rod. Also shown are predictions for the same problem from Wang et al. [11] and Kang and Im [15]. As seen from this figure, improved predictions are obtained with the new method. For example, the rise in the temperature at the centre of the cylinder due to phase transformation heat release is exactly predicted by the present algorithm. For clarity, Figure 4.10 shows the current predictions and the experimental data. This figure shows that the experimental data were predicted excellently by the present algorithm.

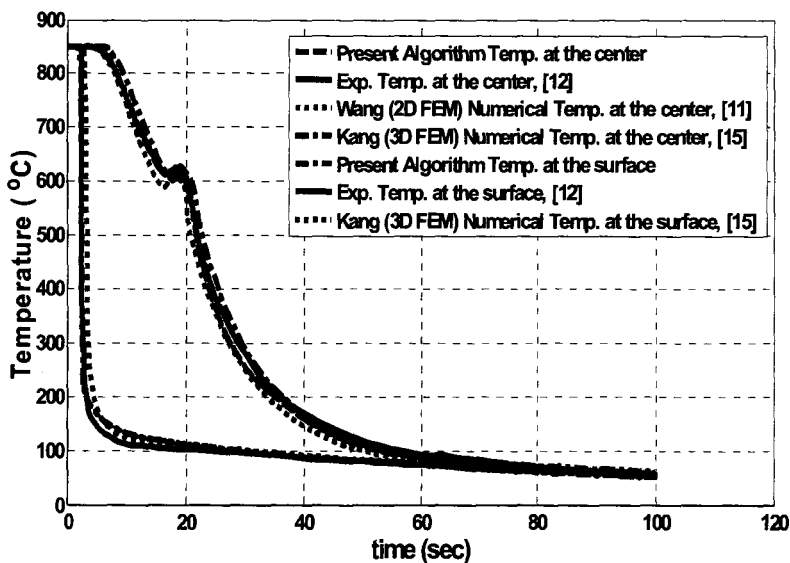


Figure 4.9 A comparison between the transient temperatures of different numerical algorithms and the experimental data reported in [12].

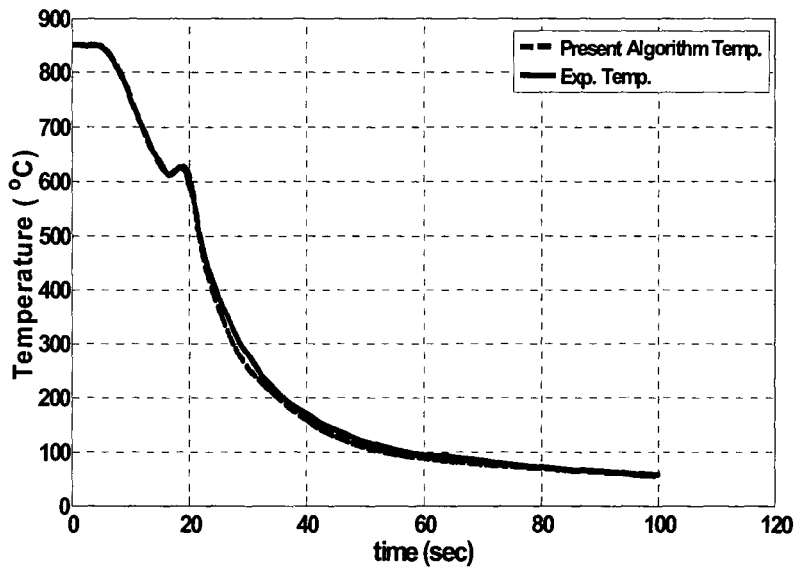


Figure 4.10 A comparison between the temperature profile at the rod center predicted by the present algorithm and the experimental data reported in [12].

Figure 4.11 shows a comparison between the volume fraction of austenite, pearlite and martensite of the quenched 1080 carbon steel rod predicted by the three previous numerical algorithms and the present algorithm. The results of the present algorithm are between the other numerical results and showing the same trend.

Figure 4.12 shows the pearlite volume fraction of three different locations along the radius of the cylinder. It is clear that there is no austenite to pearlite transformation at the surface of the rod due to the rapid cooling and only martensitic transformation occurred. Partial austenite to pearlite transformation took place at a deeper location from the surface ($r=12.03$ mm), while a complete transformation occurred at a point closer to

the centre ($r=4.01\text{mm}$) where the rod microstructure is totally pearlite. These results are in a good qualitative agreement with the expected distribution.

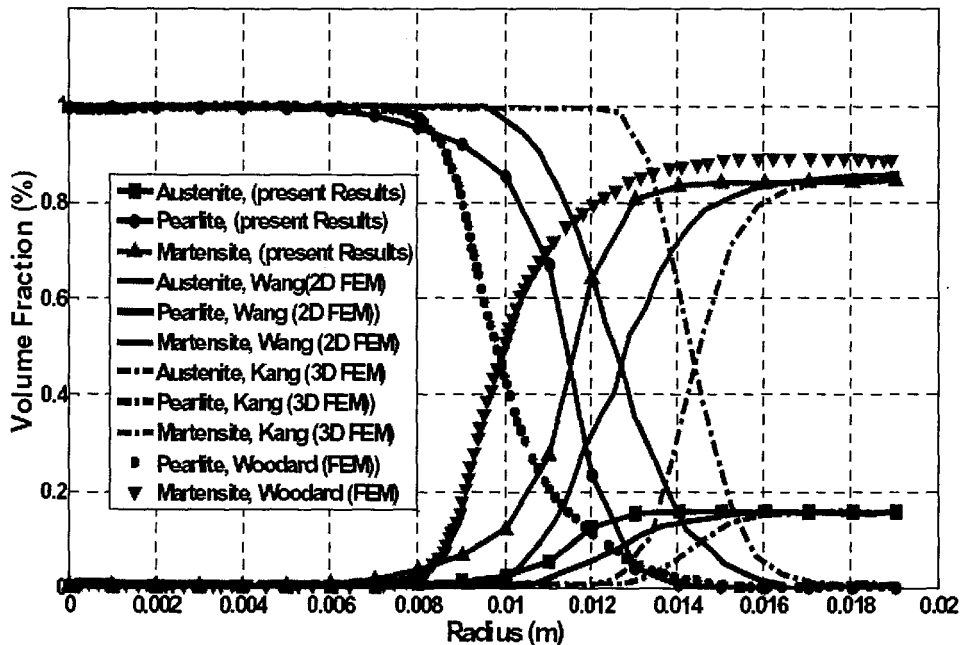


Figure 4.11 A comparison between the microstructure distributions predicted by the previous algorithms [11, 13 and 15] and the present algorithm.

Figure 4.13 shows the evolution of the three considered phases (austenite, pearlite and martensite) at a point inside the rod ($r=12.03\text{ mm}$) with time. The variation of composition as a function of time is significant and as such thermophysical properties must incorporate the mixture law.

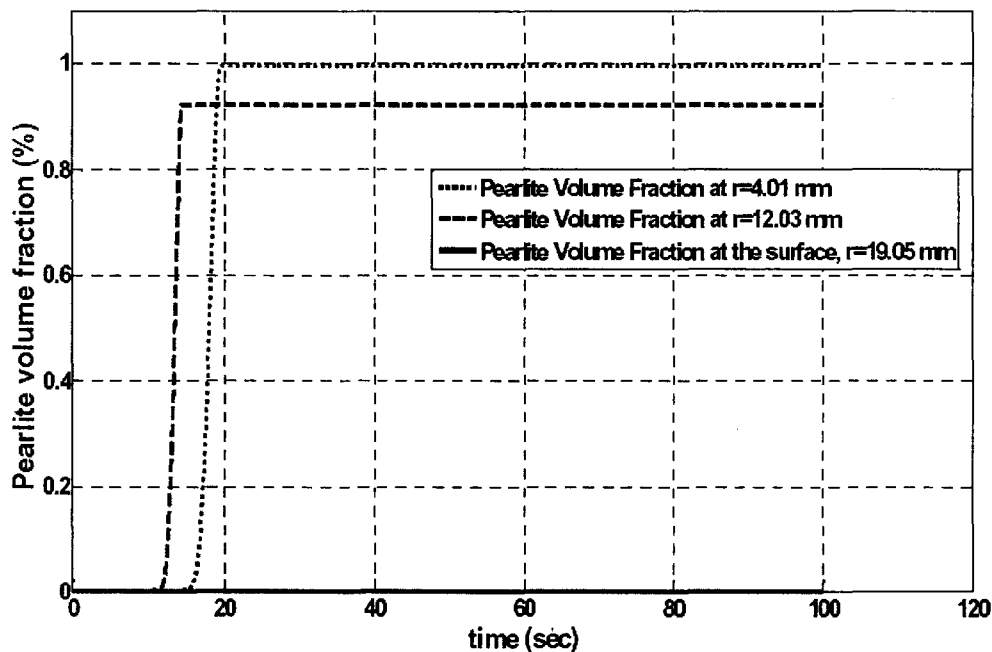


Figure 4.12 The volume fraction of pearlite at three different locations inside the rod as a function of time.

The effect of including the heat generation due to phase transformation has been investigated in this study and the results are shown in Figure 4.14. The results are also compared with the results of the previous investigation of Woodard [13]. It is clear that heat generation due to phase transformation has a very significant impact on the microstructure of the quenched steel rod. If the heat generation is neglected, the volume fraction of the pearlite at the centre varied from 100% to 32%; while the volume fraction of the martensite changed from 0% to 58% at the same location. This significant difference in the predicted microstructure may result into wrong prediction of the

expected distortion, thermal and residual stresses, as well as the expected hardness distribution within the part.

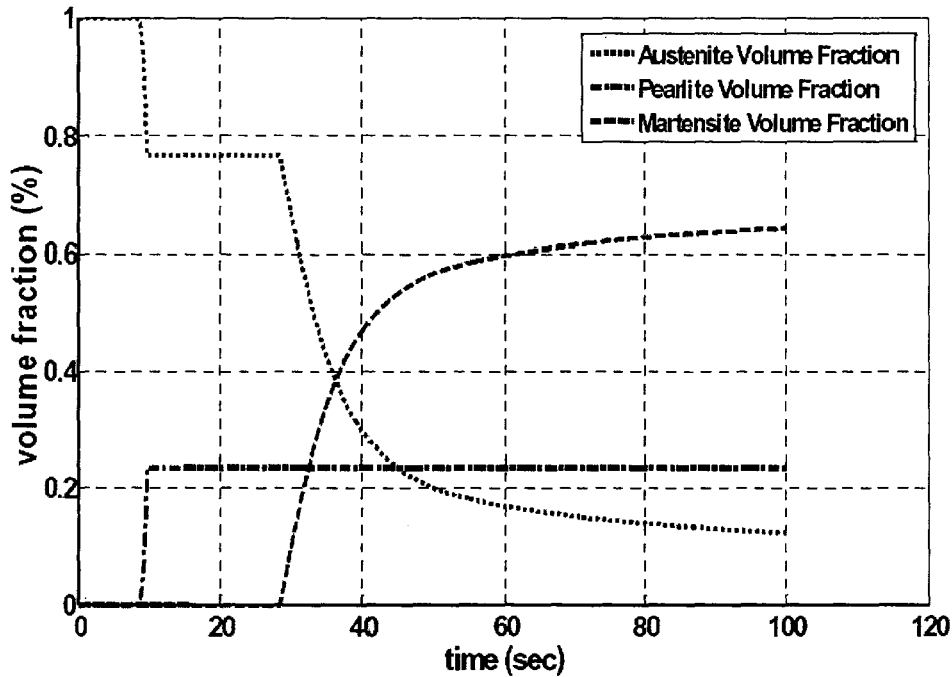


Figure 4.13 Variation of the volume fraction of Austenite, Pearlite and martensite at $r=12.03$ mm with time

Figure 4.15 gives a comparison between the temperature profile at the rod center predicted by the present study and that predicted by Woodard et al. [13] for the case of no heat generation. This figure shows that the numerical solution is unable to capture the rise in the temperature due to the phase transformation at the centre of the rod when the heat generation due to phase transformation is neglected. Although the microstructure calculations showed that there is a phase transformation at the center, yet its effect on the

thermal field is suppressed by neglecting the heat generation term. This figure also shows that the experimental data have been overestimated by Woodard's algorithm [13].

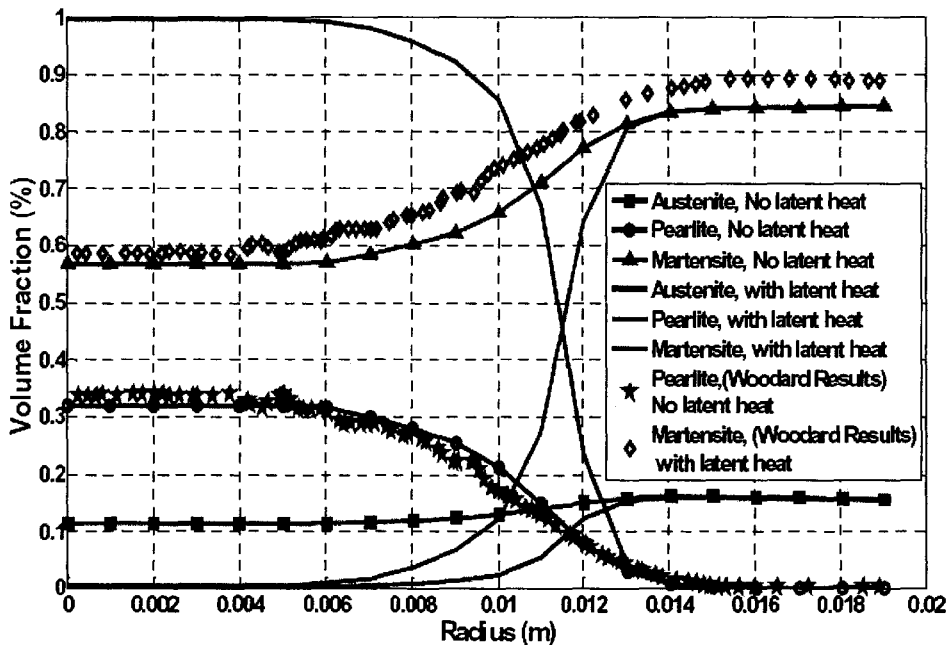


Figure 4.14 A comparison between the microstructure distributions of different numerical algorithms presenting the effect of heat generation.

Most of the previous numerical algorithms [8-15] have neglected the non-linear term, $(1/\rho Cp) (\partial k/\partial T) \{\partial T/\partial r\}^2$, in the heat equation, Equation 4.6. Neglecting this term is a result of employing an explicit linearization method to handle the nonlinearity of the thermophysical properties (being temperature dependent). In contrast, the present algorithm handles the quenching problem without any linearization and hence the effect of the above nonlinear term has been investigated using the present algorithm.

Figure 4.16 shows a comparison between the predicted temperature profile using the present algorithm with the experimental temperatures for two cases. The first case considers the nonlinear term and results in very good agreement with the experimental data. In the second case, where the nonlinear term has been neglected, the predicted temperatures deviated from the experimental data. Furthermore, without the nonlinear term, the algorithm is not able to accurately predict the rise in the rod temperature that resulted from the heat released during phase transformation.

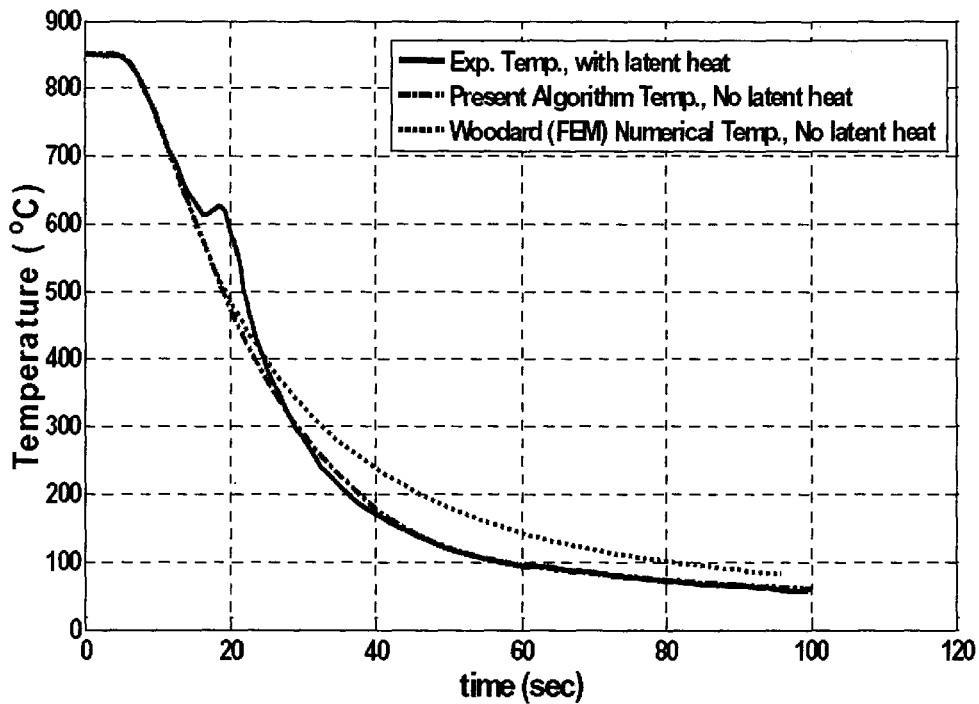


Figure 4.15 A comparison between the temperature profile at the rod center predicted by the present algorithm and those predicted by Woodard while neglecting the effect of heat generation.

A comparison between different numerical results when the nonlinear term is neglected with experimental data is shown in Figure 4.17. This figure shows that the results of the present algorithm coincide with that of Wang et al. [12] in the first 15 seconds. However, the rise in temperature at the center of the rod due to pearlitic transformation predicted by the present algorithm took place before that of Wang. The above discussion indicates that the nonlinear term has a significant impact on the results of the present algorithm.

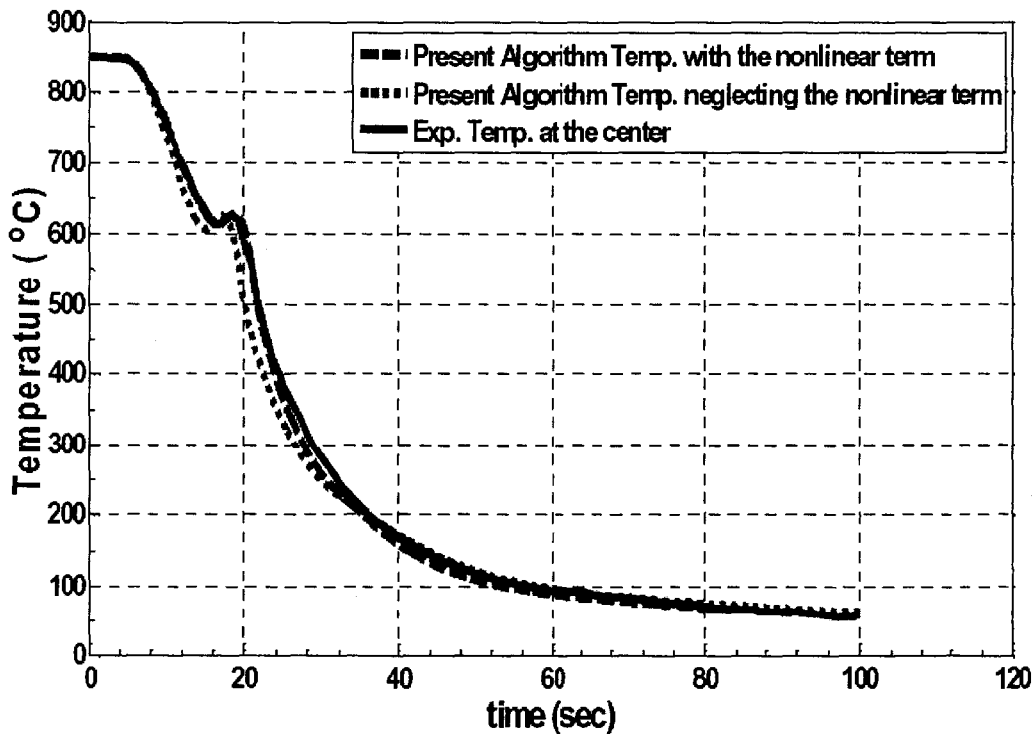


Figure 4.16 The effect of the nonlinear term on the thermal field of the quenched steel rod.

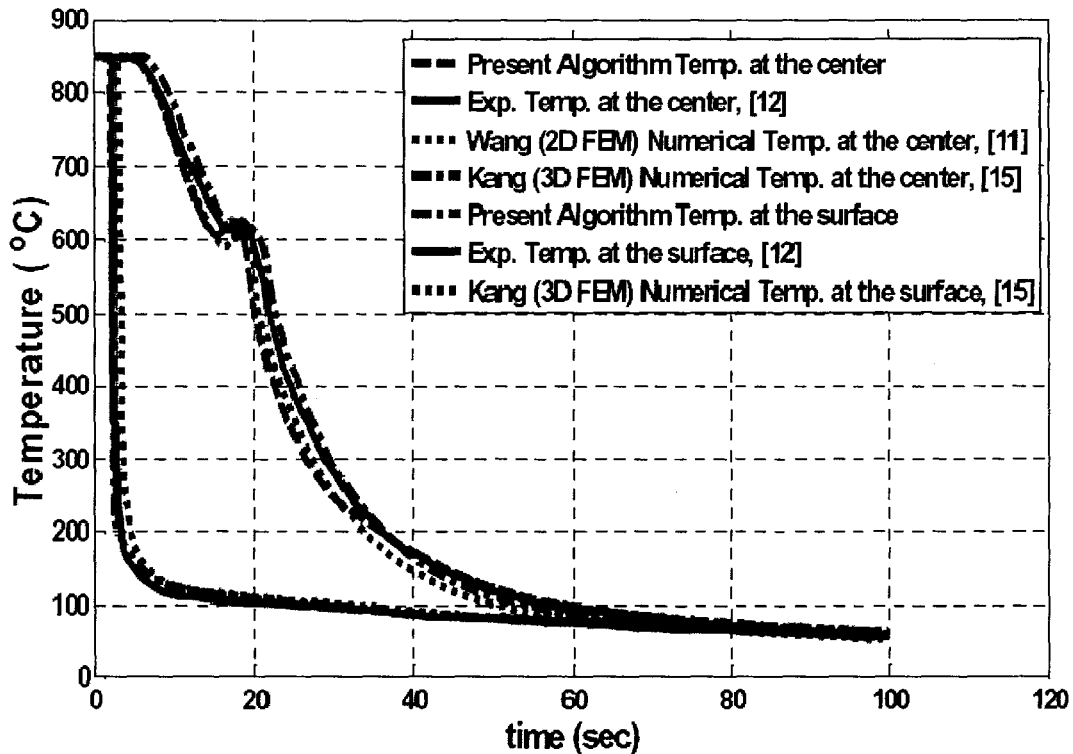


Figure 4.17 A comparison between the temperature profiles predicted by different numerical algorithms with experimental data when the nonlinear term is neglected.

4.6 Summary and Conclusions

A new numerical algorithm has been proposed to solve the thermal and microstructure fields during the quenching of an infinite 1080 carbon steel rod. The algorithm solves the full nonlinear form of the heat conduction equation. Contrary to previous models where a linear form of the heat conduction equation was solved using a linear solver employing an iterative procedure, in the present work, the nonlinear heat equation was solved using a 4th order Runge-Kutta nonlinear solver. No linearization was needed as the

thermophysical properties were taken as function of the current temperature that is being solved. Furthermore, no iteration is required during the solution of the thermal and microstructure fields. The results of the proposed algorithm showed improved predictions over the previous models. Since iteration is not required, the algorithm is computationally more efficient.

4.7 Acknowledgments

This work is supported and funded by the natural Sciences and Engineering Research Council of Canada (NSERC), the Centre for Materials and Manufacturing/Ontario Centres of Excellence (OCE-CMM), and the OCE-McMaster thermal processing Consortium.

4.8 References

1. Johnson, W. A., and Mehl, R. F., Reaction Kinetics in Process of Nucleation and Growth, *Trans. AIME*, Vol. 135, pp. 416-458, 1939.
2. Avrami, M., Kinetics of Phase Change I, *J. Chem. Phys.*, Vol. 7, pp. 1103-1112, 1939.
3. Scheil, E., Anlaufzeit der Austenitumwandlung, *Arch. Eisenhüttenwes.*, Vol.12, pp. 564-567, 1935.
4. Koistinen, D. P., and Marburger, R. E., A General Equation Prescribing the Extent of the Austenite-Martensite Transformation in Pure Iron-Carbon Alloys and plain Carbon Steels, *Acta Metall.*, Vol. 7, pp. 59-60, 1959.
5. Inoue, T., and Takana, K., An Elastic-Plastic Stress Analysis of Quenching when Considering a Transformation, *Int. J. of Mechanical Science*, Vol. 17, pp. 361-367, 1975.

6. Inoue, T., Ju D. Y., and Amrimoto, K., Metallo-Thermo-Mechanical Simulation of Quenching Process-Theory and Implementation of Computer Code, HEARTS, Proceedings of the first international conference on quenching and control of distortion, ASM International, Chicago, pp. 205-212, 1992.
7. Inoue, T., and Amrimoto, K., Development and implement of CAE System “HEARTS” for Heat Treatment Simulation Based on Metallo-Thermo-Mechanics, J. Mater. Eng. Perform., ASM International, Vol. 6, Issue 1, pp. 51-60, 1997.
8. Fernandes, F. M. B, Denis, S., and Simon, A., Mathematical Model Coupling Phase Transformation and Temperature Evolution During Quenching of Steels, Materials Science and Technology, Vol. 1, pp. 838-844, 1985.
9. Denis, S., Sjostrom, S., and Simon, A., Coupled Temperature, Stress, Phase Transformation Calculation Model Numerical Illustration of the Internal Stresses Evolution During Cooling of a Eutectoid Carbon Steel Cylinder, Metal. Trans. A, Vol. 18A, pp. 1203-1212, 1987.
10. Denis, S., Farias, D., and Simon, S., Mathematical Model Coupling Phase Transformation and Temperature Evolution in Steels, ISIJ international, Vol. 32, No. 3, pp.316-325, 1992.
11. Wang, K. F., Chandrasekar, S., and Yang, H. T. Y., An Efficient 2D Finite Element Procedure for the Quenching Analysis with Phase Transformation, Journal of engineering for Industry, Feb., Vol. 115, pp. 124-138, 1993.

12. Wang, K. F, Chandrasekar, S., and Yang, H. T. Y., Experimental and Computational study of the Quenching of Carbon Steel, *Journal of Manufacturing science and engineering*, August, Vol. 119, pp. 257-265, 1997.
13. Woodard, P. R., Chandrasekar, S., and Yang, H. T. Y., Analysis of Temperature and Microstructure in quenching of steel Cylinders, *Metallurgical and Materials transaction B*, August, Vol. 30B, pp. 815-822, 1999.
14. Homberg, D., A Numerical Simulation of the Jominy End Quench Test, *Acta Materialia*, Vol. 44, Issue 11, November, pp. 4375-4385, 1996.
15. Kang, H. K., and Im, Y. T., Three-Dimensional Finite Element Analysis of the Quenching Process of Plain-Carbon Steel with Phase Transformation, *Metallurgical and Materials transaction A*, September, Vol. 36A, pp. 2315-2325, 2005.
16. Chapra, S. C., and Canale, R. P., *Numerical Methods for Engineers*, Fourth Edition, McGraw-Hill, New York, 2002.

4.9 Supplementary Material

This part comprises another case study that includes a comparison of numerical simulation of the pearlite volume fraction distribution obtained by the present algorithm with the experimental data of Fernandes et al. [8]. It involves cooling of a plain-carbon 1080 steel cylinder of diameter 4 mm and length of 20 mm at a cooling rate of 8 K/s.

This cooling process has been simulated by the present algorithm and the obtained results are shown in Figures 4.18 and 4.19. Figure 4.18 shows a comparison between the temperature profile at the center of the cylinder with the experimental temperatures.

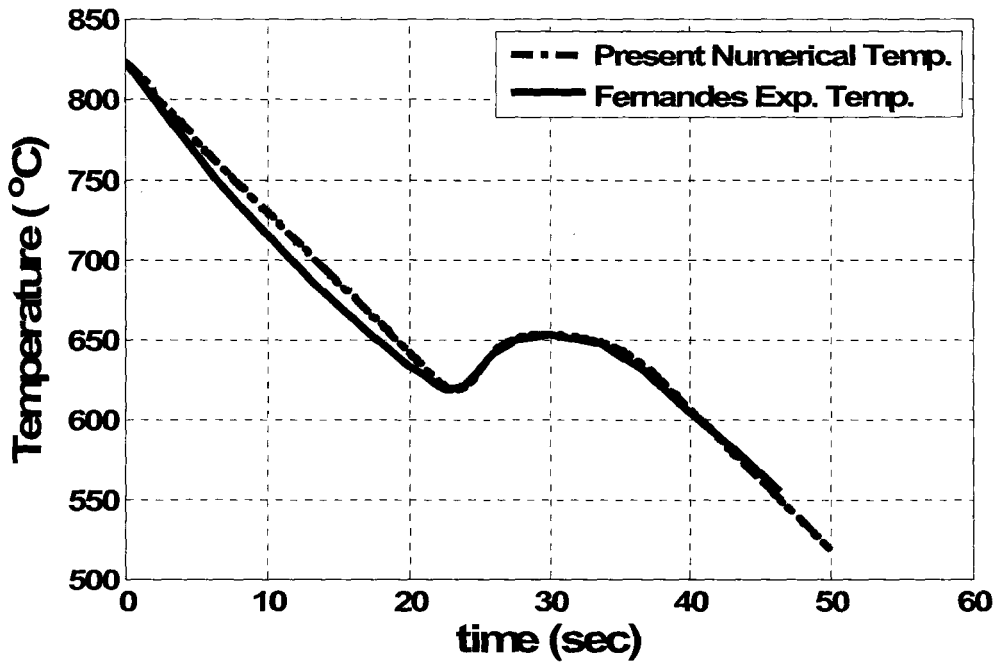


Figure 4.18 A comparison between the temperature profiles predicted by the numerical algorithm with the experimental data of Fernandes et al. [8].

Although there is some deviation between the numerical and experimental results before the starting of the phase transformation, the temperature rise due to the pearlitic phase transformation has been accurately predicted.

Figure 4.19 shows a good agreement between the numerical results of the pearlite volume fraction and the experimental data reported in [8]. This indicates that the microstructure model is reliable in predicting steel microstructure distribution during quenching.

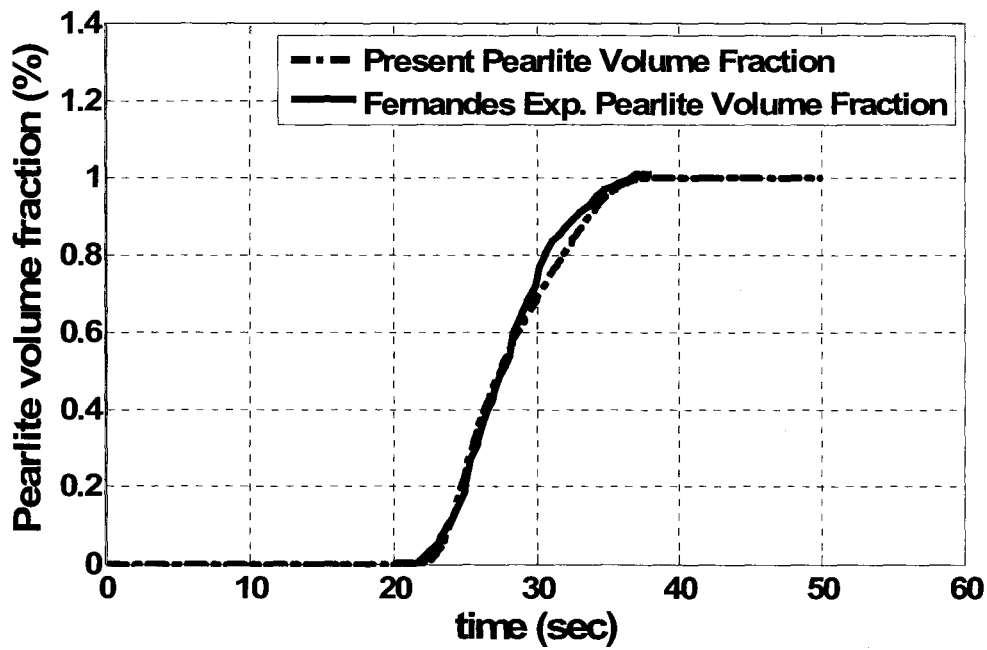


Figure 4.19 A comparison between the pearlite volume fraction predicted by the numerical algorithm with the experimental data of Fernandes et al. [8].

***A MODIFIED ONLINE INPUT ESTIMATION ALGORITHM
FOR INVERSE MODELING OF STEEL QUENCHING***

CHAPTER 5

Chapter Five Preface

This work has been submitted to the Journal of Numerical Heat Transfer/ Part B.

- Ali, S. K., Hamed, M. S., and Lightstone, M. F., A Modified Online Input Estimation Algorithm for Inverse Modeling of Steel Quenching, Submitted to the Journal of Numerical Heat Transfer/ B.

A Modified Online Input Estimation Algorithm for Inverse Modeling of Steel Quenching

Abstract

The surface temperatures and surface heat flux of a 1080 steel cylinder during quenching process are estimated by the application of inverse heat transfer analysis. The conventional online input estimation algorithm has been modified and used for the first time to handle this coupled nonlinear problem. The nonlinearity of the problem is treated explicitly which results in a non-iterative algorithm suitable for real time controlling of steel quenching process. The obtained results have been validated using experimental data and numerical results obtained by solving the direct problem. Results showed that the algorithm could efficiently estimate the convective heat transfer coefficient.

Nomenclature

a_1	state coefficient matrix
A	state transition matrix
A_T	temperature dependent coefficient
b_1	input coefficient matrix
B	second sensitivity matrix
B_T	temperature dependent coefficient
c_1	coefficient matrix of heat generation
C	first sensitivity matrix

C_p	specific heat
D	input matrix
F	input matrix of heat generation
F_f	pearlite finishing volume fraction
F_m	volume fraction of phase m
F_s	pearlite starting volume fraction
h	heat transfer coefficient
H	measurement matrix
I	identity matrix
k	discretized time index
K	Kalman gain
K_b	input gain
M	first sensitivity matrix
n	heat flux onset time
Nr	total number of spatial nodal points
P	state error covariance matrix
P_b	input estimate error covariance matrix
P_r	any material property
q	boundary heat flux (input vector)
Q	modeling error covariance
\dot{Q}_g	latent heat of phase transformation
r	radius of the cylinder

r_{meas}	measurement location
R	measurement error covariance
R_o	outer radius
s	innovation covariance
t	time
T	temperature (state vector)
T_o	initial temperature
T_∞	temperature of the quenchant
w	modeling noise vector
z	measurement vector
\bar{z}	innovation sequence

Greek Symbols

α_M	Koistinen and Marburger coefficient
γ	forgetting factor
δ	Kronecker delta function
Δr	radial step size
Δt	temporal step size (sampling interval)
κ	thermal conductivity
v	measurement noise vector
ρ	density

σ	standard deviation
τ_f	Phase transformation ending time
τ_s	Phase transformation starting time

Subscripts

a	Austenite
M	Martensite
m	Any phase
p	Pearlite
i	spatial index
j	temporal index

Superscripts

$\hat{}$	estimated
$*$	mismatched Kalman filter estimate
T	transpose of matrix

5.1 Introduction

Inverse heat conduction problems (IHCPs) are concerned with the estimation of thermal conditions at the boundary of a body using some internal transient temperature measurements. These problems occur in many industrial applications. They are ill-posed problems because their solutions are unstable and not unique [1, 2]. Therefore, some regularization techniques are required to overcome this ill-posedness and obtain a stable and unique solution.

There are many methods in the literature that have been used to solve IHCPs employing different regularization techniques. For example, the function specification method of Beck uses a number of future temperatures [2], Tikhonov regularization method uses zero, first- and second-order regularization parameters [3], while Alifanov iterative method uses the number of iterations as a stopping criterion to stabilize the solution [4]. Most of these computationally expensive solution methods are batch form techniques where the whole data of internal transient temperatures must be available before starting the solution. In contrast, with the online input estimation algorithm, the unknown boundary heat flux can be estimated in real time at each time step once the measurement is made available. This algorithm was developed by Tuan et al. [5] and has been successfully applied for many inverse heat conduction applications [6-23]. The real time estimation feature of this algorithm is very important in many industrial processes where the boundary heat fluxes and the convective heat transfer coefficients need to be estimated, adjusted and updated frequently during the process such as steel quenching.

In the steel quenching process, the surface heat flux determines the temperature distribution and cooling rates inside the quenched part. These cooling rates directly influence the steel microstructure. The quenching conditions applied at the boundary are conventionally obtained by an extensive empirical work [24]. Ultimately, these conditions are used to provide the optimal microstructure and mechanical properties that avoid deformation, distortion and cracking. Nevertheless, this way of obtaining the quenching conditions is very expensive and it does not provide detailed information about thermal and microstructure fields during the quenching process. As a result, millions of dollars are lost every year in unsatisfactory steel quenching processes [24]. There is thus a need to develop an online algorithm to control the cooling rates in quenching processes by real-time adjusting and updating the surface heat flux.

The first application of the inverse solution to steel quenching was in 1992 by Hernandez-Morales et al. [25]. The sequential function specification method of Beck [2] using future temperature measurements was used to estimate laboratory controlled quenching conditions of flat stainless steel samples quenched by water. This algorithm was subsequently modified for quenching of carbon steel cylinders by air. Only the thermal field was calculated and no attention was given to the microstructure field in this investigation.

Archambault and Azim [26] used the space marching inverse solution technique to estimate the transient surface temperature and boundary heat flux for aluminum and steel quenching. In this method the spatial domain is divided into a direct region for which all boundary conditions are known, and an inverse region for which the boundary

conditions are partially known. The implicit finite-difference method is used first to estimate the thermal field in the direct region and the solution is then marched into the inverse region where both the thermal field and the boundary heat flux are calculated. Although this method was applied for steel quenching, it did not consider heat of phase transformation.

The above inverse method was subsequently applied by Archambault et al. [27] for steel quenching where the heat generation due to phase transformation was considered. The numerical results showed that this method is very sensitive to spatial and temporal step sizes. Furthermore, the effect of measurement errors on the numerical results was not investigated.

Smith [28] developed an optimization based inverse approach to calculate the surface heat transfer coefficients using experimental cooling curves. The algorithm was applied to simulate the quenching of automotive steel components in molten salts in an industrial heat-treatment process. The applicability of the computed results was investigated by simulating quenching of helical transmission gear. The finite-element method was used to discretize the problem domain and the solution is based on adjusting the cooling curves until the measured temperatures are matched by using an unconstrained optimization method. Since this method is an iterative solution technique, this algorithm is relatively computationally expensive.

Heming et al. [29, 30] developed an inverse method to estimate the convective heat transfer coefficient for a steel cylinder undergoing phase transformation during high pressure gas quenching as well as liquid quenching. This algorithm was based on

optimizing the cost function, the difference between the calculated and the measured temperatures, with respect to the convective heat transfer coefficient. The finite-difference scheme was used to discretize the heat equation and explicit linearization technique was adapted to solve the nonlinear heat equation using an iterative linear solver. The results provided some insights about the relationship between the convective heat transfer coefficient and the surface temperature. Similar to the previous technique, this optimization method is iterative solver and hence is relatively computationally expensive.

Recently Azim et al. [31] used two inverse methods to estimate the surface heat flux of a solid steel cylinder during heat treatment. The methods used are the space marching method [26] and the function specification method [1]. Two sets of experiments were conducted to validate the numerical results for two different cases. The first case was a superficial heat treatment applied to XC42 (steel C1045) to induce martensitic transformation while in the second case a homogenous quenching was applied to XC80 (steel C1080) to induce pearletic transformation. For pearletic transformation, the results were affected by the impact of the internal stresses on the transformation kinetics. Also, both methods showed instability in the calculation of the surface heat flux. However, the stability of the function specification method was improved by using some future temperature measurements. The stability of the space marching technique was enhanced by reducing the time step. Nevertheless, it was found that using relatively small time steps caused an inaccurate description of the rapid macrostructure phase transformation.

Based on the above literature review, it appears that the applicability of inverse analysis to solve steel quenching with phase transformation problems is relatively new. As described above, three solution techniques have been used: space marching, function specification and optimization-based solution techniques. The space marching technique is proven to be unstable [26]. Function specification solution method is also unstable unless some future temperatures are incorporated [31], and therefore it cannot be used for online identification. The optimization-based solution method is a batch form technique however it is computationally expensive. An alternative approach is the online input estimator which consists of two estimators: the Kalman Filter estimator and the real-time recursive least squares estimator. The Kalman filter is an online recursive statistical estimator which can better represent the stochastic nature of the experimental measurements. It also provides some information about the quality of the estimate as well as its performance at each time step. Furthermore, it has been successfully used in solving inverse problems for different applications [6-19]. However, in all previous work, the online input estimation has dealt with the thermal field only. Furthermore, to the authors' best knowledge, there has been no work in the literature to date about using the Kalman filter for solving coupled inverse heat conduction problems such as steel quenching process where the thermal field is coupled with the microstructure field through the heat generation due to phase transformation.

Thus, the main objective of this work is to investigate the feasibility of using an online input estimation algorithm for the coupled inverse heat conduction problem of steel quenching. The success in developing such an algorithm can lead to efficiently

controlling the process of steel quenching. This algorithm incorporates a steel microstructure model with the online input estimation algorithm in order to obtain a new computational algorithm that is capable of predicting quenching conditions for which a desired steel microstructure can be achieved.

5.2 Problem Formulation

Steel quenching process is a coupled problem that can be solved by either a direct solver [32-36] or an inverse solver [25-31]. In the former the convective heat transfer coefficient or equivalent boundary conditions must be known beforehand. In the latter the convective heat transfer coefficient is part of the solution where it can be adjusted in real time to obtain the desired mechanical properties. The solution of the direct problem of steel quenching starts with the calculation of the thermal field given the convective heat transfer coefficient and the microstructure distribution of steel phases are then calculated using the calculated thermal field by incorporating the data from the Time-Temperature-Transformation (TTT) diagram of the material [34]. In the inverse problem, which is the focus of the present work, the thermal field along with the heat transfer coefficient of the quenching process are estimated using the online input estimation algorithm given some transient temperature measurements. The obtained thermal field is used by the microstructure model to calculate the volume fraction of the steel phases using the data from the TTT diagram.

5.2.1 Thermal Field Model

Consider an infinitely long cylinder of diameter $2R_o$, initially at a uniform temperature T_0 as shown in Figure 5.1. The cylinder is quenched by exposing its surface to a coolant at a temperature T_∞ . The governing equation of this problem is the one-dimensional heat conduction equation in cylindrical coordinates given by:

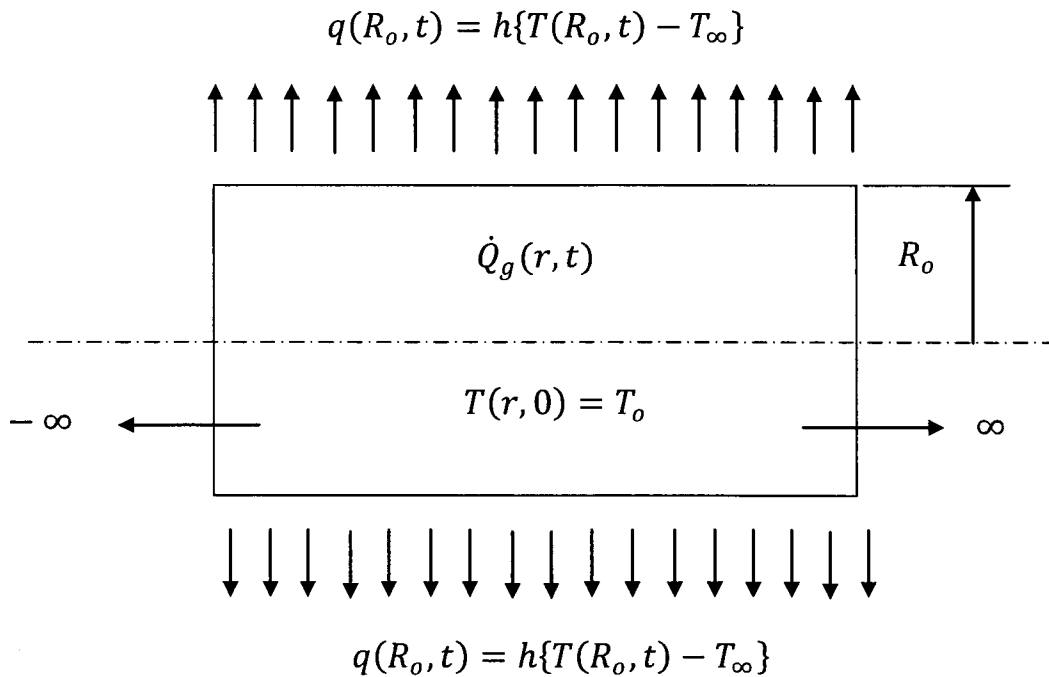


Figure 5.1 One-dimensional quenching problem

$$\rho(T)c_p(T) \frac{\partial T}{\partial t} = \kappa(T) \frac{\partial^2 T}{\partial r^2} + \frac{\kappa(T)}{r} \frac{\partial T}{\partial r} + \dot{Q}_g(r, t) \quad (5.1)$$

where $\rho(T)$ is the density, $C_p(T)$ is the specific heat, $\kappa(T)$ is the thermal conductivity and $\dot{Q}_g(r, t)$ is the latent heat generated due to phase transformation.

The cylinder is subjected to the following set of boundary and initial conditions:

At $r = 0$

$$\frac{\partial T(0, t)}{\partial r} = 0 \quad (5.2)$$

At $r = R_o$

$$q(R_o, t) = -\kappa(T) \frac{\partial T}{\partial r} = h(t) (T(R_o, t) - T_\infty) \quad (5.3)$$

$$T(r, 0) = T_0 \quad (5.4)$$

$$\dot{Q}_g(r, 0) = 0 \quad (5.5)$$

Temperature measurements at $r=r_{meas}$ are given by:

$$z(r_{meas}, t) = T(r_{meas}, t) + v(t) \quad t > 0 \quad (5.6)$$

Where R_o is the outer radius of the cylinder, $h(t)$ is an unknown heat transfer coefficient that needs to be estimated by the developed algorithm, $T(R_o, t)$ is the temperature at the cylinder surface, and $v(t)$ is the measurement errors assumed to be zero mean Gaussian white noise.

Using central finite-difference approximations to discretize the spatial derivatives,

Equation 5.1 can be written as follows:

$$\begin{aligned} \frac{\partial T(i, t)}{\partial t} = & \frac{\kappa(T)}{\rho(T)C_p(T)} \left\{ \frac{T_{i+1} - 2T_i + T_{i-1}}{\Delta r^2} \right\} + \frac{\kappa(T)}{\rho(T)C_p(T)} \frac{1}{r_i} \left\{ \frac{T_{i+1} - T_{i-1}}{2\Delta r} \right\} \\ & + \frac{\dot{Q}_g(i, t)}{\rho(T)C_p(T)} \quad \text{for } i = 1, 2, \dots, \dots, Nr \end{aligned} \quad (5.7)$$

Equation 5.7 can be rearranged in the following form:

$$\begin{aligned} \frac{\partial T(i, t)}{\partial t} = & \frac{\kappa(T)}{\rho(T)C_p(T)} \left\{ \frac{1}{\Delta r^2} - \frac{1}{2r_i\Delta r} \right\} T_{i-1} - \frac{2\kappa(T)}{\rho(T)C_p(T)} \frac{1}{\Delta r^2} T_i \\ & + \frac{\kappa(T)}{\rho(T)C_p(T)} \left\{ \frac{1}{\Delta r^2} + \frac{1}{2r_i\Delta r} \right\} T_{i+1} + \frac{\dot{Q}_g(i, t)}{\rho(T)C_p(T)} \quad \text{for } i \\ & = 1, 2, \dots, Nr \end{aligned} \quad (5.8)$$

where Nr is the total number of spatial nodal points shown in Figure 5.2, and Δr is the radial step size.

Applying the boundary condition, Equation 5.2, at the center of the cylinder ($i=1$) in Equation 5.8 yields:

$$\frac{\partial T(1, t)}{\partial t} = \frac{2\kappa(T)}{\rho(T)C_p(T)} \frac{1}{\Delta r^2} T_2 - \frac{2\kappa(T)}{\rho(T)C_p(T)} \frac{1}{\Delta r^2} T_1 + \frac{\dot{Q}_g(1, t)}{\rho(T)C_p(T)} \quad (5.9)$$

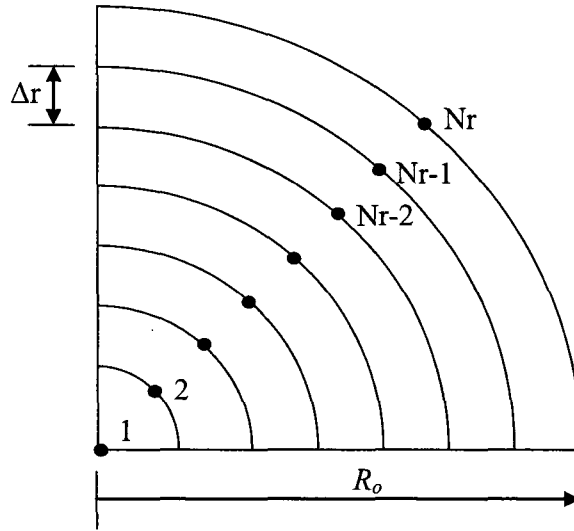


Figure 5.2 The computational domain and the uniformly spaced nodal points.

Discretizing the boundary condition at the surface of the cylinder ($i=N_r$) using a central finite-difference expression yields:

$$T_{N_r+1} = T_{N_r-1} - \frac{2\Delta r}{\kappa(T)} q \quad (5.10)$$

Substituting Equation 5.10 in Equation 5.8 yields:

$$\begin{aligned} \frac{\partial T(N_r, t)}{\partial t} = & \frac{2\kappa(T)}{\rho(T)C_p(T)} \frac{1}{\Delta r^2} T_{N_r-1} - \frac{2\kappa(T)}{\rho(T)C_p(T)} \frac{1}{\Delta r^2} T_{N_r} \\ & - \frac{2}{\rho(T)C_p(T)} \left\{ \frac{1}{\Delta r} + \frac{1}{2r_{N_r}} \right\} q + \frac{\dot{Q}_g(N_r, t)}{\rho(T)C_p(T)} \end{aligned} \quad (5.11)$$

Equations 5.8, 5.9 and 5.11 can be rearranged in the following compact forms:

$$\frac{\partial T(1, t)}{\partial t} = C_{11}T_1 + C_{12}T_2 + C_Q(1) \dot{Q}_g(1, t) \quad \text{for } i = 1 \quad (5.12)$$

$$\begin{aligned} \frac{\partial T(i, t)}{\partial t} &= C_{ii-1}T_{i-1} + C_{ii}T_i + C_{ii+1}T_{i+1} + C_Q(i) \dot{Q}_g(i, t) \quad \text{for } i \\ &= 2, \dots, Nr - 1 \end{aligned} \quad (5.13)$$

$$\frac{\partial T(Nr, t)}{\partial t} = C_{NrNr-1} T_{Nr-1} + C_{NrNr} T_{Nr} + C_q q + C_Q(Nr) \dot{Q}_g(Nr, t) \quad \text{for } i = Nr \quad (5.14)$$

where

$$\begin{aligned} C_{ii-1} &= \frac{\kappa(T)}{\rho(T)c_p(T)} \left\{ \frac{1}{\Delta r^2} - \frac{1}{2r_i \Delta r} \right\}, \quad C_{ii} = -\frac{2\kappa(T)}{\rho(T)c_p(T)} \frac{1}{\Delta r^2}, \quad C_{ii+1} = \frac{\kappa(T)}{\rho(T)c_p(T)} \left\{ \frac{1}{\Delta r^2} + \right. \\ &\left. \frac{1}{2r_i \Delta r} \right\}, \quad C_{12} = C_{NrNr-1} = -C_{ii}, \quad C_q = -\frac{2}{\rho(T)c_p(T)} \left\{ \frac{1}{\Delta r} + \frac{1}{2r_{Nr}} \right\} \quad \text{and } C_Q(i) = \frac{1}{\rho(T)c_p(T)} \end{aligned}$$

The microstructure of the quenched steel is composed of various phases depending on the thermal field. Therefore, the thermophysical properties in the above equations were determined by using the mixture rule [34]. In this rule, the thermophysical properties of the material are considered to be a function of both temperature and volume fraction of the present phases, where any property (P_r) at any point inside the solid is assumed to be a linear combination of the corresponding property of each phase multiplied by the volume fraction of that phase, as given by the following equation [34]:

$$P_r(F_m, T) = \sum_m^{n_{ph}} P_{rm}(T) F_m \quad (5.15)$$

where P_r is any property such as density, specific heat, or thermal conductivity, n_{ph} is the number of present phases and F_m is the volume fraction of the m th phase.

In order to calculate the heat generation resulted from the transformation of austenite to pearlite and martensite, the following equation can be used [35]:

$$\dot{Q}_g(i, t) = \sum_m \Delta H_m(T) \frac{\Delta F_m}{\Delta t} \quad (5.16)$$

where $\Delta H_m(T)$ is the temperature dependent enthalpy change due to the phase transformation. Depending on the type of phase transformation, this enthalpy change can be calculated for 1080 carbon steel using the following equations:

1) For austenite to pearlite transformation [34, 35]:-

$$\Delta H_{a-p}(J/m^3) = 1.56 \times 10^9 - 1.5 \times 10^6 T \quad (5.17)$$

or

$$\Delta H_{a-p}(J/m^3) = (953 + 0.409T - 0.0012T^2) \times 10^6 \quad (5.18)$$

2) For austenite to martensite transformation [34]:-

$$\Delta H_{a-M}(J/m^3) = 640 \times 10^6 \tag{5.19}$$

From Equations 5.12, 5.13, and 5.14 and considering the fictitious process noise inputs [37], the continuous time state equation of steel quenching process can be written in the following form:

$$\frac{dT}{dt} = a_1(T)T(t) + b_1(T)[q(t) + w(t)] + c_1(T)Q_g(t) \tag{5.20}$$

where T is the (Nr x 1) temperature state vector, $w(t)$ is the process noise, which is assumed to be Gaussian white noise of zero mean and independent of the measurement noise $v(t)$, $a_1(T)$ is (Nr x Nr) coefficient matrix, $b_1(T)$ is an (Nr x 1) input coefficient matrix, and $c_1(T)$ is (Nr x 1) coefficient matrix related to the heat generation of the phase transformation. The matrices $a_1(T)$, $b_1(T)$, and $c_1(T)$ are given by the following equations:

$$a_1(T) = \begin{bmatrix} C_{11} & C_{12} & 0 & 0 & 0 & \dots & 0 & 0 \\ C_{ii-1} & C_{ii} & C_{ii+1} & 0 & 0 & \dots & 0 & 0 \\ 0 & C_{ii-1} & C_{ii} & C_{ii+1} & 0 & \dots & 0 & 0 \\ 0 & \cdot & \cdot & \cdot & \dots & \dots & \cdot & \cdot \\ \cdot & \cdot \\ \cdot & \cdot \\ \cdot & \cdot \\ 0 & \dots & \cdot & 0 & C_{ii-1} & C_{ii} & C_{ii+1} & 0 \\ 0 & \dots & \cdot & 0 & 0 & C_{ii-1} & C_{ii} & C_{ii+1} \\ 0 & \dots & \cdot & 0 & 0 & 0 & C_{NrNr-1} & C_{NrNr} \end{bmatrix} \tag{5.21}$$

$$b_1(T) = [0 \quad 0 \quad 0 \quad 0 \quad \dots \quad 0 \quad C_q]^T \tag{5.22}$$

$$c_1(T) = [C_Q(1) \quad C_Q(2) \quad C_Q(3) \quad \dots \quad C_Q(Nr - 1) \quad C_Q(Nr)]^T \tag{5.23}$$

Equation 5.20 is integrated over time with a time step Δt to obtain the discrete time state equation:

$$T(k + 1) = A(k) T(k) + D(k) [q(k) + w(k)] + F(k) \dot{Q}_g(k) \tag{5.24}$$

and accordingly the measurement equation, Equation 5.6, becomes:

$$z(r_{meas}, k) = T(r_{meas}, k) + v(k) \tag{5.25}$$

The operators $A(k)$, $D(k)$, and $F(k)$ are the state transition matrix, the input matrix, and the input matrix of heat generation, respectively. These three operators are given by [23]:

$$A(k) = \exp(a_1(T)\Delta t) \tag{5.26}$$

$$D(k) = \int_{k\Delta t}^{(k+1)\Delta t} \exp[a_1(T)(k + 1)\Delta t - \tau] b_1(T) d\tau \tag{5.27}$$

$$F(k) = \int_{k\Delta t}^{(k+1)\Delta t} \exp[a_1(T)(k + 1)\Delta t - \tau] c_1(T) d\tau \tag{5.28}$$

The variance of the process noise input vector, $w(k)$, and the measurement noise vector, $v(k)$, are given by $E\{w(k)w^T(j)\} = Q\delta_{kj}$ and $E\{v(k)v^T(j)\} = R\delta_{kj} = \sigma^2\delta_{kj}$, respectively. The parameter Q is the model error covariance matrix, δ is the Kronecker delta function. The operator R is the measurement noise covariance matrix and σ is the standard deviation of the measurement error.

5.2.1.1 Online input estimation algorithm for Steel Quenching Process

Online input estimation algorithm of steel quenching consists of two estimators. The first estimator is the Kalman filter by which the thermal field (temperature state vector) is estimated given some internal transient temperature measurements. The thermal field is used to generate the residual innovations which are defined as the difference between the measured temperatures and the predicted temperatures. The second estimator is the real time recursive least squares estimator by which the boundary heat flux is estimated using a linear regression relationship between the residual innovations and the unknown boundary heat flux.

The Kalman filter estimator employs two Kalman filters. The first Kalman filter assumes zero input (heat flux) while the second Kalman filter assumes known input (heat flux). The first Kalman filter is called the mismatched Kalman filter while the second one is called the hypothetical Kalman filter [38].

Let:

$\hat{T}^*(k)$ = the state estimate of the mismatched Kalman filter

$\hat{T}(k)$ = the state estimate of the hypothetical Kalman filter.

Using Equation 5.24 for the mismatched Kalman filter (zero input), the state prediction equation becomes:

$$\hat{T}^*(k+1/k) = A(k) \hat{T}^*(k/k) + F(k) \dot{Q}_g(k) \quad (5.29)$$

Since the last term, $F(k) \dot{Q}_g(k)$, is a deterministic sequence, it does not have any effect on the prediction error. Thus, the prediction error covariance matrix is:

$$\hat{P}^*(k+1/k) = A(k) \hat{P}^*(k/k) A(k)^T + D(k) Q D(k)^T \quad (5.30)$$

The updated estimate [39] is:

$$\begin{aligned} \hat{T}^*(k+1/k+1) \\ = [I - K(k+1)H(k+1)] \hat{T}^*(k+1/k) + K(k+1)z(k+1) \end{aligned} \quad (5.31)$$

The updated estimate error covariance matrix is:

$$\hat{P}^*(k+1/k+1) = [I - K(k+1)H(k+1)] \hat{P}^*(k+1/k) \quad (5.32)$$

Substituting Equation 5.29 in Equation 5.31 and replacing the index $k+1$ by k yields:

$$\hat{T}^*(k/k) = [I - K(k)H(k)][A(k) \hat{T}^*(k/k) + F(k) \dot{Q}_g(k)] + K(k)z(k) \quad (5.33)$$

Using Equation 5.24 for the hypothetical Kalman filter (known input), the prediction equation becomes:

$$\hat{T}(k + 1/k) = A(k) \hat{T}(k/k) + D(k) q(k) + F(k) \dot{Q}_g(k) \quad (5.34)$$

The prediction error covariance matrix is the same as that of the mismatched Kalman filter, Equation 5.30, since q is also a deterministic sequence.

The updated estimate [39] is:

$$\begin{aligned} \hat{T}(k + 1/k + 1) \\ = [I - K(k + 1)H(k + 1)] \hat{T}(k + 1/k) + K(k + 1) z(k + 1) \end{aligned} \quad (5.35)$$

If the index $(k + 1)$ is replaced by (k) , Equation 5.35 becomes:

$$\hat{T}(k/k) = [I - K(k)H(k)] \hat{T}(k/k - 1) + K(k) z(k) \quad (5.36)$$

Substituting Equation 5.34 in Equation 5.36 yields:

$$\begin{aligned} \hat{T}(k/k) = [I - K(k)H(k)] [A(k) \hat{T}(k/k) + D(k)q(k) + F(k)\dot{Q}_g(k)] \\ + K(k) z(k) \end{aligned} \quad (5.37)$$

Assuming that the input heat flux ($q(k)$) is applied at $k = n$ and that it is constant for an interval $n < k \leq L$

At

$$k = n, \quad q(k - 1) = 0 \quad (5.38)$$

and

$$\hat{T}(k) = \hat{T}^*(k) \quad \text{at } k \leq n \quad (5.39)$$

Let

$$\Delta\hat{T}(k + 1/k + 1) = \hat{T}(k + 1/k + 1) - \hat{T}^*(k + 1/k + 1) \quad (5.40)$$

Substituting Equations 5.33 and 5.37 in Equation 5.40 yields:

$$\begin{aligned} \Delta\hat{T}(k + 1/k + 1) = & [I - K(k + 1)H(k + 1)]\{A(k)[\hat{T}(k + 1/k + 1) - \\ & \hat{T}^*(k + 1/k + 1)] + D(k)q\} \end{aligned} \quad (5.41)$$

$$\begin{aligned} \Delta\hat{T}(k + 1/k + 1) \\ = [I - K(k + 1)H(k + 1)]\{A(k)\Delta\hat{T}(k/k) + D(k)q\} \end{aligned} \quad (5.42)$$

Since q is applied at $k = n$, therefore for $k = n$, $\Delta\hat{T}(n/n) = 0$ as can be also concluded from Equation 5.39.

$$\begin{aligned} \Delta\hat{T}(k + 1/k + 1) \\ = \begin{cases} 0 & \text{for } k \leq n \\ [I - K(k + 1)H(k + 1)]\{A(k)\Delta\hat{T}(k/k) + D(k)q\} & \text{for } k > n \end{cases} \end{aligned} \quad (5.43)$$

If recursively, substituting in Equation 5.43 for the index $k+1$ by $k=n, n+1, n+2, n+3, \dots, n+L$ and assuming that $\Delta\hat{T}(k/k) = M(k)D(k)q$, the following recursive equation can be obtained for the sensitivity matrix $M(k)$ [40, 41]:

$$\begin{aligned}
 &M(k/k) \\
 &= \begin{cases} 0 & \text{if } k \leq n \\ [I - K(k)H(k)]\{A(k-1)M(k-1) + I\} & \text{if } k > n \end{cases} \quad (5.44)
 \end{aligned}$$

The residual innovation sequence for the mismatched Kalman filter is given by:

$$\bar{z}^*(k+1) = z(k+1) - H(k+1) \hat{T}^*(k+1/k) \quad (5.45)$$

$$\bar{z}^*(k+1) = z(k+1) - H(k+1) [A(k) \hat{T}^*(k/k) + F(k) \dot{Q}_g(k)] \quad (5.46)$$

and for the hypothetical Kalman filter is given by:

$$\bar{z}(k+1) = z(k+1) - H(k+1) [A(k) \hat{T}(k/k) + D q + F(k) \dot{Q}_g(k)] \quad (5.47)$$

Subtracting Equation 5.47 in Equation 5.46 yields:

$$\bar{z}^*(k+1) = \bar{z}(k+1) + H(k+1) [A(k)M(k) + I]D(k) q \quad (5.48)$$

this can be written as:

$$\begin{aligned}
 &\bar{z}^*(k+1) \\
 &= \begin{cases} \bar{z}(k+1) & \text{if } k \leq n \\ \bar{z}(k+1) + H(k+1) [A(k)M(k) + I]D(k) q & n < k \leq n+L \end{cases} \quad (5.49)
 \end{aligned}$$

$$\bar{z}^*(k) = \begin{cases} \bar{z}(k) & \text{if } k \leq n \\ \bar{z}(k) + C(k) q & n < k \leq n+L \end{cases} \quad (5.50)$$

where $C(k)$ is the sensitivity matrix given by:

$$C(k) = H(k) [A(k-1)M(k-1) + I]D(k) \quad (5.51)$$

Equation 5.50 can be considered as a measurement equation for the boundary heat flux q where the recursive least squares parameter estimation procedure can be applied to estimate the parameter q . The details of this procedure can be found in [5]. The final equations of the Kalman filter as well as those of the real time recursive least squares estimator are given below:

Kalman filter equations

State prediction

$$T(k+1/k) = A(k)T(k/k) + F(k) \dot{Q}_g(k) \quad (5.52)$$

State covariance prediction

$$P(k+1/k) = A(k)P(k/k)A(k)^T + D(k)QD(k)^T \quad (5.53)$$

Innovation covariance

$$s(k+1) = H P(k+1/k) H^T + R \quad (5.54)$$

Filter gain

$$K(k+1) = P(k+1/k) H^T s^{-1}(k+1) \quad (5.55)$$

Update state covariance

$$P(k+1/k+1) = [I - K(k+1)H] P(k+1/k) \quad (5.56)$$

Innovation

$$\bar{z}(k+1) = z(x_{x_{meas}}, k+1) - H T(k+1/k) \quad (5.57)$$

Update state estimate

$$T(k+1/k+1) = T(k+1/k) + K(k+1) \bar{z}(k+1) \quad (5.58)$$

Recursive least squares equations

First sensitivity matrix

$$C(k+1) = H [A(k) M(k) + I] D(k) \quad (5.59)$$

Second sensitivity matrix

$$M(k+1) = [I - K(k+1)H][A(k) M(k) + I] \quad (5.60)$$

Gain

$$K_b(k+1) = \gamma^{-1} P_b(k) C^T(k+1) * [C(k+1) \gamma^{-1} P_b(k) C^T(k+1) + s(k+1)]^{-1} \quad (5.61)$$

Error covariance of the input estimate

$$P_b(k+1) = [I - K_b(k+1)C(k+1)] \gamma^{-1} P_b(k) \quad (5.62)$$

Input estimation

$$\hat{q}(k+1) = \hat{q}(k) + K_b(k+1) * [\bar{z}(k+1) - C(k+1) \hat{q}(k)] \quad (5.63)$$

where H is the measurement matrix, K_b is the input gain, and γ is a scalar called the “forgetting factor” which works as a weighting factor in the recursive least square estimator.

The calculated thermal field is then corrected using the estimated heat flux since it is primarily calculated using the mismatched Kalman filter assuming zero boundary heat flux. The thermal field is corrected by using the following equation [41]:

$$T_{Corr}(k+1/k+1) = T(k+1/k+1) + M(k+1) * D(k) * \hat{q}(k+1) \quad (5.64)$$

5.2.2 Microstructure Model

The phase transformation during steel quenching can be classified into: (1) diffusional transformation such as austenite to pearlite transformation and (2) diffusionless transformation such as austenite to martensite transformation. The former depends on temperature and time while the latter depends on the temperature only.

Two periods are involved in the diffusional transformation. The first period is called the incubation period, also known as nucleation period. The transformation in this period is estimated by using the Scheil’s additivity method. In this method, the cooling curve on the Time-Temperature-Transformation (TTT) diagram, see Figure 5.3, is

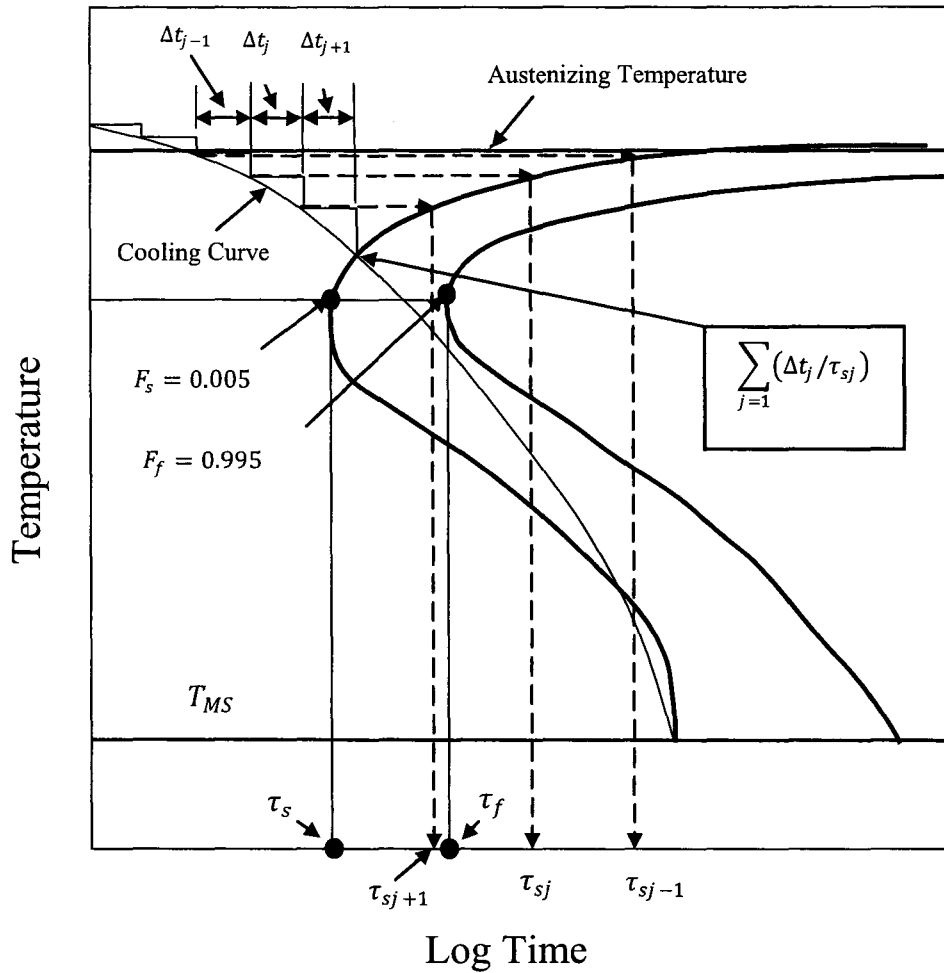


Figure 5.3 Schematic representation of the Scheil's additivity principle and the calculation of the of the Temperature dependant parameters AT(T) and BT(T) from TTT diagram.

divided into a series of small isothermal intervals corresponding to the number of time steps and connected by unit step temperature changes. The quantity $(\Delta t_j / \tau_{sj})$ is calculated

at each time step j , where Δt_j is time step size and τ_{sj} is the incubation time or the transformation starting time taken from the TTT diagram based on the temperature. The incubation period of the diffusional transformation is completed when the following summation reaches one:

$$\sum_j (\Delta t_j / \tau_{sj}) = 1 \quad (5.65)$$

The second period of the diffusional transformation is called the growth period. The volume fraction of the transformed phase in this period is estimated by using the following Johnson-Mehl-Avrami (JMA) equation [35]:

$$F_m(t) = 1 - \exp[-A_t(T) \times t_j^{B_t(T)}] \quad (5.66)$$

where $F_m(t)$ is the volume fraction of phase m , $A_T(T)$ and $B_T(T)$ are temperature dependent parameters which can be calculated from the isothermal TTT diagram, t_j is the transformation time representing the time elapsed from the beginning of the diffusional transformation and can also be considered as the current time excluding the incubation time. t_j is given by:

$$t_j = \Delta t_j + \left[\frac{\ln \left\{ \frac{1}{1 - F_m^{(j-1)}} \right\}}{A_T(T)} \right]^{1/B_T(T)} \quad (5.67)$$

Where $F_m^{(j-1)}$ is the volume fraction of the m^{th} phase present at the previous time step, $j-1$, and Δt_j is the current time step.

The JMA equation was mainly derived and applied for isothermal transformation. However, it has been used successfully for many nonisothermal transformations [32-36] by updating the two parameters $A_T(T)$ and $B_T(T)$ at each time step using the following equations [36]:

$$B_T(T) = \frac{\ln\{\ln(F_f)\} - \ln\{\ln(F_s)\}}{\ln\{\tau_s(T)\} - \ln\{\tau_f(T)\}} \quad (5.68)$$

$$A_T(T) = -\ln(F_f) \tau_s^{-B_T(T)} \quad (5.69)$$

Where F_s and F_f are the starting and the finishing volume fractions of the austenite to pearlite diffusional transformation represented by the two C-curves on the TTT diagram, Figure 5.3. The pearlite volume fractions on the first and second curves are assumed to be 0.005 and 0.995 respectively. The quantities $\tau_s(T)$ and $\tau_f(T)$ are the starting and ending time of the diffusional transformation, respectively, taken from the TTT diagram at each time step.

For the martensitic diffusionless transformation, the volume fraction of the generated martensite is function of temperature only and can be estimated by the following Koistinen-Marburger equation [36]:

$$F_M(T) = [1 - \exp\{-\alpha_M(T_{MS} - T)\}] \quad (5.70)$$

where $F_M(T)$ is the volume fraction of the martensite, α_M is the Koistinen and Marburger coefficient and it is equal to $1.1 \times 10^{-2} K^{-1}$ for 1080 carbon steel, T_{MS} is the martensitic transformation start temperature. Since pearlite, ferrite, and bainite cannot be transformed to martensite, the above equation should be multiplied by $(1 - \sum_m F_m)$ as follows:

$$F_M(T) = [1 - \exp\{-\alpha_M(T_{MS} - T)\}] \left(1 - \sum_m F_m\right) \quad (5.71)$$

5.3 Computational Procedure

The procedure of the present algorithm is shown in Figure 5.4. The computation is initialized by entering the following data: the initial conditions, the physical geometry, and data taken from the isothermal Time-Temperature-Transformation (TTT) diagram of the material.

Firstly, the thermal field is calculated using the Kalman filter, Equation 5.58. Secondly, the real time recursive least squares estimator is used to estimate the boundary heat flux, Equation 5.63. The thermal field is then corrected using Equation 5.64. Finally, the convective heat transfer coefficient of the quenching process is estimated using Newton's law of cooling, Equation 5.3.

After calculating the thermal field, the calculation of the microstructure transformations starts by employing the additivity rule, Equation 5.65, incorporating the data from the TTT diagram to calculate the incubation period. Once the incubation period is completed, the growth transformation is calculated by using the Johnson-Mehl-Avrami

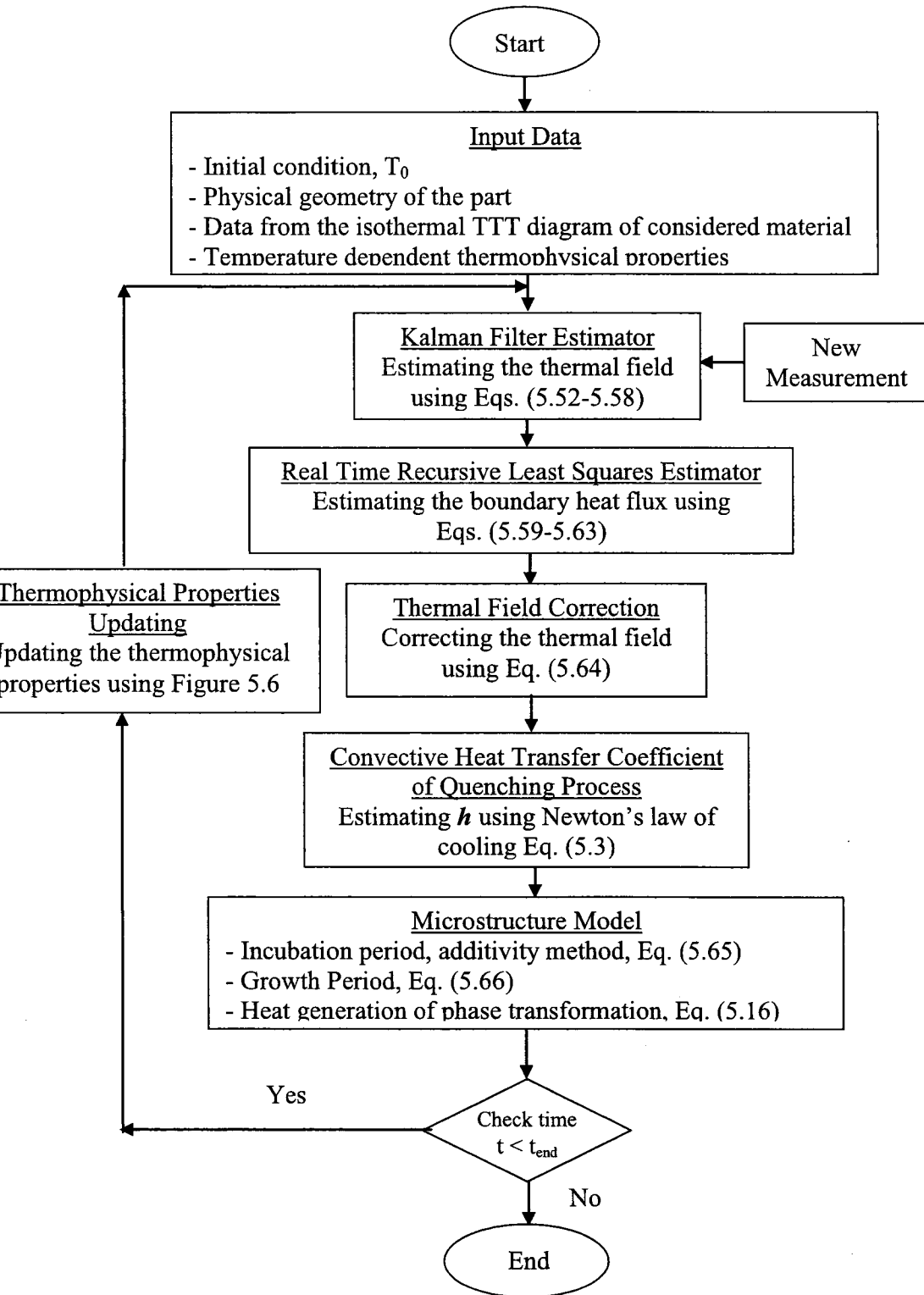


Figure 5.4 Simplified flow chart of the computational procedure of the present inverse algorithm.

equation, Equation 5.66. In this study only the austenite to pearlite transformation is considered and is assumed to only take place above the nose of the TTT diagram [32].

The temperature of each node is compared with the martensitic transformation starting temperature (T_{Ms}) and if it is smaller, the martensite volume fraction is calculated using the Koistinen-Marburger equation, Equation 5.71.

In the previous works [27, 31], where the heat generation due to phase transformation was considered, the thermal field calculation at each time step are carried out assuming no heat generation primarily. At the same time step, upon completing the microstructure calculation and if there is heat generation due to phase transformation, this heat generation is added to the heat equation and the calculation of the thermal field is repeated along with the microstructure calculation. This iterative solution procedure continues until a specific convergence criterion is satisfied. The computational procedure of the previous algorithms is therefore very time consuming and cannot be implemented for real time estimation. In contrast, the heat generation of the phase transformation is handled in the present algorithm explicitly, where it is calculated at the end of each time step from the microstructure calculations, and then used in the heat equation to calculate the thermal field of the next time step.

The quenching process is a highly nonlinear problem due to the thermophysical properties being temperature dependant. This nonlinearity is treated in the present work by explicit linearization. Thermophysical properties of the present time step are calculated based on temperatures of the previous time step. At the end of each time step the thermophysical properties are updated in order to use them in the next time step. This

procedure eliminates the need for the iterative procedure adapted by the previous models, and hence the computational time of the present algorithm is reduced significantly. This feature makes this computational procedure very suitable for real time controlling of steel quenching process.

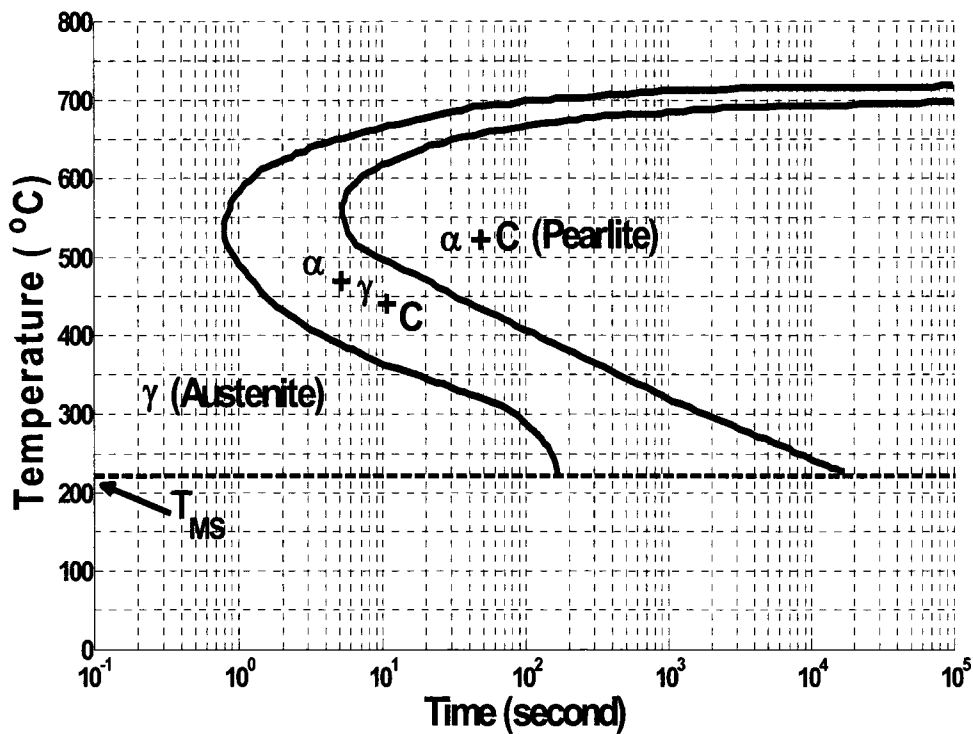


Figure 5.5 TTT diagram for Plain Carbon 1080 Steel.

5.4 Case Study

The above procedure has been applied to simulate the quenching process of infinitely long plain-Carbon 1080 steel cylinder of radius 19.05 mm. The TTT diagram of this material is shown in Figure 5.5. The direct solution of this quenching problem had been experimentally and numerically investigated by many researchers [32-36]. These experimental and the numerical results will be used to validate the predictions of the present work. Three thermocouples have been used and are located at the surface, close to the surface and at the centre of the cylinder. The dependency of the thermophysical properties on the temperature of 1080 carbon steel is shown in Figure 5.6 [34].

The cylinder is initially kept at the austenizing temperature of 850 °C and then quenched in 22.5 °C water. The direct problem (where the heat transfer coefficient is known) of this steel quenching process is first solved using a fourth order Runge-Kutta nonlinear solver [36] to generate transient temperatures at a distance of 1 mm below the surface. Then these temperatures are corrupted by Gaussian white noise of zero mean to simulate the actual temperature measurements. These transient temperature measurements are then used as an input to the inverse algorithm.

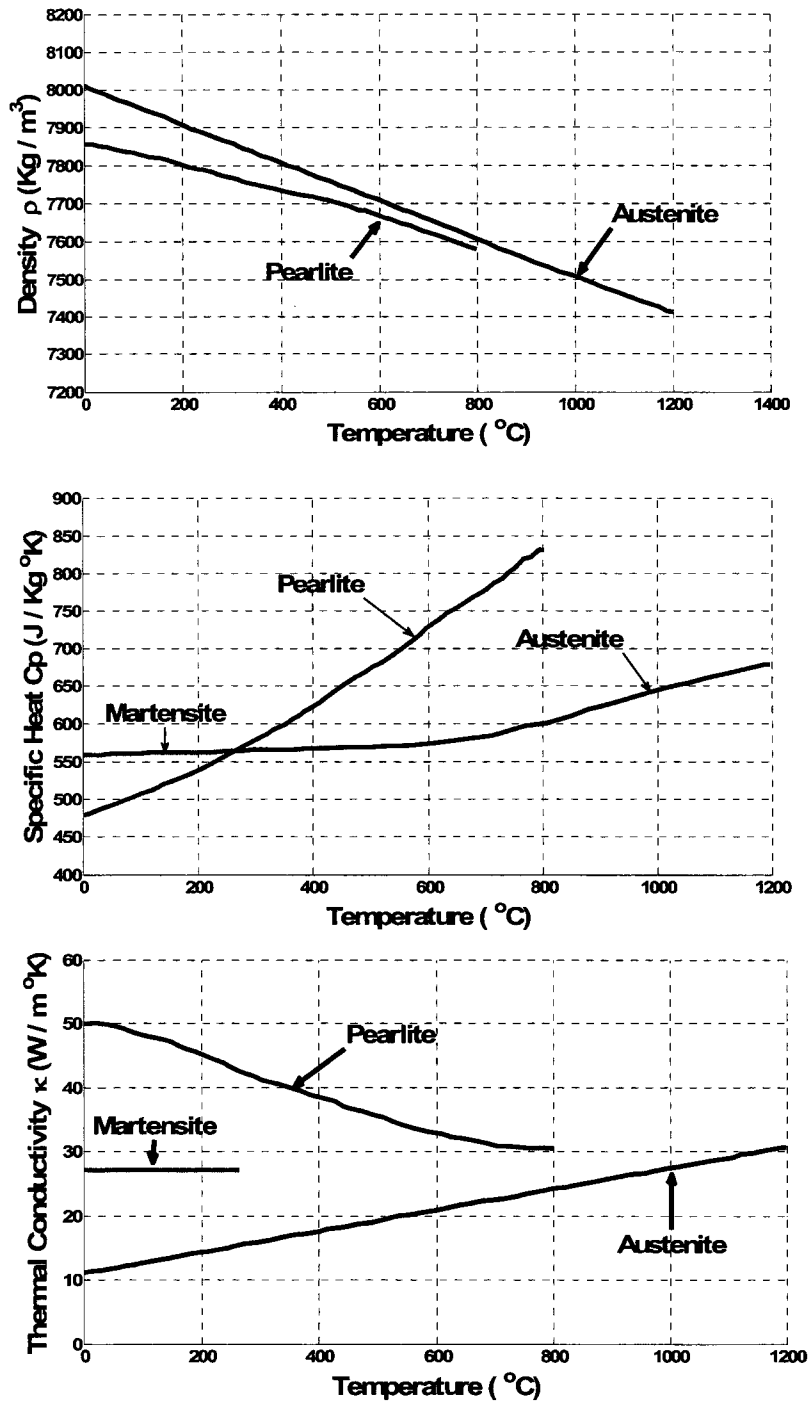


Figure 5.6 The variation of thermophysical properties with temperature used in the case study

5.5 Results and Discussion

The online input estimation algorithm coupled with the steel microstructure model has been used to solve the quenching problem of a 1080 carbon steel cylinder described in the previous section. The present results have been compared with the direct solution of the same problem solved by a fourth order Runge-Kutta method [36]. They are also compared with the experimental data reported in [33], as well as the available numerical results reported in [32, 34, 35].

The physical domain of the problem is discretized into 20 equally spaced nodes. Thus, the coefficient matrices a_I , b_I , and c_I are given by 20 x 20, 20 x 1 and 20 x 1, respectively. The measurement matrix H is 1 x 20 given by $[0 \ 0 \ 0 \ 0 \ \dots \ \dots \ \dots \ \dots \ 0 \ 0 \ 1 \ 0]$ for the considered problem where the thermocouple is located at $i=Nr-1$.

The optimality of the Kalman filter depends on the exact knowledge of the process noise covariance matrix Q in the process model, Equation 5.53, and the measurement error covariance matrix R , Equation 5.54. This operator R is usually given based on the accuracy of the temperature measurements. For the present problem, the standard deviation of the measurement error is assumed equal to 0.001 while the Kalman filter stabilizing parameter, Q , is equal to 9.5×10^{14} [18, 19]. The forgetting factor γ in the recursive least square estimator is taken equal to 0.85. The state error covariance matrix in the Kalman filter is initialized with $P(0/0) = \text{diag}[10^5]$, while the error covariance of the estimated input vector, $P_b(0/0)$, in the real time recursive least squares estimator is initialized with 10^{22} . The sensitivity matrix in Equation 5.59 is initialized with $M(0)=0$.

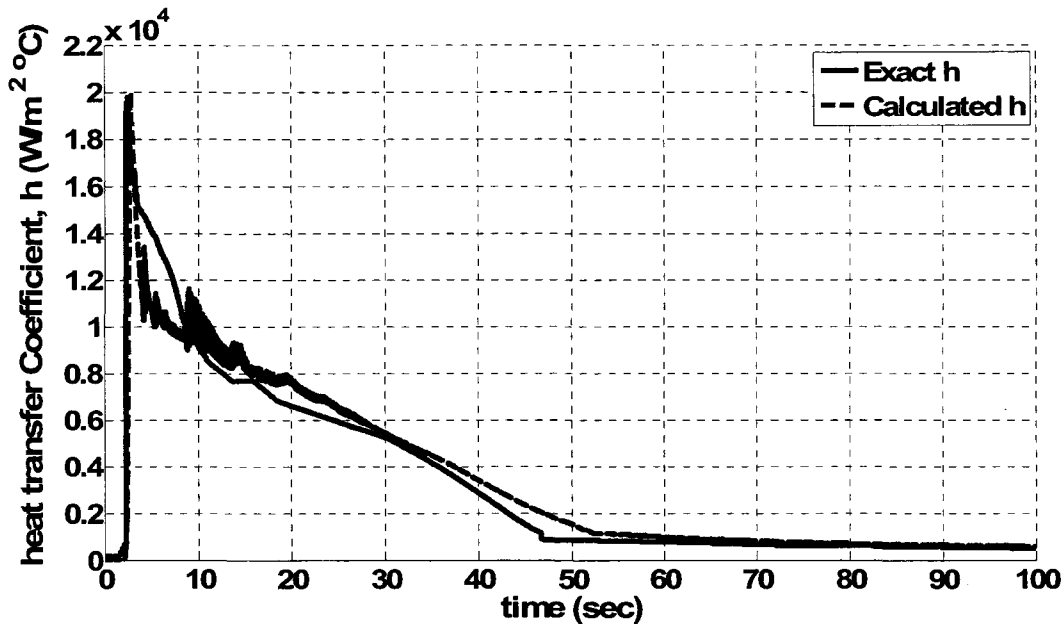


Figure 5.7 A comparison between the exact and the estimated convective heat transfer coefficient of steel quenching process.

For the purpose of comparison, the simulation time of the present problem was chosen equal to 100 second to match that reported in [32-36]. The time step size $\Delta t = 0.05s$ and the spatial step size $\Delta r = 0.001m$. The impact of the grid spacing and time step on the numerical solution is also studied.

Figure 5.7 shows a comparison between the exact and the reconstructed heat transfer coefficient by the online input estimation algorithm. The shape of the heat transfer coefficient is quite well reproduced especially the peak value at the early stage of the steel quenching process. Therefore, this figure indicates that the present model can be used efficiently to estimate the heat transfer coefficient of steel quenching process.

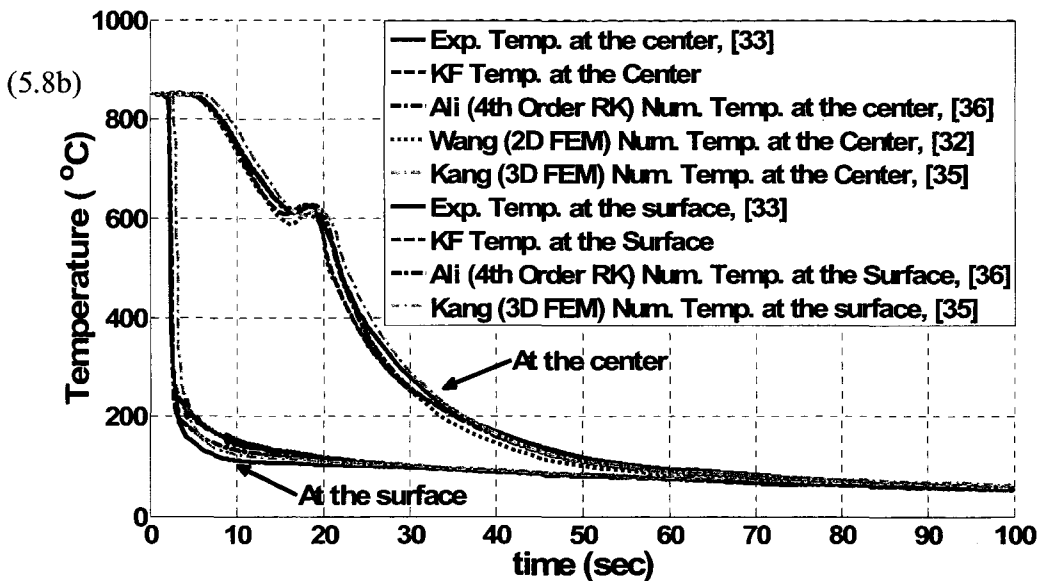
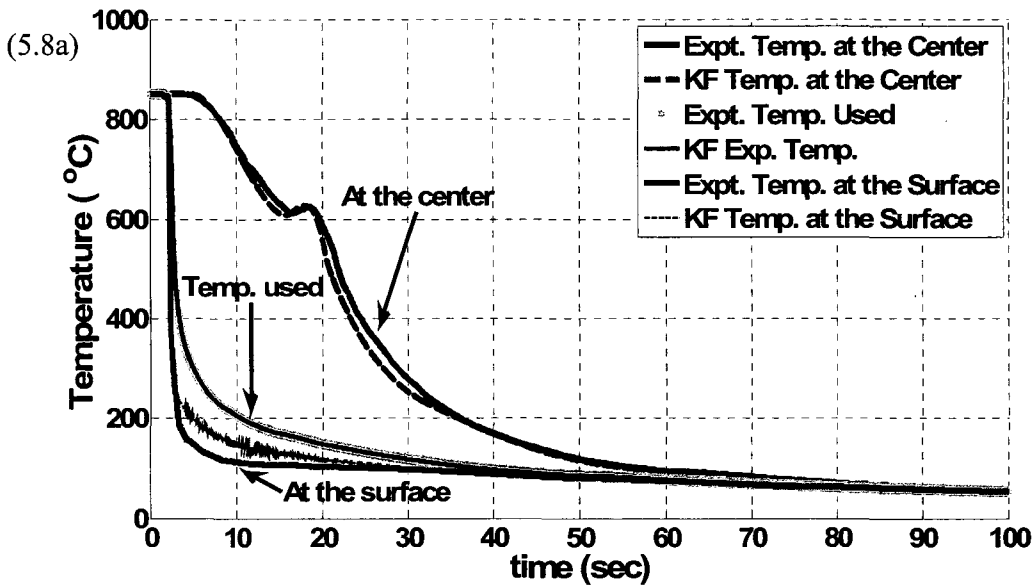
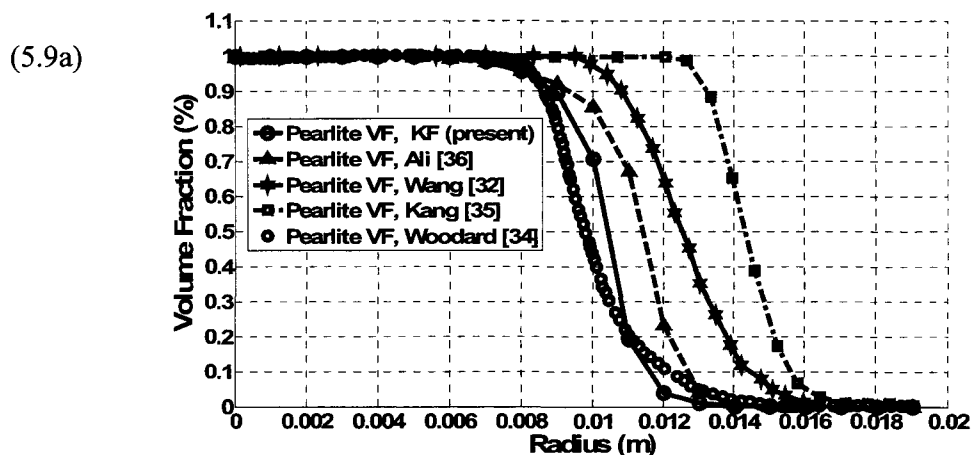


Figure 5.8 A comparison between (a) the temperature profile predicted by the present algorithm and the experimental data reported in [33], and (b) the transient temperatures of the Kalman filter, different direct numerical algorithms and the experimental data reported in [33].

Figure 5.8a shows a comparison between the inversely estimated and the experimental temperatures at two different locations in the quenched steel cylinder. Also shown are the experimental temperatures used as an input for the online input estimation algorithm and its prediction by the Kalman filter. This figure shows a very good agreement between the estimated and the experimental temperatures especially at the center where the rise in the temperature due to phase transformation heat release is excellently estimated by the present algorithm.

Figure 5.8b displays a comparison between the inversely predicted temperatures and the experimental temperatures, [33], as well as other numerical predictions of the direct problem of the same case study [32, 34, 35, 36]. As seen from this figure, the Kalman filter gives excellent results at the center while there are some fluctuations in temperature predictions at the surface. These fluctuations are expected in any inverse solver due to the measurement errors. However, these fluctuations are removed at the center because of the damping effect resulted from the diffusive nature of the heat conduction process [2].



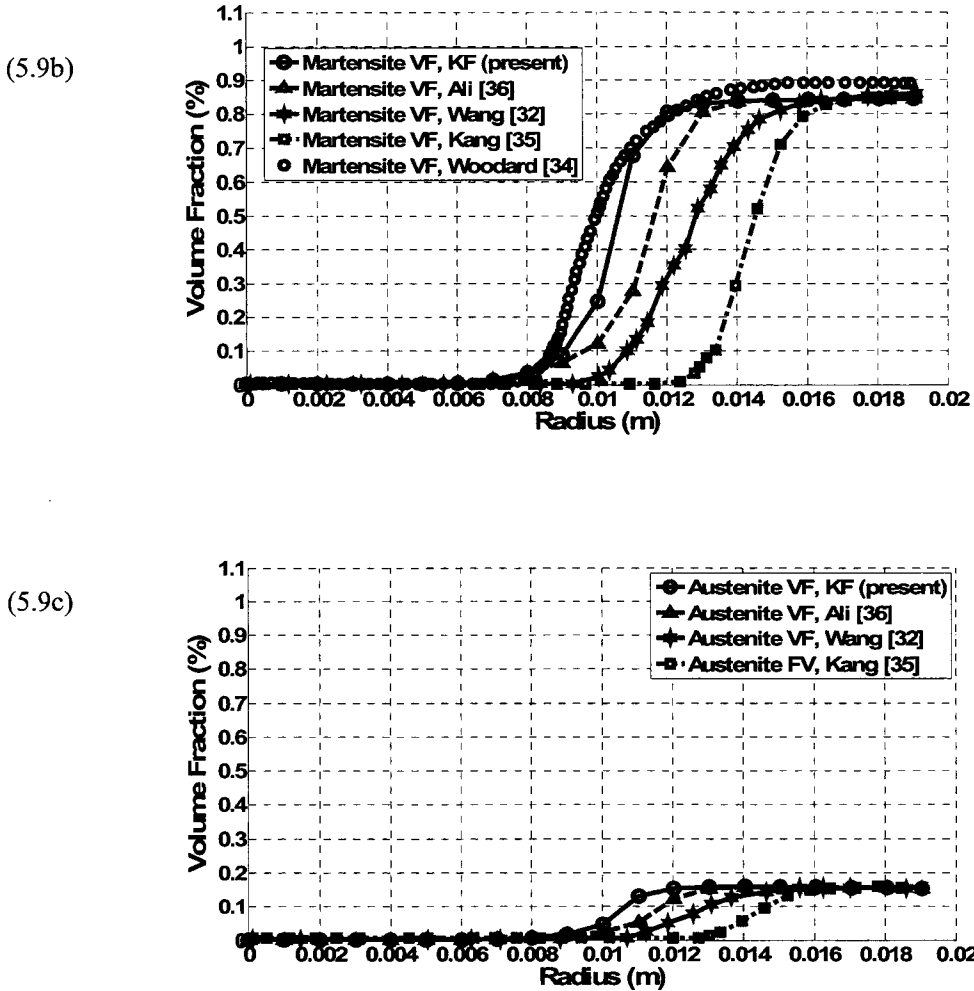


Figure 5.9 A comparison between (a) the pearlite volume fraction (b) the martensite volume fraction and (c) the retained austenite volume fraction predicted by the previous direct solution algorithms [32,34,35,36] and the present inverse algorithm.

Figure 5.9 shows a comparison between the volume fraction of pearlite, martensite, and austenite of the quenched 1080 carbon steel cylinder predicted by the inverse solver and the previous four direct numerical algorithms at the end of the

simulation time, respectively. The results of the inverse solution are between the other direct numerical results and showing the same trend. However, as previously discussed, the advantage of the inverse solution is that the convective heat transfer coefficient is part of the solution while in the direct solution algorithms it must previously be known. It is worth noting here that the volume fraction of the retained austenite has not been reported in Woodard et al. [34].

Comparison between the pearlite volume fraction calculated by the present algorithm and that calculated by a fourth order Runge-Kutta method with time at two locations in the cylinder, ($r = 19.04$ mm and $r = 4.01$ mm) is shown in Figure 5.10. This figure shows very good results of the present inverse algorithm comparing to the direct solver.

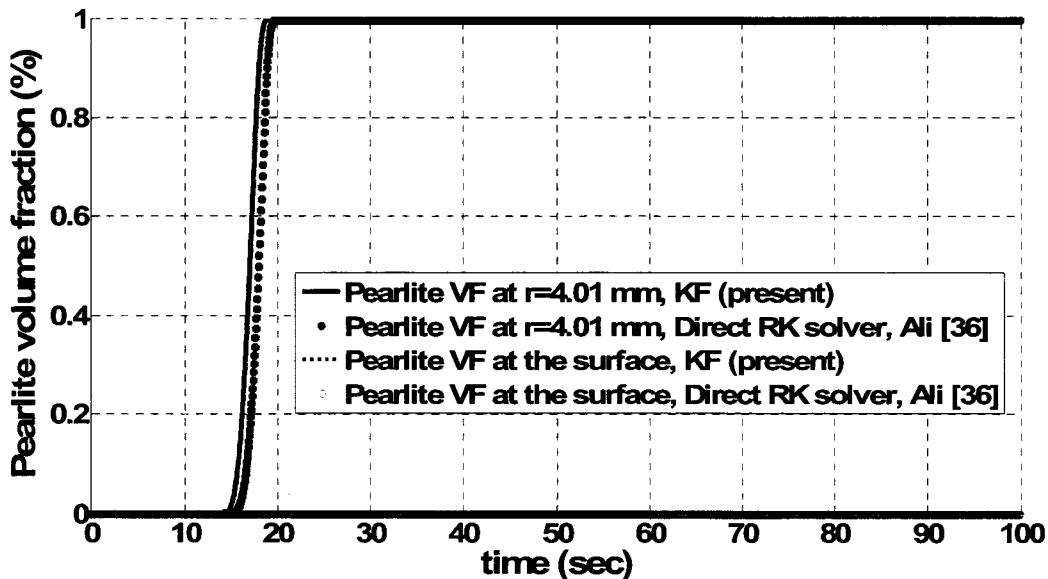


Figure 5.10 A comparison between the inverse solver pearlite volume fraction and that of the direct solver with time for two locations.

However, Figure 5.11 shows there is a difference between the phases volume fraction calculated from the inverse and direct solvers. The reason for this difference can be explained by using Figures 5.12 and 5.13.

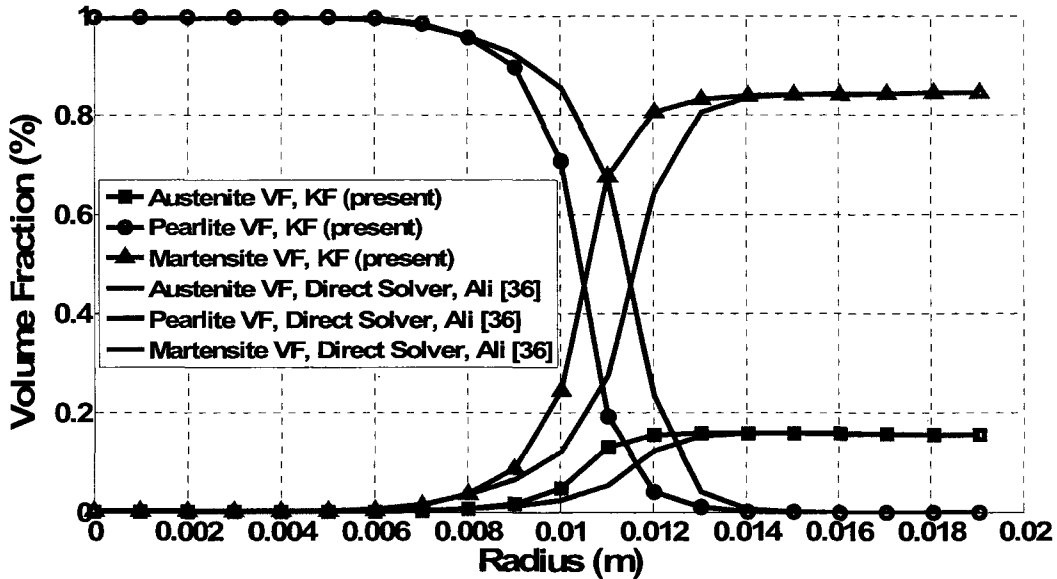


Figure 5.11 A comparison between the inverse solver volume fraction of different phases and these of the direct solver.

Figure 5.12 shows variation of the pearlite volume fraction at four locations in the cylinder with time. As previously shown, at $r=4.01$ mm, the agreement between the inverse and direct solver is excellent because the entire steel microstructure at this point is pearlite. The cooling curve at this point crosses the right C-curve on the TTT diagram where the pearlite volume fraction is one, as shown in Figure 5.13.

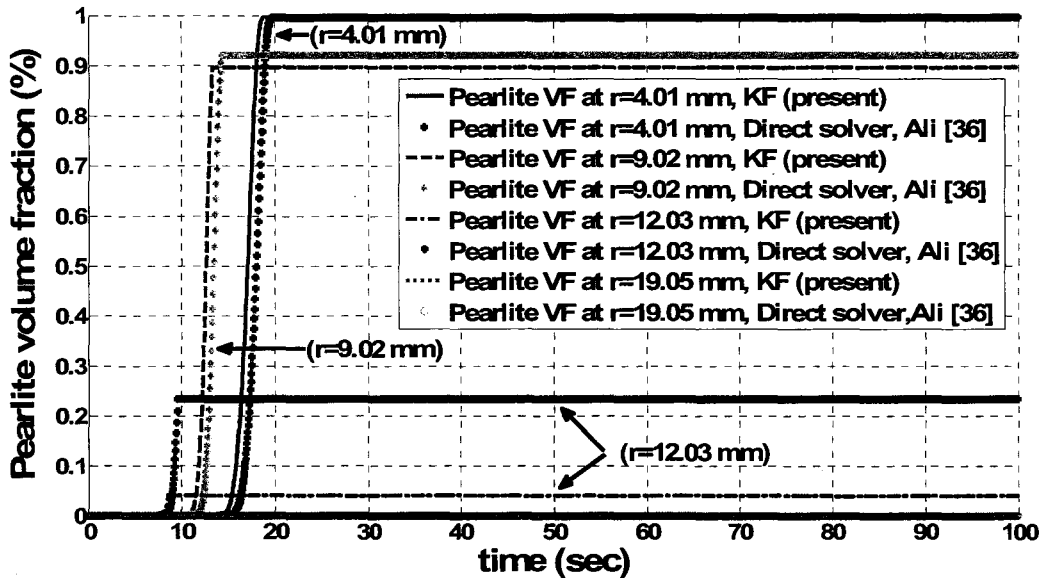


Figure 5.12 A comparison between the inverse solver pearlite volume fraction and that of the direct solver with time for four locations.

Similarly, the agreement at the surface is good where there is not any pearlitic transformation and only martensitic transformation took place. The cooling curve at this point does not cross the left C-curve on the TTT diagram, Figure 5.13.

The difference appears in the intermediate points (from $r = 8$ mm to $r = 14$ mm), Figure 5.11, due to the pearlitic partial transformation as well as the small difference in the cooling curves at the same points estimated by the inverse and direct solvers. This small difference in the temperature distribution of the inverse and direct solvers causes this noticeable difference in the pearlite volume fraction due to the exponential nature of

the pearlite microstructure model. This may be the reason for the wide discrepancy in the pearlite volume fractions estimated by different researchers [32-36], shown in Figure 9a.

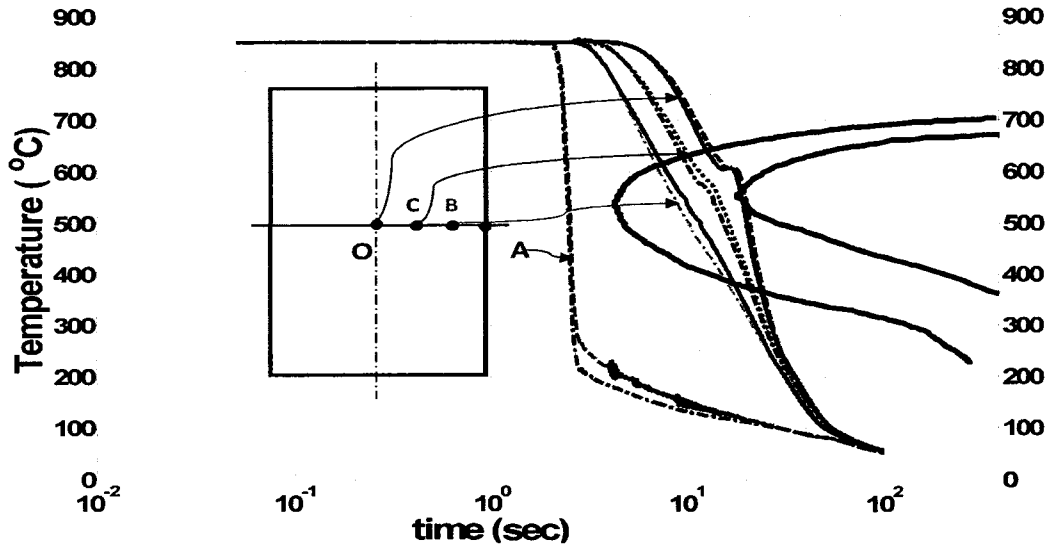


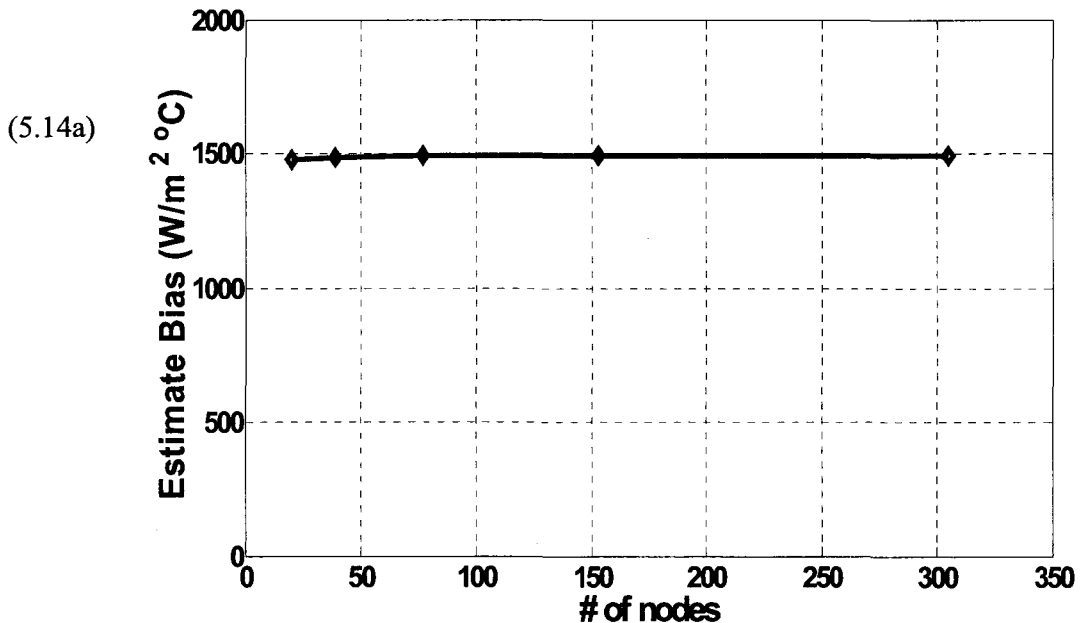
Figure 5.13 Schematic representation of the cooling curves for four locations inside the quenched cylinder on the TTT diagram.

In order to study the effect of temporal and spatial discretization as well as the measurement error on the performance of the present algorithm, the estimate bias is used as a performance measure of the algorithm. This estimate bias is calculated by using the following equation [23]:

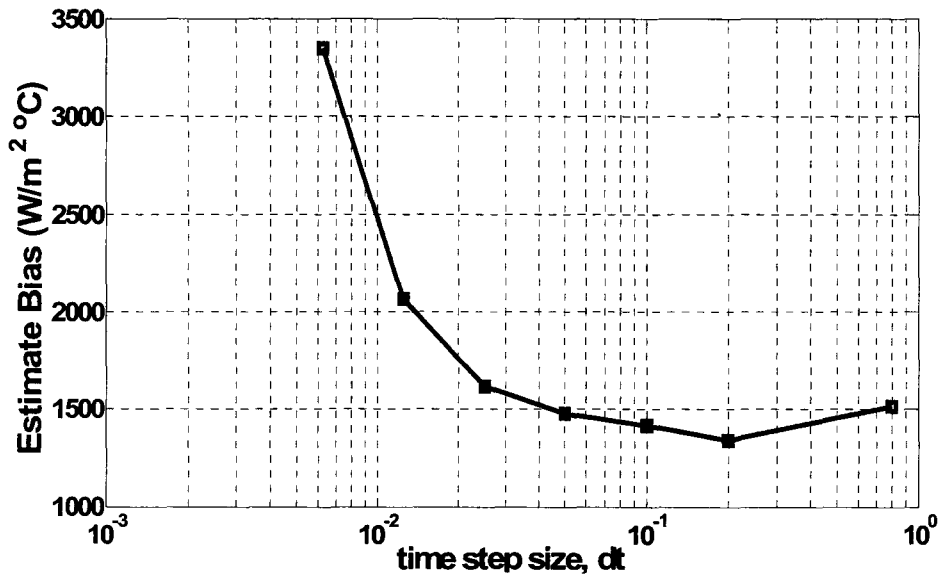
$$Bias = \left[\frac{1}{n_T} \sum_{k=1}^{n_T} (h_k - \hat{h}_k)^2 \right]^{1/2} \quad (5.72)$$

where h_k and \hat{h}_k are the exact and estimated convective heat transfer coefficients, respectively, and n_T is the total number of the time steps. This measure of the bias includes the effect of both the model errors and the temperature errors.

The performance of the present algorithm is not affected by the spatial step size as can be seen from Figure 5.14a. The effect of the temporal step size on the algorithm performance is shown in Figure 5.14b. As previously concluded in [22], there is a specific time step size that gives the minimum estimate bias. This time step size satisfies the trade-off between the deterministic bias and the sensitivity to the measurement error [42].



(5.14b)



(5.14c)

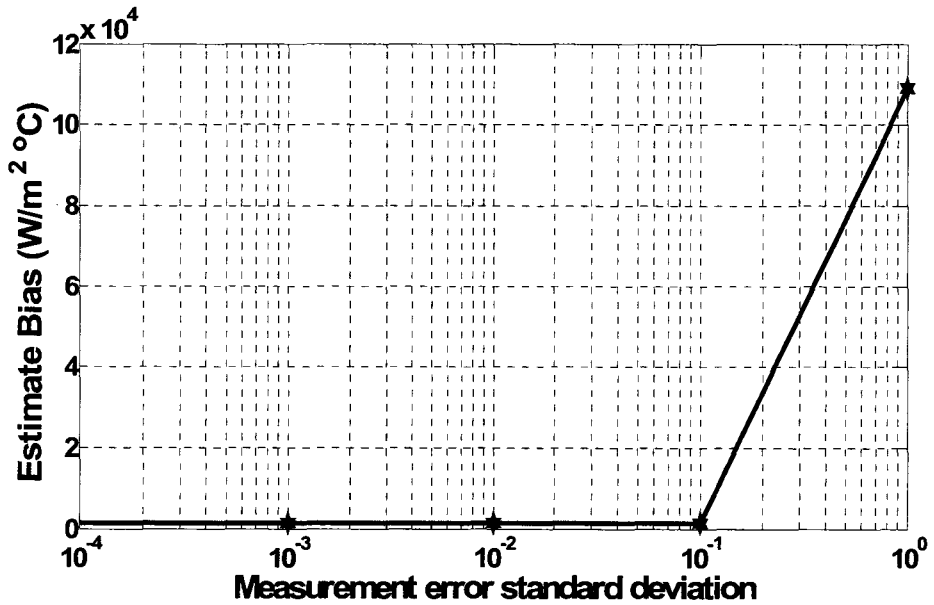


Figure 5.14 Variation of the Estimate Bias with (a) the spatial step size, (b) the time step size, and (c) the measurement error standard deviation

Figure 5.14c shows the effect of the measurement error on the estimate bias of the present algorithm. As seen from the figure, the algorithm is not sensitive to the change in the measurement error when the standard deviation of the measurement error is less than or equal to 0.01. However, as expected, above this value the estimate bias increases when the measurement error increases.

Finally, it is worth mentioning that the total computational time to solve this case study was about 95 seconds using a personal computer with a Pentium 4 processor and 2 GB RAM. The computational time is less than the measuring time period used in the direct problem (100 seconds). This indicates the strength of the computational efficiency of this algorithm which makes it very suitable for real-time controlling of steel quenching processes.

5.6 Conclusion

A new computational algorithm has been developed for real-time control of the process of steel quenching. The algorithm combines an online input estimation algorithm with a steel microstructure model to solve the nonlinear inverse heat conduction problem of steel quenching. The nonlinearity of the problem is treated explicitly where the thermophysical properties are calculated and updated at the end of each time step. Also, the heat generation due to phase transformation is handled in the present work explicitly where it is calculated at the end of each time step from the microstructure calculations, and then used in the heat equation to calculate the thermal field of the next time step. This way of handling the nonlinearity and the heat generation resulted in a more efficient

algorithm where no iterations were required without a large degradation in the accuracy of the estimation. This feature makes the present algorithm very suitable for real-time control of steel quenching processes.

5.7 Acknowledgments

This work is supported and funded by the Natural Sciences and Engineering Research Council of Canada (NSERC), the Centre for Materials and Manufacturing/Ontario Centres of Excellence (OCE-CMM), and the OCE-McMaster Thermal Processing Consortium.

5.8 References

1. Blanc, G., Beck, J. V., and Raynaud, M., Solution of the Inverse Heat Conduction Problem with a Time-Variable Number of Future Temperatures, *Numerical Heat Transfer B*, vol. 32, pp. 437-451, 1997.
2. Beck, J. V. , Blackwell, B., and Clair, C. R. St., *Inverse heat conduction-III Posed Problems*, New York, John Wiley, 1985.
3. Tikhonov, AN, and Arsenin, VY. , *Solution of ILL-Posed problems*, Washington DC., John Wiley, 1977.
4. Alifanov, O. M., *Inverse Heat Transfer Problem*, New York, Springer-Verlag, 1994.
5. Taun, P. C., Ji, C. C., Fong, L. W., and Huang, W. T., An Input Estimation Approach to On-line Two-Dimensional Inverse Heat Conduction Problem, *Numerical Heat Transfer B*, vol. 29, pp. 345-363, 1996.

6. Tuan, P. C., Lee, S. H., and Hou, W. T., An Efficient On-line Thermal Input Estimation Method Using Kalman Filter and recursive Least Square Algorithm, *Inverse Problems in Engineering*, vol. 5, pp. 309-333, 1997.
7. Ji, C. C., Tuan, P. C., and Jang, H. Y., A Recursive Least-Squares Algorithm for On-Line 1-D Inverse Heat Conduction Estimation, *International Journal of Heat and Mass Transfer*, vol. 40, no. 9, pp. 2081-2096, 1997.
8. Tuan, P. C., and Hou, W. T., Adaptive Robust Weighting Input Estimation Method For the 1-D Inverse Heat Conduction Problem, *Numerical heat Transfer B*, vol. 34, pp. 439-456, 1998.
9. Tuan, P. C., and Ju, M. C., The Validation of the Robust Input Estimation Approach to Two-Dimensional Inverse Heat Conduction Problems, *Numerical Heat Transfer B*, vol. 37, pp. 247-265, 2000.
10. Cheng, T. C., Adaptive Weighting Input Estimation Method To Contact Conductance During Metal Casting Problem, *Numerical Heat Transfer B*, vol. 39, pp. 405-419, 2001.
11. Tuan P. C., and Chen, T. C., Inverse Problem Of Estimating Interface Conductance Between Periodically Contacting Surface Using the Weighting Input Estimation Method, *Numerical Heat Transfer B*, vol. 41, pp. 477-492, 2002.
12. Chen T. C., and Tuan, P. C., Input Estimation Method Including Finite-Element Scheme for Solving Inverse Heat Conduction Problems, *Numerical Heat Transfer B*, vol. 47, pp. 277-290, 2005.

13. Jang, H. Y., Tuan, P. C., Chen, T. C., and Chen, T. S., Input estimation Method Combined With the Finite-Element Scheme to Solve IHCP Hollow-Cylinder Inverse Heat Conduction Problem, *Numerical Heat Transfer A*, vol. 50, 263-280, 2006.
14. Ji C. C., and Jang, H. Y., Experimental Investigation in Inverse Heat Conduction Problem, *Numerical Heat Transfer A*, vol. 34, 75-91, 1998.
15. Tuan P. C., and Ju, M. C., Adaptive Weighting Input Estimation Algorithm for One Dimensional Cylindrical Inverse Heat Conduction Problems, *Proc. Natl. Sci. Council. ROC (A)*, Vol. 25, No. 3, pp. 163-171, 2001.
16. Tuan, P. C., and Fong, L. W., An IMM Tracking Algorithm with Input Estimation, *International Journal of System Science*, vol. 27, no. 7, 629-639, 1996.
17. Lee, W. S., Ko, Y. H., and Ji, C. C., A Study of an Inverse Method for the Estimation of Impulsive Heat Flux, *Journal of the Franklin Institute*, vol 337, 661-671, 2000.
18. Wang, H. M., Chen, T. C., Tuan, P. C., and Den, S. G., Adaptive-Weighting Input-Estimation Approach to Nonlinear Inverse Heat-Conduction Problems, *Journal of Thermophysics and Heat Transfer*, vol. 19, no. 2, 209-216, 2005.
19. Chen, T. C., Cheng, C. H., Jang, H. Y., and Tuan, P. C., Using Input Estimation to Estimate Heat Source in Nonlinear Heat Conduction Problem, *Journal of Thermophysics and Heat Transfer*, vol. 21, no. 1, 166-172, 2007.
20. Chen, T. C., Liu, C. C., Jang, H. Y., and Tuan, P. C., Inverse Estimation of Heat Flux and Temperature in Multi-Layer Run Barrel, *International Journal of Heat and Mass Transfer*, vol. 50, pp. 2060-2068, 2007.

21. Cheng, T. C., and Liu, C. C., Inverse Estimation of Time-varied Heat Flux and Temperature on 2-D Gun Barrel using Input Estimation Method with Finite-element Scheme, *Defence Science Journal*, vol. 58, pp. 57-76, January 2008.
22. Ali, S. K., Lightstone, M. F., and Hamed, M. S., Parametric Study of Input estimation Algorithm Used for Inverse Heat Conduction Problems, 15th Annual Conference of the CFD Society of Canada, Ontario, Canada, May 27-31, 2007.
23. Ali, S. K., Hamed, M. S., and Lightstone, M. F., Numerical study of the modeling error in the online input estimation algorithm used for inverse heat conduction problems (IHCPs), *Journal of Physics: Conf. Ser.* 135 012004, 2008.
24. Shuhui, M., Aparna, S. V., Makiko, T., and Darrell, K. R., Quenching-Understanding, Controlling and Optimizing the Process, *Proceeding of the Fourth International Conference on Quenching and Control of Distortion*, 20-23 may, Beijing, 2003.
25. Hernandez-Morales, B., Brimacombe, J. K., and Hawbolt, E. B., Application of Inverse Techniques to Determine Heat-Transfer Coefficients in Heat-Treating Operations, *Journal of Materials Engineering and Performance*, vol. 1, pp. 763-771, 1992.
26. Archambault, P., and Azim, A., Inverse resolution of the Heat Transfer Equation: Application to Steel and aluminum Alloy quenching, *Journal of Materials Engineering and Performance*, vol. 4, no. 6, pp. 730-736, 1995.
27. Archambault, P., Denis, S., and Azim, A., Inverse Resolution of the Heat transfer equation with Internal heat source: application to the quenching of steels with Phase Transformation, *Journal of Materials engineering and Performance*, vol. 6, pp. 240-246, 1997.

28. Smith, D. E., Optimization-Based inverse Heat Transfer Analysis or salt Quenching of Automotive Components, *International Journal of Vehicle Design*, vol. 25, nos 1/2, Special Issue, 2001.
29. Heming, C., Xieqing, H., and Jiabin, X., Comparison of Surface Heat-Transfer Coefficients Between Various Diameter Cylinders During Rapid Cooling, *Journal of Materials Processing and Technology*, vol. 138, pp. 399-402, 2003.
30. Heming, C., Xieqing, H., and Jiabin, X., Determination of Surface Heat Transfer Coefficients of Steel Cylinder With Phase Transformation During Gas Quenching With High Pressure, *Computational Materials Science*, vol. 29, pp. 453-458, 2004.
31. Azim, A., Archambault, P., Denis, S., and Rhamin, H., Experimental Validation of Inverse Heat Conduction Method: Quenching of steels XC42 and XC80, *The European Physical journal applied Physics*, vol. 34, pp. 243-251, 2006.
32. Wang, K. F., Chandrasekar, S., and Yang, H. Y. Y., An Efficient 2D Finite Element Procedure for the Quenching Analysis with Phase Transformation, *Journal of engineering for Industry*, vol. 115, pp. 124-138, 1993.
33. Wang, K. F., Chandrasekar, S., and Yang, H. Y. Y., Experimental and Computational Study of the Quenching of Carbon Steel, *Journal of Manufacturing Science and Engineering*, vol. 119, pp. 257-265, 1997.
34. Woodard, P. R., Chandrasekar, S., and Yang, H. T. Y., Analysis of Temperature and Microstructure in Quenching of Steel Cylinders, *Metallurgical and Materials transaction B*, vol. 30 B, pp. 815-822, 1999.

35. Kang, H. K., and Im, Y. T., Three-Dimensional Finite Element Analysis of the Quenching Process of Plain-Carbon Steel with Phase Transformation, Metallurgical and Materials transaction A, vol. 36 A, pp. 2315-2325, 2005.
36. Ali, S. K., Hamed, M. S., and Lightstone, M. F., An Efficient Numerical Algorithm for the Prediction of Thermal and Microstructure Fields during Quenching of Steel Rods, Journal of ASTM International, vol. 5, no. 10, 2008.
37. Jazwinski, H., Stochastic Processes and Filtering Theory, New York, Academic Press, 1970.
38. Shalom, Y. B., Li, X. R., and Kirubarajan, T., Estimation with Applications to Tracking and Navigation: Theory Algorithms and Software, John Wiley, New York, 2001.
39. Haykin, S., Kalman Filtering and Neural Networks, John Wiley, 2001.
40. Bogler, P. L., Tracking a Maneuvering Target Using Input Estimation, IEEE Transactions on Aerospace and Electronic Systems, vols. AES-23, no. 3, May, 1987.
41. Hou, M., and Shaanxi, X., Comments on Tracking a Maneuvering Target Using Input Estimation, IEEE Transactions on aerospace and Electronic Systems, vols. AES-25, no. 2, March 1989.
42. Raynaud, M., and Beck, J. V., Methodology for Comparison of Inverse Heat Conduction Methods, Transaction of ASME, vol. 110, pp. 30-37, February, 1988.

***RESEARCH CONTRIBUTIONS AND RECOMMENDATIONS
FOR FUTURE WORK***

CHAPTER 6

6.1 Research Contributions

There are many industrial processes that require their thermal boundary conditions to be controlled in real time. One important application is the steel quenching process. The quenching process of steel is mainly used to improve the mechanical properties of steel by controlled cooling without changing part dimensions. Thus, the cooling process should be controlled in such a way that the desired mechanical properties can be achieved.

There have been financial consequences in the industry every year caused by non-optimal material properties resulting from uncontrolled quenching. The reason for these financial consequences is that the conditions of the quenching process are obtained by using extensive experimental work that does not provide detailed information about the steel microstructure during the process.

Addressing this need, an online inverse coupled heat conduction/microstructure algorithm has been developed in this study to simulate steel quenching process and estimate, adjust, and update the convective heat transfer coefficient in real time in order to achieve the desired steel microstructure that leads to optimal material properties.

The developed real-time estimation algorithm is capable of handling the coupled problem of steel quenching. The development of the algorithm involved a four-stage plan.

In stage one, a thorough literature review has been performed to explore most of the inverse heat conduction solution techniques. Inverse heat solution methods have been classified into three categories, namely; the direct inverse category, optimization based

category and the observer based category. Unlike the first and second categories, the solution methods of the third category are derived based on the optimal control theory using the dynamic observer concept which provides the possibility of real time estimating, identifying, and controlling of different industrial processes.

Of many available dynamic observers, the Kalman filter dynamic observer has been chosen to be used in this work as a part of the online input estimation algorithm due to its stochastic structure as well as its capacity in treating noisy measurements efficiently. Kalman filter also provides a quantitative measure of the estimate at each time step and most importantly its recursive nature makes it very suitable for real time estimation. This feature enhanced the computational efficiency and reduced the required computer memory.

Although, the online input estimation algorithm has been successfully applied for many industrial applications, it has not been yet used for a coupled problem such as steel quenching and has only been used for solving thermal field in pure inverse heat conduction problems. In order to modify this algorithm for steels quenching problem, the effect of many important parameters on the algorithm performance had to be systematically investigated and understood. Such investigation has not been carried out before.

The parametric study has been carried out for a one-dimensional inverse heat conduction problem in Cartesian coordinates employing different forms (functions) of boundary heat fluxes that cover most of the industrial boundary heat flux shapes. Many important parameters have been considered including, spatial step size, temporal step

size, temperature sensor location, stabilizing parameter, measurement noise level, initial state error covariance matrix in the Kalman filter and input error covariance matrix in the recursive least squares estimator. Another important investigation that has also not been carried out before is the use of different types of Kalman filters with the online input estimation algorithm. Four different types of Kalman filters have been implemented and tested. These types are the conventional continuous time state Kalman filter, implicit Kalman filter, Crank-Nicholson Kalman filter, and the explicit Kalman filter. In this investigation, both numerical stability and computational time of the algorithm have been investigated. The most significant observation of the conducted investigations in stage one and two of this study can be summarized as follows:

1. A robust range of the stabilizing parameter has been obtained for the transient heat flux considered.
2. There is an optimal time step that gives a minimum estimate bias.
3. There is no effect for the spatial step size on the performance of the filter.
4. The thermocouple should be located as close as possible to the active boundary to reduce the estimate bias.
5. Reasonable values for both P and Pb have been determined and recommended. These values can be assumed based on the prior information of the initial conditions of a given problem.
6. it was found that the implicit and Crank-Nicholson schemes are better than the explicit scheme due to their stability.

The heuristic study of the effect of changing the stabilizing parameter on the algorithm performance gave a general guide on how to design an optimal Kalman filter for particular problems of similar applications.

The contribution of the third stage of this work is developing a new, very efficient algorithm for simulating the direct problem of steel quenching. Previous researchers have mostly focused on solving the direct problem of steel quenching employing the linear form of the heat conduction equation and an iterative linear solver. The nonlinearity of the problem resulted from the thermophysical properties being temperature dependent was treated by explicit linearization. The computational time was an issue in these types of solvers.

Conversely, the proposed algorithm employed the full nonlinear form of the heat conduction equation in cylindrical coordinates. In addition, the thermophysical properties of the quenching problem in this algorithm were treated as a function of temperature. The full nonlinear heat conduction equation was solved by using a fourth order Runge-Kutta nonlinear solver.

Considering the full nonlinear heat conduction equation in simulating the quenching problem as well as the way of handling the nonlinearity of the thermophysical properties, the present direct algorithm is more computationally efficient algorithm that does not require any iteration. Furthermore, the comparison of the results of the proposed algorithm with the experimental data as well as with numerical results of previous investigations showed the improved performance and predictions obtained by the present algorithm.

The most profound contribution of this research is the work conducted in stage four where an online input estimation algorithm has been successfully developed for the first time to simulate a coupled heat conduction/microstructure problem of steel quenching. This algorithm can be used to control steel quenching process in order to produce optimal mechanical properties.

The nonlinearity of the thermophysical properties of steel quenching was treated explicitly. They have been updated at the end of each time step. The modeling error resulted from this type of linearization has been accounted for by changing the scale of the stabilizing parameter in the process equation of Kalman filter. This parameter also account for all sources of error in the model, which shows the advantage of using a stochastic estimator.

The technique used to handle the nonlinearity in the modified online input estimation algorithm did not require any iteration and thus the algorithm is very suitable for real-time control of steel quenching processes.

Finally, the two main aspects of steel quenching process have been successfully addressed by this study. The first aspect concerned with solving the direct problem of steel quenching has been addressed by the work conducted in stage three. The second aspect concerned with solving the inverse problem of steel quenching which has been addressed by the work conducted in stage four. It is worth noting that this is the first time that the above two aspects have been considered in the same study. The algorithms developed in this study provide an integral tool that can be used to optimize steel

quenching processes. This tool can also be used to replace the traditional experimental way of obtaining the right quenching conditions.

6.2 Recommendations for Future Work

Considering the available information in the literature and the insight gained from this research, the following recommendations are proposed for future work:

1. The present algorithms can be extended to tackle two and three dimensional geometries.
2. The other aspect of numerical simulation of quenching process is to predict the deformation, residual stresses, and hardness. The present algorithms did not consider this aspect. Therefore, an important recommendation for future work is to extend the present algorithm to include these important mechanical behaviors of the quenched parts.
3. Applying the developed algorithms for cases where there is more than one diffusional transformation such as transformation from austenite to ferrite and bainite. These phase transformations can be treated similar to the way adapted in the present research for diffusional transformation of austenite to pearlite. Although, the proposed algorithms have accounted for these types of transformations, they have not been examined with all possible diffusional transformations and they have been only validated against available experimental data that involves only austenite to pearlite transformation.

4. Investigate the applicability of the present algorithm for the whole heat treating cycle including the heating process.
5. Apply the present algorithm for quenching of materials that have no phase transformations such as aluminum.
6. The proposed algorithms can be applied to situations where steel is quenched by gas. This case is very interesting since many industrial quenching processes use gases for cooling and hence it could be a focus for future work.
7. In deriving the online input estimation algorithm the input (unknown boundary heat flux) has been assumed constant over a moving slide time window to obtain the measurement equation for the input in terms of the biased innovation sequence (mismatched innovation) for the real time recursive least squares estimator. It would be interesting to investigate the effect of other assumptions such as linear function form.
8. Finally, the developed algorithm is an efficient online algorithm that could potentially be used to control steel quenching process to obtain a desired steel microstructure. However, the application and implementation of this algorithm for such a purpose is a subject of future work.